ISTANBUL TECHNICAL UNIVERSITY ★ GRADUATE SCHOOL OF SCIENCE ENGINEERING AND TECHNOLOGY

ADSORPTION SIMULATIONS OF THIOPHENE REMOVAL FROM LPG BY MOFs

M.Sc. THESIS

Masoud TEYMOURFAMIANASL

Department of Chemical Engineering
Chemical Engineering Programme

JANUARY 2016

ISTANBUL TECHNICAL UNIVERSITY ★ GRADUATE SCHOOL OF SCIENCE ENGINEERING AND TECHNOLOGY

ADSORPTION SIMULATIONS OF THIOPHENE REMOVAL FROM LPG BY MOFs

M.Sc. THESIS

Masoud TEYMOURFAMIANASL
(506131023)

Department of Chemical Engineering

Chemical Engineering Programme

Thesis Advisor: Prof. Dr. M. Göktuğ AHUNBAY

JANUARY 2016

İSTANBUL TEKNİK ÜNİVERSİTESİ ★ FEN BİLİMLERİ ENSTİTÜSÜ

LPGDE BULUNAN TİYOFENİN MOFLARDA ADSORPSİYON SİMÜLASYONU

YÜKSEK LİSANS TEZİ

Masoud TEYMOURFAMIANASL
(506131023)

Kimya Mühendisliği Anabilim Dalı

Kimya Mühendisliği Programı

Tez Danışmanı: Prof. Dr. M. Göktuğ AHUNBAY

OCAK 2016

Masoud Teymourfamianasl, a M.Sc. student of ITU Graduate School of Science Engineering and Technology student ID 506131023, successfully defended the thesis entitled "ADSORPTION SIMULATIONS OF THIOPHENE REMOVALFROM LPG BY MOFs ", which he prepared after fulfilling the requirements specified in the associated legislations, before the jury whose signatures are below.

Thesis Advisor :	**Prof. Dr. M. Göktuğ AHUNBAY** Istanbul Technical University	.....
Jury Members :	**Prof.Dr. Ş. Birgül ERSOLMAZ** Istanbul Technical University	.....
	Prof.Dr. Ahmet Erhan AKSOYLU Boğaziçi University	.....

Date of Submission : 24 November 2015
Date of Defense : 7 January 2015

To my family,

FOREWORD

I would like to express my great appreciation to my supervisor, Prof. Dr. Mehmet Göktuğ AHUNBAY, who really gave me a lot of helpful advice during my study.

I would like to express my appreciation to all my friends for their motivation and mind expanding discussions during this study.

Finally, my heartfelt gratitude goes to my family for the support and encouragment they provided throughout the duration of this project.

DECEMBER 2015

Masoud Teymourfamianasl
(Chemical Engineer)

TABLE OF CONTENTS

Page

ABBREVIATIONS

LPG	**:** Liquified petrolium gas
CFC	**:** Chlorofluorocarbon
PSA	**:** Pressure swing adsorption
TSA	**:** Temperature swing adsorption
MOF	**:** Metal-organic framework
MD	**:** Molecular dinamic
MC	**:** Monte carlo
PCP	**:** Porous coordination polymers
NGV	**:** Natural gas vehicles
MRI	**:** Magnetic resonance imaging
DBT	**:** Dibenzothiophene
MMM	**:** Mixed Matrix Membranes
BD	**:** Brownian Dynamics
QM	**:** Quantum Mechanical
GCMC	**:** Grand canonical monte carlo
UA	**:** United atom
LJ	**:** Lennard-Jones

LIST OF TABLES

Page

LIST OF FIGURES

Page

ADSORPTION SIMULATIONS OF THIOPHENE REMOVAL FROM LPG BY MOFs

SUMMARY

Recently besides the well known usages of the LPG gas such as fuel in transportation system, some other sectors are added to LPG demanding market such as aerosol sector. Chlorofluorocarbons (CFCs) were used to be used in this sector but because of the environmental issues it is now almost been abandoned and safer gases like LPG are decided to be used in this sector. LPG provides the propellant pressure to push the material inside the spray containers out. So according to the environmental issues and also human health it should be completely free of sulfur containing compounds. As the only material in the LPG which causes odor, sulfur free LPG is also called odorless LPG. Sulfur causes erosion in the all mechanical parts with which it is in contact with and also is the main factor in creation of the acidic rain.

LPG is containing favorable components such as light and heavy hydrocarbons and also unfavorable component such as sulfur compounds, carbon dioxide (CO_2), nitrogen (N_2), and water (H_2O). Most of hydrocarbons are light hydrocarbons and are believed to be mostly containing Propane, n-Butane, and i-Butane. There are different methods providing LPG purification (removal of unfavorable components from LPG) and as it is related to the subject of this study it would be better o concentrate on the removal of sulfur components from LPG.

There is a wide range of sulfur containing material inside LPG such as sulfur dioxide (SO_2), hydrogen sulfide (H_2S), thiols (RSH), and thiophene family (like C_4H_4S). All these materials can lead to reduction in efficiency and value of the product, contribute to the global warming, contribute to acid rain, cause various health issues, and of course is the main reason of bad odor in the products. Among the different sulfur removal methods we can point to adsorption process with different materials, pressure swing adsorption (PSA), temperature swing adsorption (TSA), cryogenic processes, membranes and some other methods. Each of these methods has some advantages and some disadvantages and according to the sulfur removal plan design and the aimed final sulfur amount inside the final product it will be possible to choose one of them. The LPG which is going to be used in the aerosol sector is also called ultra-clean LPG which means that should be almost free of sulfur components. With normal methods it is very hard to achieve such a level so using MOFs for this aim would be so logical.

MOF based systems can work in ambient pressure and temperature which is an important advantage in comparing with other methods. On the other hand choosing different metal node and different organic part can help to have variety of the MOFs with different selectivity and adsorption feature. Then by applying proper MOF in an adsorption column in normal LPG sweetening system or after normal sweetening process it will be possible to produce ultra clean LPG. Choosing proper MOF plays a

critical role here because as mentioned before according to the chemical and also physical nature of the metal nod and organic linkers different MOFs will prefer different material. As in the LPG generally the amount of the sulfur components is less than the amount of the hydrocarbon then in normal situations it would be better for us to choose a MOF which chooses sulfur component then we would have a system in which unfavorable materials are chosen and taken out of the system.

Metal organic frameworks are known as very expensive materials at least at this moment which synthesizing of these materials is under development and from some aspects they are still costly. So doing simulations will be helpful in reduction of the costs. By getting advantages of the simulations it would be possible to do adsorption and diffusion experiments for lots of materials.

LPGDE BULUNAN TİYOFENİN MOFLARDA ADSORPSİYON SİMÜLASYONLARI

ÖZET

Metal-organik kafes yapılar (MOF) son zamanlarda gaz ayırma ve saflaştırma konusunda en sık rasladığımız uygulamalardan biridir. Ortam sıcaklığı ve basıncında çalışabilme özelliklerine sahip olması ile çevresel açıdan diğer yöntemlerden çok daha iyi olması avantajlarıyken üretim aşamasında daha henüz çok yüksek maliyete sahip olması bu madde için bir dezavantaj sayılabilir. Üretimdeki yüksek maliyetin en önemli nedeni bu yapıların üretiminin çok zor olmasıdır. Gelecekte endustriyel çapta üretilebilmesi durumunda fiyat açısından belki çok daha uygun olabilir ve o zaman çok daha yaygın bir şekilde kullanılması kesindir, ama şimdilik simülasyon yöntemleriyle ilk once hangi MOF'un uygulama için gerekli olacağı belirlenir ve bu herhangi bir yatırım yapılmadan önce MOF'ların bir sistemde nasıl davranacağını açığa çıkararak deney maliyetlerini fazlasıyla düşürebilir.

MOF'ların yapısında bulunan metaller Cu, Zn, Al, Cr, V, Zr olmak üzere periyodik tabloda bulunan çoğu metal elementleridir. Organik ligandlar ise karboksilatlar, fosfonatlar gibi bileşiklerdir. Metal ve organik bağlayıcı çeşitlerinin değişmesiyle çok farklı MOF çeşidi elde edilebilir. MOF'ların yoğunlukları oldukça düşük olduğu için kendilerine özgü gözenek hacimleri ve BET alanları onların karakteristiği için önemlidir . MOF'lar genellikle 25˚C ve 250˚C arasında değişen ortamlarda, çözelti içerisindeki ligandlar ve metal tuzları arasında gerçekleşen reaksiyonlarla sentezlenir. Çözelti olarak genellikle iyonik sıvılar kullanılır. İstenilen kafes elde edildikten sonra saflaştırma ve aktive etme işlemleri kafes üzerine uygulanır. Gözenekli kristal şeklindeki yapısı sayesinde X-ray ışınına maruz kaldığında yapıları kolaylıkla karakterize edilebilir ve böylelikle yeni ve gelişmiş MOF'lar tasarlanabilir.

Bilim dünyasına son yirmi yılda giren metal organik kafesler üzerinde yapılan çalışmalar çoğunlukla gazların depolanması, katalizörlerin ve ayırma işlemlerinin geliştirilmesi yönündedir. Son zamanlarda ise özellikle düşük kükürt içeren yakıtlar elde etmek için tiyofen gibi kükürtlü bileşiklerin model yakıtlardan ayrılması üzerine çalışmalar artmıştır.

Farklı moleküler uygulamalar için Moleküler Dinamik (MD) ve Monte-Carlo (MC) metodu gibi farklı simülasyon metodları ile daha esnek uygulamalar gerçekleştirilebilir.

Rastgele üretilen sayılardan faydalanılarak istatistiksel simülasyonlar Monte Carlo metoduyla yapılır.Deney girdileri belirli olmayan, kesin olmayan bir şekilde gelmesi bekleniyorsa ve dağılım bir fonksiyonla hesaplanabilecekse kullanılır. Monte Carlo, rastgele sayıları baz alarak tahmini sistemleri modeller. Hücre Similasyonu, Borsa Modelleri, Dağılım Fonksiyonları, Sayısal Analiz, Doğal olayların simülasyonu, Atom ve Molekül Fiziği, Nükleer Fizik ve Yüksek Enerji Fiziği modellerini test eden simülasyonlar, Deneylerde kullanılan aletlerin simülasyonu (Örneğin bir madde içerisinde x ışınlarının dağılımı).

Bu uygulamalardan en önemli olanı fosil yakıtlardan özellikle doğalgaz ya da LPG ‘den sülfür giderimidir. Normal sülfürsüz LPG’den ayrıca aerosol sektöründe kullanılan ultra temiz LPG talebi de giderek artmaktadır. Aerosollerin tamamen kokusuz ve desülfürize olması istenmektedir. İstenen bu sülfürsüzleştirme oranı, absorpsiyon kolonu ile yapılan normal desülfürizasyon işlemi ile elde edilemez. Bu problem için MOF kullanımı en olumlu sonucu elde etmemizi sağlar.

LPG içersinde çeşitli safsızlıklar bulunmaktadır. CO_2, H_2O, H_2S, SO_2 ve Tiyofen sıkça rastladığımız safsızlıklardanlardır. LPG’nin asıl koku kaynağı kükürt içeren safsızlıklardır ve onların gidermesinin aerosol üretiminde çok önemli rolu verdır. Tiyofen yapısından kaynaklanan nedenlerden dolayı, daha zor adsorplandığından dolayı bu çalışmada daha çok tiofen giderimine odaklanarak, MOF’ların bu maddeye maruz kaldığında davranışını farklı açılardan incelendi.

Simülasyonlar Accelrys Material Studio 6 program paketi kullanılarak gerçekleştirilmiştir. Tüm parametreler farklı makalelerden alınmış ve force field dökümanı manuel olarak tüm simülasyonlar için üretilmiştir. MOF kristal yapıları orjinal veritabanında bulunmakta olup simulasyon sistemleri için optimize edilmiştir.

Bu çalışmada, adsorpsiyon sistemleri için en iyi metod olan Monte Carlo simülasyon metodu kullanılmıştır. Simülasyonlar 3 farklı adımda sıcaklıklar 273K olarak başlayıp, 10K artışlarla 303K de bitecek şekilde gerçekleştirilmiştir. LPG içeriği n-Bütan, i-Bütan, Propan olarak kabul edilmiş ve ana sülfür bileşimi olarak Tiyofen kullanılmıştır. Tekil adsorpsiyon ve kampetitiv adsorpsiyon tüm komponentler için test edilmiş ve adsorpsiyon izotermleri ve seçicilik faktörleri tüm örnekler için oluşturulmuştur. Bu çalışmada C300, Z1200, Basossiv M050 ve A100, IRMOF olarak beş farklı MOF kullanılmıştır.

MOF’larin performansını oldukça iyi bir şekilde incelemek için, ilk adımda tekli adsopsiyon hesaplamaları 4 farklı sıcaklıkta ve 1E-4 ve 506 kPa basınc aralığında her bir MOF için yapıldı. İkinci aşamada koptetitiv adsorpsiyon hesaplamaları tiyofen ve LPG içeriğinde bulunan hidrokarbonlar için yapıldı ve diyagramlar çizdirildi. Üçüncü kademede sıcaklığın adsorpsiyonu nasıl etkilediğini daha iyi görmek için her MOF için adsorpsiyon izotermleri farklı sıcaklıklarda aynı diyagramda çizdirilip kıyaslandırıldı. Bir sonraki aşamada MOF’ların seçicilik özelliği incelendi. Bu aşamada LPG’de bulunan tiyofen ve hidrokarbon atom sayısında çok büyük bir fark olduğundan dolayı, kompetitive adsorpsiyon değerleri yerine tekli adsorpsiyon değerlerinin üzerine hesaplamaları yapmak zorunda kaldık. MOF’ların fiyatı daha öncede söylendiği gibi yüksek olduğundan dolayı, tekrar tekrar kullanmaya müsait olmaları gerekiyor. Bu özelliği incelemek için MOF’ların çalışma kapasitelerine bakmak gerekiyor ve bu çalışmada da bu parametre tüm MOF’lar için hesaplandi ve karşılaştırıldı.

Son aşamada MOF’ların performansı, günümüzde LPG safsızlık gideriminde en yaygın olan maddeler, yani Zeolit’ler ile karşılaştırıldı. Bu amaçla 3 tane en iyi performans gösteren MOF seçildi ve 3 farkli zeolit (All silica zeolit, MOR ,ve MFI) ile karşılaitırıldı. Bu zeolitler daha önce LPG’den tiyofen gidermek amacıyla başka gruplartarafından farklı makalelerde incelenmiştir

Sonuçlar göstermiştir ki Magnesium formate, Cu-BTC, ve IRMOF-1 diğer iki MOF’a göre absorpsiyon ve seçicilik açısından daha iyi performans sağlamaktadır. Bu üç MOF adsorplama açısından iyi performans göstermelerine rağmen, düşük çalışma kapasitesne sahiplerdir. Bu neden ile onları tekrar kullanabilmek için, yüksek

sıcaklık veye çok düşük basınçta onlardan tiyofen molecüllerini ayırmak gerekiyor ve bu MOF'lar için bir dezavantaj sayılabilir.

Zeolitler ile kıyaslandığında, MOF'ların çok daha iyi performans gösterdiğini ve çok daha fazla tiyofem adsorplayabileceğini söyleyebiliriz.

Gelecekte bu MOF'ların laboratuvar ve endüstriyel çapta denemsi önerilmektedir.

1. INTRODUCTION

Recently besides the well-known usages of the LPG gas such as fuel in transportation system, some other sectors are added to LPG demanding market such as aerosol sector. Chlorofluorocarbons (CFCs) were used to be used in this sector but because of the environmental issues it is now almost been abandoned and safer gases like LPG are decided to be used in this sector (Tiwari, Sahu et al. 2013). LPG provides the propellant pressure to push the material inside the spray containers out. So according to the environmental issues and also human health it should be completely free of sulfur containing compounds (Nevers 1987). As the only material in the LPG that causes odor, sulfur free LPG is also called odorless LPG. Sulfur causes erosion in the any mechanical parts that it is in contact with and is the main factor in creation of the acidic rain.

LPG is containing favorable components such as light and heavy hydrocarbons and also unfavorable component such as sulfur compounds, carbon dioxide (CO_2), nitrogen (N_2), and water (H_2O). Most of hydrocarbons are light hydrocarbons and are believed to be mostly containing Propane, n-Butane, and i-Butane (Anunziata, Eimer et al. 1999). There are different methods providing LPG purification (removal of unfavorable components from LPG) and as it is related to the subject of this study, it would be better to concentrate on the removal of sulfur components from LPG.

There is a wide range of sulfur containing material inside LPG such as sulfur dioxide (SO_2), hydrogen sulfide (H_2S), thiols (RSH), and thiophene family (like C_4H_4S) see Appendix D. All these materials can lead to reduction in efficiency and value of the product, contribute to the global warming, contribute to acid rain, cause various health issues, and of course is the main reason of bad odor in the products. Among the different sulfur removal methods we can point to adsorption process with different materials, pressure swing adsorption (PSA), temperature swing adsorption (TSA), cryogenic processes, membranes and some other methods. Nevertheless, one of the most dominant methods that is widely used is adsorption method. For this aim,

different materials are used as adsorbents such as Zeolites and MOFs. Adsorbents are usually loaded to adsorption columns and selective adsorption process is performed in optimized temperature and pressure and according to the components that are desired to be captured from the feed stream to the adsorption columns, type of adsorbent and operation conditions may change. Each of these methods have some advantages and some disadvantages and according to the sulfur removal plan design and the aimed final sulfur amount inside the product, it will be possible to choose one of them. The LPG, which is going to be used in the aerosol sector, is also called ultra-clean LPG that means that should be almost free of sulfur components. With normal methods, it is very hard to achieve such a level so using MOFs for this aim would be so logical.

MOF based systems can work in ambient pressure and temperature which is an important advantage in comparing with other methods (Millward and Yaghi 2005). On the other hand choosing different metal node and different organic part can help to have variety of the MOFs with different selectivity and adsorption feature. Then by applying proper MOF in an adsorption column in normal LPG sweetening system or after normal sweetening process it will be possible to produce ultra clean LPG. Choosing proper MOF plays a critical role here because as mentioned before according to the chemical and physical nature of the metal nod and organic linkers different MOFs will prefer different material. As in the LPG generally the amount of the sulfur components is less than the amount of the hydrocarbon then in normal situations it would be better for us to choose a MOF which chooses sulfur component then we would have a system in which unfavorable materials are chosen and taken out of the system (Corma, Martınez et al. 2001, De Wild, Nyqvist et al. 2006).

Metal organic frameworks are known as very expensive materials at least at this moment which synthesizing of these materials is under development and from some aspects, they are still costly. So doing simulations will be helpful in reduction of the costs. By getting advantages of the simulations it would be possible to do adsorption and diffusion experiments for lots of materials (Ting and Doan 2014).

2. METAL-ORGANIC FRAMEWORKS

Metal-Organic frameworks (MOFs) also known as porous coordination polymers (PCPs) are a class of emerging highly crystalline porous materials in one-dimensional (1D), two-dimensional (2-D), three-dimensional (3-D) networks. In particular, 2-D and 3-D coordination polymers has attracted a great attention over the past two decades in different fields of study like heterogeneous catalysis, bio-catalysis, sensors and bio-chemical applications, gas separation, and gas storage. MOFs are constructed from metal-containing nodes connected to each other by organic linkers (ligands) and compared to the other conventional porous solids such as carbons and zeolites MOFs are of particular interest because of mild synthesizing and design conditions. Both because of their facile preparation and for the variety of the metal containing nodes and linker available, there are many synthesized MOFs now, and every passing day this variation gets even more abroad. They can be tailored indifferent combination, porosity, surface area, shape, size, etc.

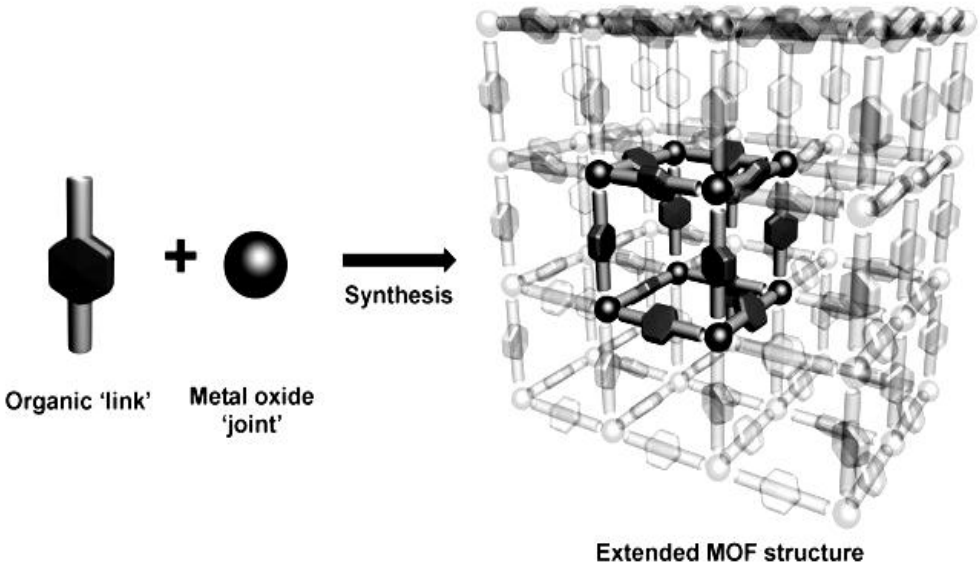

Figure 2.1: Metal-organic frameworks combine a cluster of metal ions and organic linkers to form a honeycomb-like structure.

2.1 Properties of MOFs

MOF properties are generally attributed to its framework structure. Variation of organic linker and metal nodes results in variations in behavior of the material in different conditions. Now, even it is accepted that controlling the position and sort of nodes and linkers fully results in MOF performance. MOFs are generally synthesized in water or organic solvents and indifferent temperatures ranging from room temperature up to around 250°C that was achieved in ovens or oil bathes previously but recently in order to reduce the required energy microwave system are hired in such synthesis. Besides that it is shown that microwave heating affects morphology and size of the crystals, too (Yoo, Lai et al. 2009).

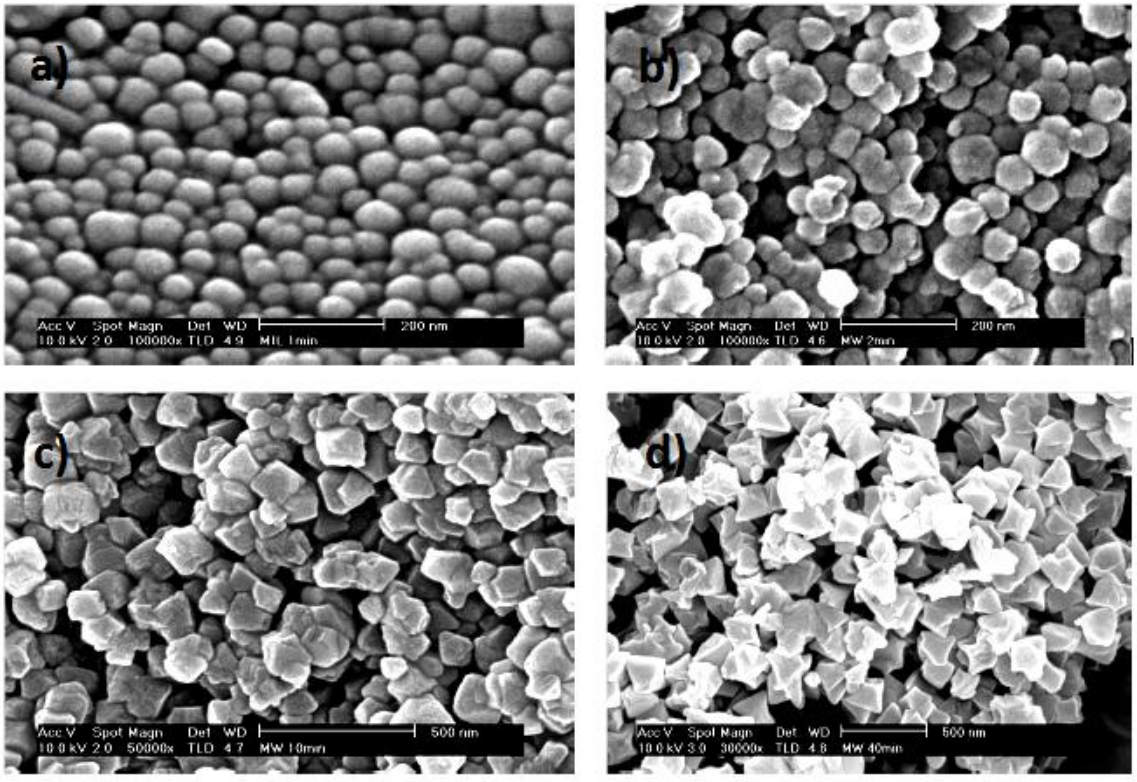

Figure 2.2: Effect of micro wave on MOFs

The other two affective properties of MOFs are surface area and pore size (Sun, Ma et al. 2006, Farha, Yazaydın et al. 2010). There are various kinds of MOFs classified by the pore size such as nanoscale MOFs and mesoporous MOFs. In addition, both metal nods and linkers are effective in pore size, it is usually accepted that the pore

size is more important and effective for this factor. High internal surface area is one of the foremost attributes of MOFs and has been shown to be highly desirable in many potential applications involving catalysis or storage. Forty tennis courts can be covered by the surface area of one gram of MOF. This incredible exclusivity lets the material to have a very large storage capacity, since there are a great number of locations for gas molecules to "stick" or adsorb to. After molecular adsorption, the immobilized materials take less space than the time they were free to move around in gas phase. This directly means that a tank filled with MOFs can take more gas in comparing with an empty tank with the same value. Desorption process of the MOFs is done simply and by getting the advantage of fully reversible uptake and release behavior of these material, and the gas can be released by putting a simple valve on the tank and opening it (Liu, Eubank et al. 2007, Férey 2008, Klontzas, Mavrandonakis et al. 2008, Allendorf, Bauer et al. 2009, Stock and Biswas 2011, Tanabe and Cohen 2011).

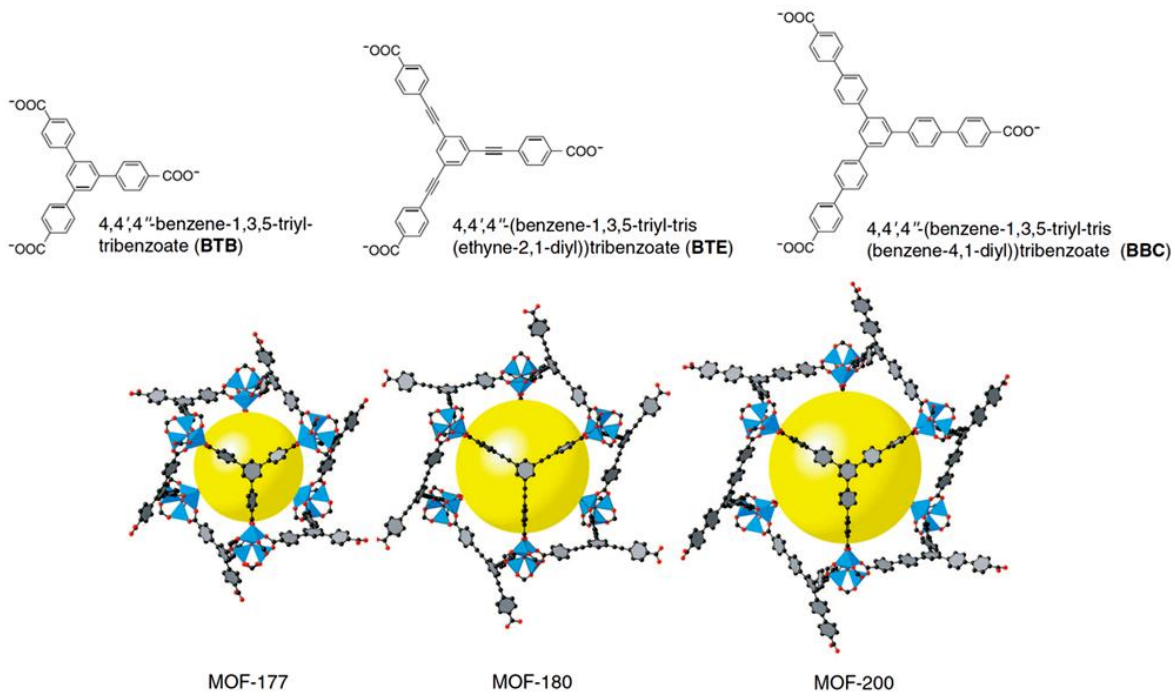

Figure 2.3: effect of organic linkers on MOF features

2.2 Applications of MOFs

Thanks to potential applications that could affect several aspects of our lives in the near future, MOFs are used in different areas. MOFs have broad industrial applications because of two key attributes: their extremely large surface-areas and the flexibility with which their structures can be varied. They are also very robust, with high mechanical and thermal stabilities. These materials are used in:

2.2.1 Carbon capture

One of the most important environmental concerns with which our civilization faces, is the sharply rising level of atmospheric carbon dioxide (CO2) resulting from the burning of fossil fuels. There is therefore a huge global drive to minimize and mitigate these emissions, concentrating on the Carbon Capture and Sequestration (CCS). CCS involves capturing carbon dioxide that would otherwise be released to the atmosphere, compressing it, transporting it to a suitable site and injecting it into deep geological formations where it will be safely trapped.

The first step in CCS is separating the CO2 from other gases in the exhaust stream and, in the process, capturing the CO2. The dominant technology in these processes has been amine scrubbing an energy-intensive and inefficient process that creates toxic byproducts. This technology itself requires 30% of the output of the power plant to operate and accounts for as much as 70% of the cost of CCS. These costs must certainly be reduced if CCS is to become viable.

MOFs are a good solution for this problem, besides that they are more environmentally friendly and efficient, capturing more CO2 and requiring less energy to regenerate. The adjustable structure of MOFs allows them to be optimized for the CO2 capture in different specified carbon capture systems such as post-combustion capture, pre-combustion capture, or oxy-fuel combustion. MOFs have been identified by the US Department of Energy as the most promising next-generation technology for carbon capture (Yazaydın, Snurr et al. 2009, Li, Ma et al. 2011, Sumida, Rogow et al. 2011).

2.2.2 Natural gas storage

Natural gas vehicles (NGVs) are getting prominent because of many advantages comparing with the gasoline-fueled vehicles such as:

a- Lower fuel costs for a mile travelled for natural gas which is around half of the gasoline
b- Lesser carbon emission production which is accepted as 30% reduction
c- Lower particulate and NO_x production
d- Lower caring costs
e- Safer using conditions (gas fuels are excepted to be safer than liquid in burning meanwhile)

The significant barrier of using NGVs has been the refueling and storage issue. A very high pressure of about 300 atm and as the result of the pressure cylindrical storage tanks of steel are needed for this aim. In addition, in order to attain this pressure special refueling stations are needed. The best solution is provided by MOFs by enabling higher storage capacities in lower pressure conditions. So it will be much cheaper and so much safer while using MOFs (Wu, Zhou et al. 2009, Mason, Veenstra et al. 2014).

2.2.3 Acetylene storage

Acetylene is one of the important raw materials for assorted industrial chemicals and every year thousands of tons of it are produced around the world. Volatility of acetylene renders it difficult to transport and dangerously explosive at twice regular atmospheric pressure. To store it safely, storage cylinders are filled porous material and some liquid solvents and for this aim, MOFs are good candidate. By using MOFs in this field, the economics of acetylene storage can be completely transformed because of vastly increasing possible storage capacities. In addition, it is possible to store more acetylene in the same volume of cylinder.

2.2.4 Hydrogen storage

Nowadays there is a considerable evolution in using non-petroleum energy to be used in transportation and hydrogen is an engaging choice because of the high energy content and clean exhaust. As the specific energy of uncompressed hydrogen is not satisfactory, decisively it should be stored in a denser way and adsorbing in a MOF structure is a logical way for this aim.

As MOFs are known as free dead-volume materials, in long-term usage no loss of storage capacity is expected. As the benefits provided by MOFs are realized in gaseous state, the only limitation in storage capacity of the MOFs is the liquid-phase density issue (Collins and Zhou 2007, Lin, Jia et al. 2007, Murray, Dincă et al. 2009, Suh, Park et al. 2011).

2.2.5 Natural gas processing and light hydrocarbon separations

Separation and purification of the chemicals that are encountered in daily life establishes a major part of global economy and a considerable part of it relies on the use of porous solids in a range of industrial processes. All the extracted natural gas includes some contaminants such as CO2 and sulfur components. These impurities are called (acid gasses) are highly corrosive and also very harmful respect to the environmental and human health issues. These contaminants must be removed at the refinery prior to the natural gas being transported and sold. Also there are various methods for this aim, but most of them are insignificant or they are highly energy intensive. MOFs are non-toxic, cost-effective, and easy to handle and also they have high adsorption capacity, greater selectivity, and long life time. Besides these they require relatively mild processing conditions. The pore size and chemical composition of a MOF can be tuned to selectively and efficiently capture each individual hydrocarbon. So they are a good alternative for most of the prior technologies (Pan, Olson et al. 2006, Li, Kuppler et al. 2009, Herm, Bloch et al. 2013).

2.2.6 Drug storage and delivery

The unique properties of the MOFs provide modern methods to manipulate, store and react to a wide variety of substances. This is leading to the rapid development of new applications in areas such as pharmaceuticals, medical imaging and sensing. The development of huge number of promising drug candidates has been abandoned due to poor bioavailability, i.e. the controlled delivery of the drug to where it is needed cannot be achieved. Non-toxic and biodegradable MOFs have been shown to be suitable for the encapsulation and controlled delivery of a large number of therapeutic molecules, including several challenging antitumor and antiretroviral drugs. By tailoring the pore sizes of the MOF, large storage capacities and long release times can be achieved for specific drug molecules. Research is also underway on MOFs built from the drug molecule itself (Horcajada, Serre et al. 2006, Horcajada, Serre et al. 2008, Della Rocca, Liu et al. 2011).

2.2.7 Medical imaging

MRI and some other medical imaging systems are mainly depended on large doses of administered contrast agents in order to find the difference between diseased tissues and the normal ones. The most important challenge in this area is developing more sensitive and flexible methods for early and accurate diagnosis of illnesses with minimal amounts of contrast agent. MOFs are intrinsically biodegradable, and their high porosity makes them ideal for targeted delivery of entrapped agents. Trials have also shown that can be specifically targeted to certain regions of the body (Taylor, Rieter et al. 2008, Horcajada, Chalati et al. 2010).

2.2.8 Sensors

In such fields like air quality monitoring, food spoilage and explosive detections some sensors called Chemiresistive sensors are widely used. Typically metal oxides and carbon-based nanomaterials including graphene are used for this aim. The problem that users of this method are facing with is the tuning of the material

structure which is very hard to handle at atomic levels. In contrast, MOFs are affirmative for tuning in response to their chemical properties. The tailorable nanoporosity and ultrahigh surface area of MOFs make them ideal candidates for recognizing analytes in sensing applications. MOFs have the potential to overcome many of the challenges of selectivity that plague other sensor materials and form the basis of robust, highly-sensitive and compact sensing devices (Lu and Hupp 2010, Kreno, Leong et al. 2011).

2.3 Academic study background

Since the 1990s, this area has performed a supreme development not only in the field of research papers but also in laboratory experiments. Also not many experiments or simulations have been performed for the application of sulfur compound removal from LPG especially for the thiophene like sulfur components but the rapid increase in work performed in this areas is easily sensible. In a study in 2012, Zhang et al. have tested adsorption behavior of MOFs for thiophenic sulfur for diesel oil using Cu-BTS, Cu-BDC, Cr-BTC, and Cr-BDC. Two different metal nodes and two different organic parts are selected to survey in this study in order to realize the effect of these parameters. As the result of this study, it is believed that π-electron number and the electron density on the S-atom is the main factor that is affecting the adsorptive activity. All MOFs used in this study can be easily washed and regenerated to be used again (Zhang, Huang et al. 2012).

In another study performed by Khan et al. Me-BDC is been taken to be studied in which 'Me' is the symbol for metal node and Al, Cr, and V are placed in this position in three different MOFs. $CuCl_2$ is a different item that is added to the structure of each of the MOFs in order to see the change in the adsorption capacity of them. It is reported so that, Cu^{3+} is almost affective just for the MOF with the V as the metal node. This study is suggesting careful deliberation of metal nodes before choosing MOFs for all applications such as catalysis and adsorption (Khan and Jhung 2013).

Adsorption of organo-sulfur compounds of liquid fuels are studied by Blanco-Brieva et al. for different MOFs and compared with Y-type zeolite in order to show the

better performance of the MOFs in comparing with the zeolites and also see the performance of the MOFs in comparing with each other. According to their study, all studied MOFs have shown much better performance than the Y-type zeolite. Adsorption processes where performed for dibenzothiophene (DBT) and it is been proved that DBT adsorption strongly depends on the MOF type and among C300, A100, and F300 which are the MOFs studied in this project, C300 performs better than other two. The very high adsorption capacity of this substrate makes it a potential candidate to be employed in the removal of remaining refractory S-compounds in previously desulfurized liquid fuels.

One of the fastest growing branches of the membrane technology for gas separation is using selective transport ability of the polymeric membranes. Nevertheless, it seems that existing polymeric membrane materials are deficient to fully accomplish the application opportunities of these materials on industrial scales. Improvement in selectivity causes may cause reduction in and vice versa. The most recent type of membrane material is emerging by application of Mixed Matrix Membranes (MMMs) composed of homogeneously interpenetrating of the polymeric and inorganic particle matrixes. One of the best candidates for particle matrix part are MOFs. Applying appropriate MOF inside proper polymer structure either can affect both selectivity and permeability of the polymer positively or increases the physical properties of the MOF part. A high performance membrane adsorber including MOF has been fabricated in study performed by Lin et al. in order to see its effect on sulfur removal of hydrogen source fuels used in fuel cells in the year 2013. The three-dimensional channels formed by reciprocal interaction of polyimide, as the polymer part material and Cu-BTC as the MOF are believed to be affective factor in this study. The properties of the MOF based adsorber, including the adsorption contribution, regeneration behavior and effect of fuel species, have been investigated. They proved that inlet fuel can be desulfurized up acceptable levels for fuel cell applications (Blanco-Brieva, Campos-Martin et al. 2011).

In another study performed by Achmann et al. in the year 2009, several MOFs were investigated to determine the sorption characteristics of sulfur compounds from fuels. Low-sulfur gasoline and diesel fuels were produced for this study in the laboratory as model fuels. Thiophene and tetrahydrothiophene (THT) were chosen as model

substances. Cu3(BDC)2, MOF-5, Zn4O(BDC)3, Cu-DABCO, and Cu-iso-MOF are the MOFs used in this study and according to their reports only Cu3(BDC)2 shows a high efficiency for sulfur removal from fuels and model oils of this study. Time-resolved measurements performed in this study shows that sorption process for sulfur components occurs only in the first 60 minutes after the contact between MOF and adsorbate comes true (Achmann, Hagen et al. 2010).

3. MOLECULAR SIMULATIONS

3.1 Introduction to molecular simulation

In the modern analysis and testing age, simulation based analysis methods are obligatory beneficial to production of new materials and either physical or chemical prob of various material on a molecular level. All these methods are based on unic properties of any species, like molecules and porous material, that are examined. Quantities of interest, whether in macroscopic scale or microscopic scale, could be derived from these approaches both qualitatively and quantitatively.

So called “Molecular Simulation” methods which are delineated by Monte Carlo (MC) and Molecular Dynamic (MD) methods figure out the motion of separate single molecules in gas, liquid, or solid models (Haile 1992). Also MD and MC are known as major simulation methods, there are some other methods used in special cases such as Brownian Dynamics (BD) which is used for simulating brownian motion of particles like pollen grain dispersed in a liquid (Satoh 2003) or Dissipative Particle Dynamics (DPD) or lattice Boltzman methods which are used for simulating either particle dispersions or pure liquid systems as composition of virtual fluid particles (Koelman and Hoogerbrugge 1993, Chopard and Droz 1998).

Molecular simulation innovation is parallel with development of computers. It is believed that Metropolis et al. Executed the first molecular simulation in 1953 for a liquid system based on MC method. Later in 1957 and 1959, MD method was introduced by Alder and Wainwright for scrutinizing equations of motion for intermolecular interactions in a system for momenta chenge experienced by indevidual molecules (Sadus 2002).

3.2 The monte carlo method

The MC method is known as a stochastic technique and depends on probabilities. Transition between various configurations and states is a fundamental factor in simulating a system is accomplished by three steps:

a- Developing a random configuration
b- Appraising an ‘acceptance criterion’ by considering the changes in different parameters such as energy in developed configuration
c- Comparing this acceptance criterion with a random number in order to accept or reject the configuration

In MC analyzing process, a new configuration is generally achieved by adding a molecule, exchanging the old molecule with new one, displacing the desired molecule or removing it. In each of this choices again probabilities are involved and nature of transition probabilities for any of them is depended on the chosen ensemble for the system (Sadus 2002)So a short survey on ensemble matter would be useful in this part**.**

3.3 Statistical ensembles

Statisticle ensemble is generally known as collection of compilation of various states of the assumed system which have different compositions and velocities for component particles. There are different kinds of satatisticle ensemble in order to represent appropriate probability distribution of component related properties. By a galance to the history of ensemble applcation in MC based simulations we will see that metroplis et al. Have applied constante particle number, volume, and temporature (NVT) ensemble in 1993 to their system (Huelsenbeck and Ronquist 2001) or the application of Isothermal-Isobaric ensemble was performed by McDonlad for binary mixtures in 1972 (McDonald 1972) . Grand Canonical ensemble and Microcononical Ensembles had been applied by Vallue and Cohen , and Ray in the year 1980 and 1991 (Valleau and Cohen 1980, Ray 1991)

Table 3.1: Statistical ensembles.

Ensemble	Imposed Variables	Partition Function(Z)	P_i
Isothermal-Isobaric	N, P, T	$\sum_i e^{\beta pV_i} Z_{NVT}$	$\frac{e^{-\beta(E-PV_i)}}{Z_{NPT}}$
Micro canonical	N, V, E	$\sum_i \delta(E_i - E)$	$\frac{\delta(E_i - E)}{Z_{NVE}}$
Canonical	N, V, T	$\sum_i e^{-\beta E_i(N,V)}$	$\frac{e^{-\beta E_i(N,V)}}{Z_{NVT}}$
Grand canonical	V, T, μ	$\sum_i e^{\beta N\mu} Z_{NVT}$	$\frac{e^{-\beta(E_i-\mu N)}}{Z_{VT\mu}}$

The partition function which is shown in Z in the table 3.1 shows the summation of all possible conditions in each ensemble and P_i refers to the possibility of each ensemble in step i. β is named Boltzman factor, k ($k = 1.381\times10^{-23}$ $J.K^{-1}$) is Boltzman constant and T stands for Temporature. β can be calculated by using equation below:

$$\beta = \frac{1}{kT} \quad \textbf{(3.1)}$$

Each of the statisticle ensembles in table 3.1 is stated by related characteristic thermodynamic function. By using this function for it is possible to calculate Gibbs number to be used in isothermal-isobaric ensemble as by using euqation below:

$$G = -kTlnZ_{NPT} \quad \textbf{(3.2)}$$

microcanonical ensemble calculations require entropy (S) and it be calculated as follow:

$$A = klnZ_{NVT} \quad \textbf{(3.3)}$$

The helmholtz function which is used in simulations based on canonical ensemble is as:

$$A = -TlnZ_{NVT} \quad \textbf{(3.4)}$$

And the desired factor in garand canonicle ensembl is pressure (P) and we can can calculate it by using following equation:

$$PV = -kTlnZ_{\mu VT} \quad \textbf{(3.5)}$$

In isothermic-isobaric or NPT ensemble at constante pressure and temperatur, then volume and enerjy will be falactuating factors. So the anticipation for a given state will eproportional to :

$$Exp(-\beta E_j - \beta PV_j) \quad \textbf{(3.6)}$$

In which E_j is total energy and V_j total volume of the system. This ensemble can be used for calculating average volume by :

$$<V> = \frac{1}{n} \sum_{j=1}^{n} V_j \quad \textbf{(3.7)}$$

Or can be used for estimating average energy using:

$$<E> = \frac{1}{n} \sum_{j=1}^{n} E_j \quad \textbf{(3.8)}$$

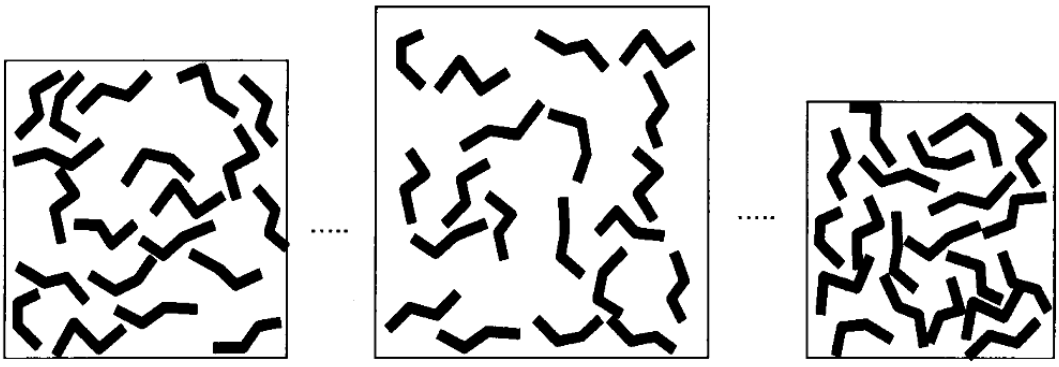

Configuration 1 configuration j configuration n

(V_1, E_1) (Vj, Ej) (Vn, En)

Figure 3.1: Schematic representation of the NPT ensemble

For micro canonical or ensemble NVE, total volume, number of molecules, and total internal energy is supposed to be constant. In NVE, all the states of the system have

the same anticipation and temperature fluctuate. For each single state temperature can be calculated throw the following equation:

$$T = \frac{2<K>}{kN_f} \quad \textbf{(3.9)}$$

In which K is the kinetic energy of the system and is a function of mass and velocity as follow:

$$k = \sum_{i=1}^{n} \frac{m_i v_i^2}{2} \quad \textbf{(3.10)}$$

Moreover, N_f is the total amount of the degree of the freedom and can be computed by:

$$N_f = 3N\text{-}N_c \quad \textbf{(3.11)}$$

N in this equation is the total number of all atoms N_c is global amount of independent constraints. Bond lengths and angles are good examples for these constraints.

The canonical or NVT ensemble is used for a system with constant volume and temperature and imposed number of particles. The variable factors for this ensemble are energy and pressure which differ from a state to another. We can calculate pressure by using equation below:

$$P_j = \frac{e^{-\beta E_j}}{Q_{NVT}} \quad \textbf{(3.12)}$$

Where:

$$\mathbf{QNVT} = \frac{1}{N!} \sum_{r_i} \sum_{p_i} e^{-\beta E(r_i, p_i)} \quad \textbf{(3.13)}$$

Alternatively:

$$Q_{NVT} = \frac{1}{h^{3N} N!} \int_{r_i} \int_{p_i} e^{-\beta E(r_i, p_i)} dr_i dp_i \quad \textbf{(3.14)}$$

And the average energy will be equal to:

$$<E> = \frac{1}{n}\sum_{i=1}^{n} E_i \qquad \textbf{(3.15)}$$

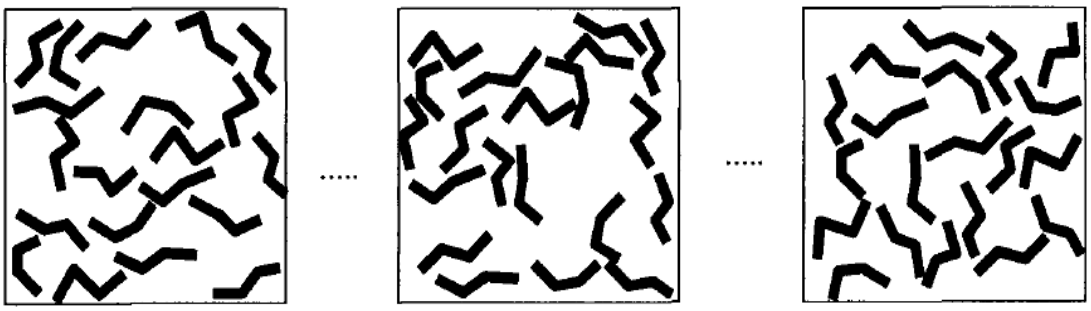

Configuration 1 (Total energy E1) ..... **configuration j** (Total energy Ej) ..... **configuration n** (Total energyEn)

Figure 3.2: Schematic representation of the NVT ensemble.

If we desire to simulate a system in order to examine adsorption isotherms, what I have done in my thesis, we have to use grand canonical or μVT ensemble. Because for simulating either pure compounds or multicomponent systems we need to impose temperature and partial pressure to be able to simulate each given point. In this system mole number of the desired particles will change. The average number of molecules (<N>) will be:

$$<N> = \frac{\sum_{N=0}^{\infty} e^{(\beta N \mu^* - lnN!)} \int_{\Omega} N e^{(-\beta E)} d\alpha^N}{Z_{\mu YT}} \qquad \textbf{(3.16)}$$

Where

$$\mu^* = \mu^{excess} + kTln<N> \qquad \textbf{(3.17)}$$

and

$$\alpha = r_i / L \text{ (length of flactuating cube)} \qquad \textbf{(3.18)}$$

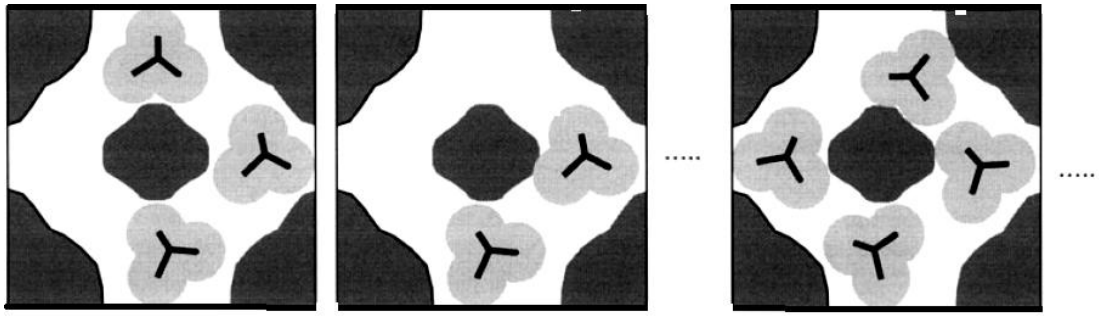

Configuration 1 Configuration 2 Configuration i

Figure 3.3: Schematic representation of the μVT ensemble

3.4 Molecular forcefield

There are some methods to calculate the total energy of the system which is going to be simulated like Quantum Mechanical (QM) method or Molecular Force-field method. In MC simulation we do not need to calculate the kinetic energy because in this method we analyze the equilibrium states which is not time depended. So accepting the potential energy as the total energy of the system would be so logical. As it is too expensive to use QM method for only such a system, the best choice for us would be molecular force-field method. We can use force-field based calculation method for:

1- Calculating normal modes of vibration and vibration frequencies.
2- Analyzing intra-molecular and inter-molecular interactions in terms of residue–residue or molecule molecule interactions, energy per residue, or interactions within a radius.
3- Calculating diffusion coefficients of small molecules in a polymer matrix.
4- Calculating thermal expansion coefficients of amorphous polymers.
5- Calculating the radial distribution of liquids and amorphous polymers.

The total potential energy of any molecular system is the sum of intra-molecular energy and inter-molecular energy. So the total energy would be equal to the sum of stretch energy (U_{str}), bending energy (U_{bend}), torsion energy (U_{tors}), cross energy (U_{cross}) as components of inter-molecular energy and van der Waals energy (U_{vdW}), electrostatic energy (U_{el}), and polarization energy (U_{pol}) as intra-molecular energy.

$$U(r^N) = U_{str} + U_{bend} + U_{tors} + U_{cross} + U_{vdW} + U_{el} + U_{pol} \quad \textbf{(3.19)}$$

U_{str} is the energy related to the variation of the bond length between two atmos. There are two different methods to calculate this energy. One of them is harmonic potential energy as:

$$U_{str} = \frac{1}{2} k_{str} (r-r_0)^2 \quad \textbf{(3.20)}$$

And the other one is Morse method as:

$$U_{str} = D (1-e^{\alpha r})^2 \quad \textbf{(3.21)}$$

As the Morse method is very expensive from the aspect of calculation, using the harmonic method is mostly preferred.

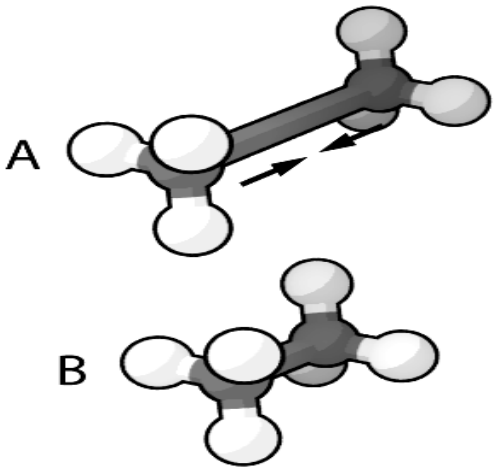

Figure 3.3: Schematic representation of bond strech

Again, for U_{bend} that represents the expanding energy about equilibrium position we may prefer harmonic equation as:

$$U_{bend} = \frac{1}{2} k_{bend} B_{oltzmann} (\Theta - \Theta_0)^2 \quad \textbf{(3.22)}$$

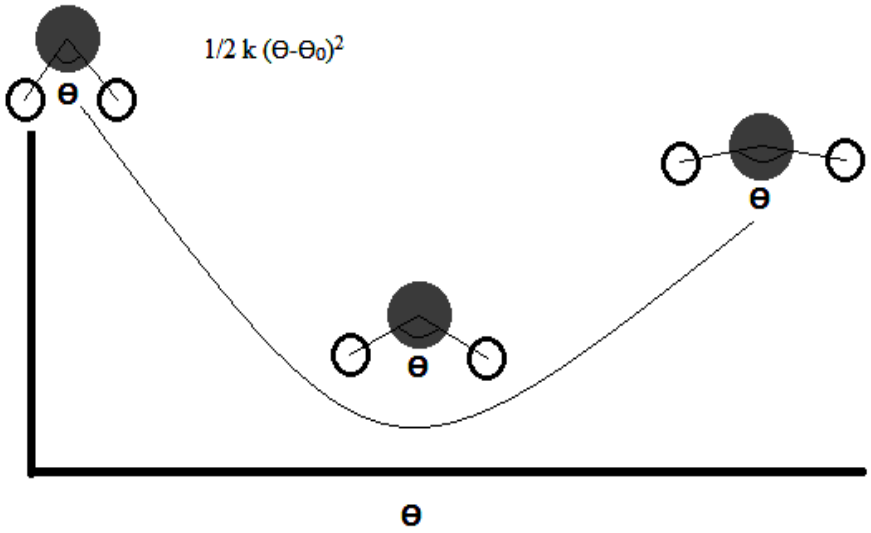

Figure 3.4: Schematic representation of bend stretch

U_{tor} is a factor we face with in the case of three or four atom interaction. It directly depends on the dihedral angle (ϕ). A simple way to show how this factor is calculated can be represented as below:

$$U_{tor} = \sum_n U_n \cos(n\phi) \qquad \textbf{(3.23)}$$

In simulations, it is possible to face with more minimal torsion energy for structure and it is important to choose the correct one. As an example for linear alkanes computations will result to three torsion angles as 180°, and ±60° and it would be the best to choose the 180° one.

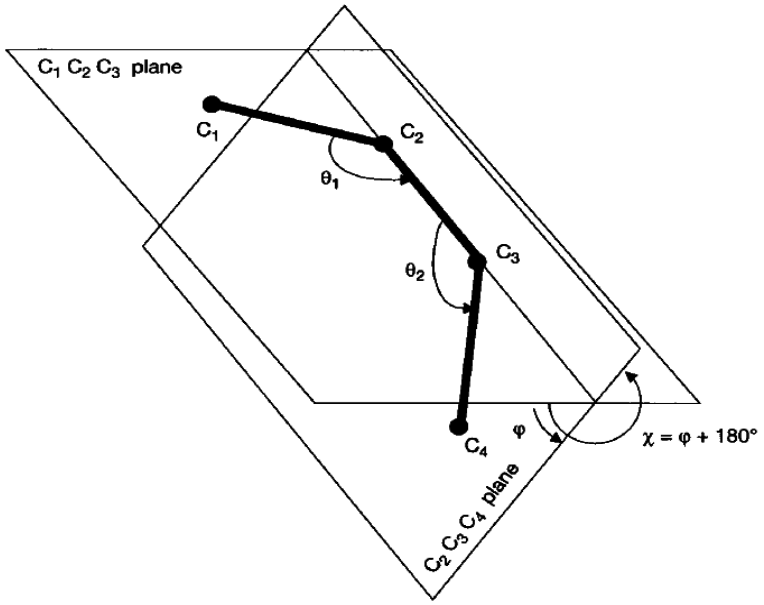

Figure 3.5: Schematic representation for torsion bend

The electrostatic potential energy can be calculated by considering charge distribution in different points of the atoms. In such situation, it is possible to face with different cases in the format of dipole or higher order moments. The equation below lets us to compute this potential for our structures:

$$U_{el} = \sum_{\substack{i,j \\ i<j}} \frac{1}{4\pi\varepsilon_0} \frac{q_i q_j}{r_{ij}} \qquad \textbf{(3.33)}$$

U_{pol} is the factor in which charge redistribution is considered according to the influence of the surrounding molecules. For this aim simulator does iterative computations as:

a- evaluating electric field acting on each charge due to other charges

b- adjusting charges according to polarizability and electric field

c- re-computing electric field and repeat to convergence

Generally, we use formula below to calculate U_{pol}:

$$U_{pol} = -\frac{1}{2} \alpha_p E^2 \qquad \textbf{(3.34)}$$

In fact, we may be able to suppose U_{vdW} is consisted from dispersion energy and repulsive energy. The most comprehensive expression containing dispersion energy and repulsive energy is Lenard-Jones potential. There are different formulas according to the variation of power of the energy also variation of separation distance power. The formula that we used for this aim is:

$$U_{LJ} = U_{rep} + U_{disp} = 4\varepsilon \left(\left(\frac{\sigma}{r}\right)^{12} - \left(\frac{\sigma}{r}\right)^{6}\right) \qquad \textbf{(3.35)}$$

In the cases that our system contains of different atom types, it will be like:

$$U_{LJ} = \sum_{\substack{i,j \\ i<j}} 4\varepsilon \left(\left(\frac{\sigma_{ij}}{r_{ij}}\right)\left(\frac{\sigma_{ij}}{r_{ij}}\right)\right) \qquad \textbf{(3.36)}$$

In which all pairs of atoms of different molecules are included.

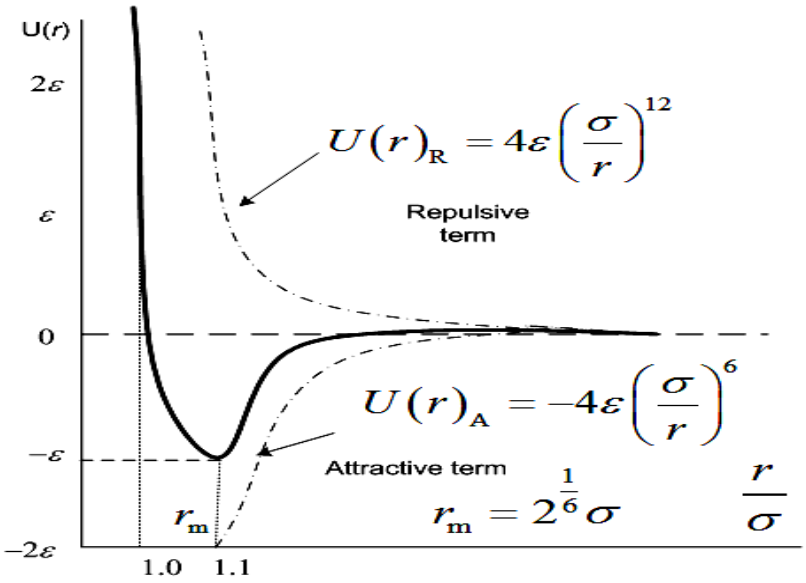

Figure 3.6: Schematic representation Lenard-Jones energy

Parameters σ_{ij} and ε_{ij} are related to the pair of atoms. It is necessary to use combining rules in order to calculate them from the same parameters related to pure components. The most widespread expression used for combining is Lorentz-Berthelot method as:

$$\sigma_{ij} = \frac{\sigma_i + \sigma_j}{2} \qquad \textbf{(3.37)}$$

and

$$\varepsilon_{ij} = \sqrt{\varepsilon_i \varepsilon_j} \qquad \textbf{(3.38)}$$

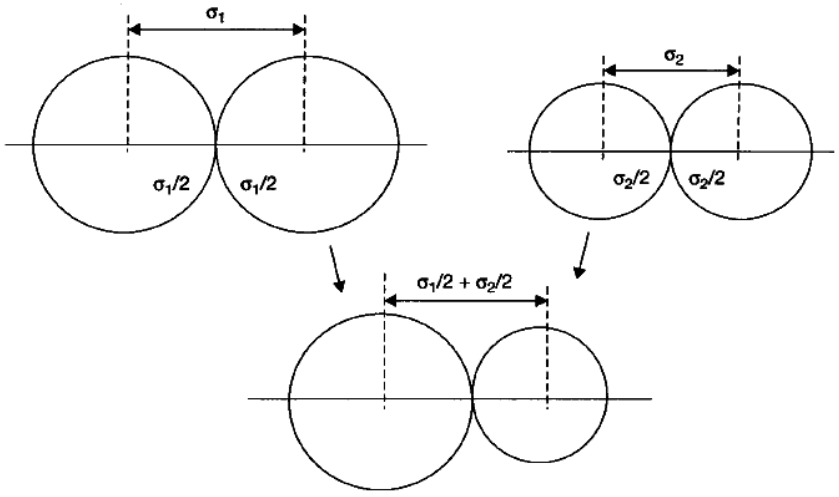

Figure 3.7*:* Figure 3.8 Schematic representation for σ

3.5 Periodic boundary

Besides the short-range inter molecular potentials we have to be aware of the long-range interactions. One of the most popular techniques for handling long-range interactions is Ewald sum method. If we supposed to have a central simulation box of length L there will be six periodic images of it with just the same properties in three dimensions surrounding. Therefore, there will be N atoms in each of these boxes and the electrostatic interaction between them will be equal to:

$$E = \frac{1}{2} \sum_{box=1}^{6} \sum_{i=1}^{N} \sum_{j=1}^{N} \frac{q_i q_j}{r_{ij} r_{box}} \quad \textbf{(3.39)}$$

Now it is possible to assume further five images for each of the added boxes and this action can be continued until any step we desire according to the accuracy that we expect from our simulation.

$$E = \frac{1}{2} \sum_{n=0}^{\infty} \sum_{i=1}^{N} \sum_{j=1}^{N} \frac{q_i q_j}{r_{ij}+n} \quad \textbf{(3.40)}$$

The only problem we may face with in simulations, related to Ewald sum, is the converging of the system that usually is very slow and take lots of time. However, it is possible to solve this method by different mathematical methods.

3.6 Periodic boundary conditions and cut-off distance

As a standard feature of a bulk molecular simulation periodic boundary conditions is used for simulating a model by getting the advantages of smaller repeating units. Actually, we can say that periodic boundary helps us to avoid inaccuracies caused by surface effect and cut-off distance lets us to reduce the computing time but ignoring some not so much important calculations. By assuming periodic boundary conditions when a particle leaves the simulation box from any of the boundaries, another particle comes inside the box but exactly in the direction of leaving particle. Therefore, it helps us to have the same total number of the particles and same structure inside the box during the simulation without limiting the system that sure can affect it negatively.

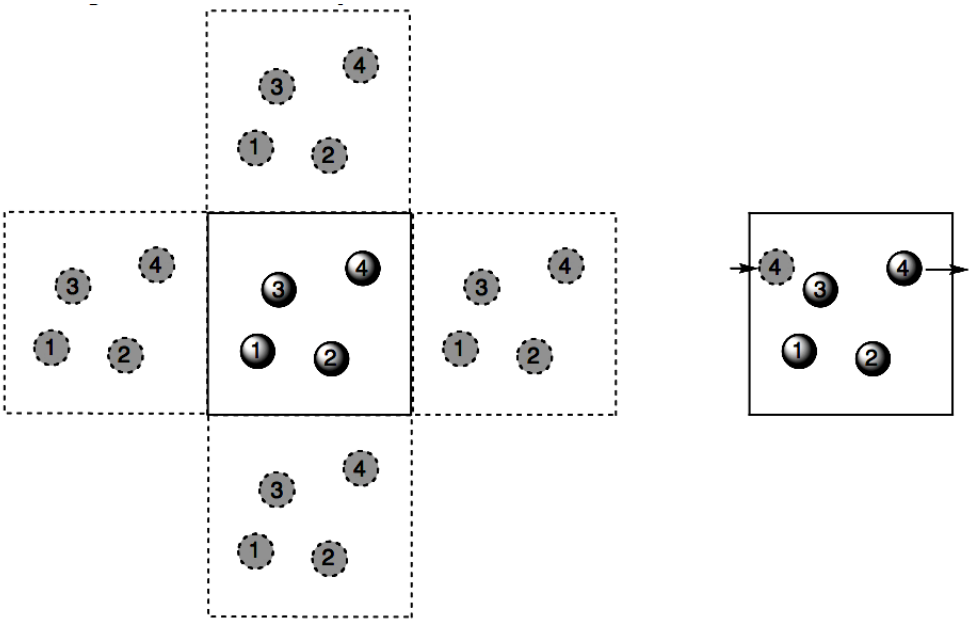

Figure 3.8: Schematic representation boundary conditions

In order to decrease the computation time for the simulations while considering the inter-molecular interactions, it would be logical to use cut-off distance. Cut-off distance will help us to ignore the effect of the potential energy of the molecules that are apart from the central molecule. This is a common procedure and the error caused by this method can be neglected most of the time.

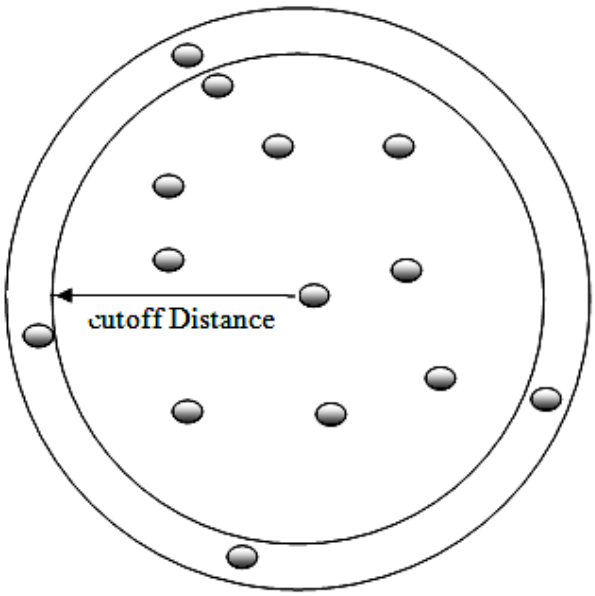

Figure 3.9: Schematic representation cut-off distance

3.7 Monte Carlo

Monte Carlo Molecular modeling is the application of Monte Carlo simulation method to a system of molecules. In addition, this it is possible to apply such a system to molecular dynamics too, but as the equilibrium statistical mechanics of the system is more important than the reproduction of the dynamic of the system for us, using MC is always preferred. MC method uses Boltzmann probabilities in order to generate different states for the system followed by Metropolis Monte Carlo simulation system. In order to determine each new state from the previous one it employs Markov chain and according to the nature of this method, each new step is accepted as random. Each trial is usually counted as a move and there are different categories for these moves. In addition, the general concept for MC simulating is the same for all molecular systems, but according to the ensemble, we choose for the system it may change a bit in calculations. As it is mentioned before, there are different ensembles such as NVT ensemble, NVE ensemble, etc. and for the adsorption systems, we need to use μVT ensemble. So it would be logical to use the reintegrated form of Monte Carlo for Grand-Canonical ensemble, it is called Grand Canonical Monte Carlo or GCMC. In adsorption experimental system, the adsorbed gas is supposed to be in equilibrium with reservoir gas. Chemical potential and temperature for the gas inside and outside is the same.

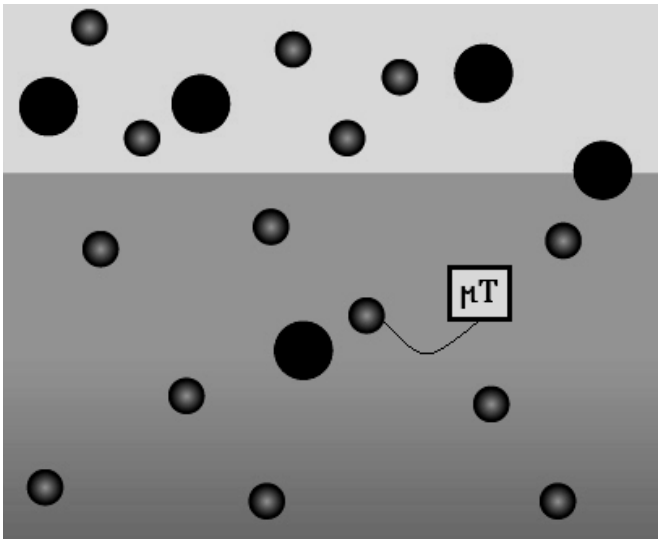

Figure 3.10: Impose of constant chemical potential and tempotature for asdorbent and ressvior gas

So knowing the temperature and chemical potential of the reservoir gas will help us to know the equilibrium inside the adsorbent then we can estimate the number of molecules fluctuating by fugacity (or pressure) in the meanwhile of simulation. Equation below introduces Metropolis sampling scheme as a computational method in order to predict the average of a function such as A (r^N) which is depended on the molecular coordinates in a so-called N-body system:

$$< A > = \frac{\int dr^N \exp(-\beta u(r^N)) A(r^N)}{\int dr^N \exp(-\beta u(r^N))} \quad \textbf{(3.41)}$$

In an N-body system, it is possible to state differences of the energies between two possible states of the system and it can be exploited in MC method. Equation below gives the partition function for a system combined of N interacting particles with volume of V that in V_0-V volume of the system there are M-N molecules of ideal gas:

$$Q(N,M,V,V_0,T) = \frac{V^N (V_0 - V)^{M-N}}{\Lambda^{3M} N!(M-N)!} \int ds^{M-N} \int ds^N \exp(-\beta u(s^N)) \quad \textbf{(3.42)}$$

This formula is for a volume exchange between two systems and we can see what happens if they can also be able to exchange particles too.

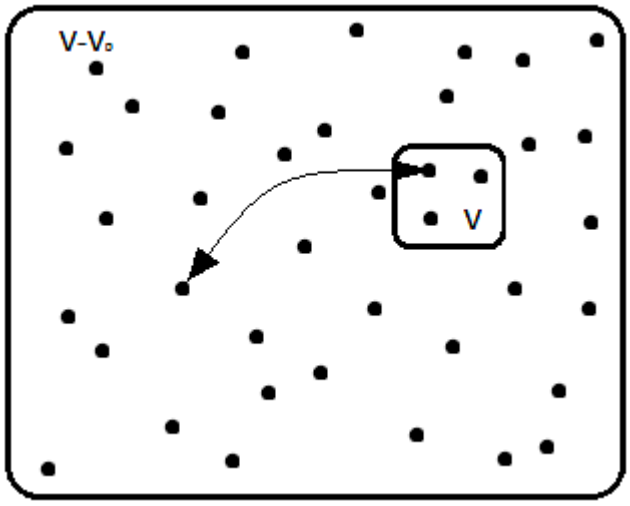

Figure 3.11: N-particle(V volume) system and ideal gas (M-N particles and V_0-V volume) exchanging particles

When a molecule, let's say molecular i, transfers from coordinate s_i in volume V_0-V to the same coordinate in volume V, the potential energy $u(s^N)$ changes to $u(s^{N+1})$. In such a situation, the total partition function will be as following for all possible distributions of the M particles in both sub-volumes:

$$\mathrm{Q(M,V,V0,T)} = \sum_{N=0}^{M} \cdot \frac{V^N (V_0 - V)^{M-N}}{\Lambda^{3M} N!(M-N)!} \int ds^{M-N} \int ds^N \exp\left(-\beta u(s^N)\right) \quad \textbf{(3.43)}$$

Now writing the equation of probability density will be local in order to find a system of M-N particles and s^{M-N} reduced coordinates with volume of V′ (V_0-V) and N particles and s^N reduced coordinates with volume of V:

$$\mathrm{N}(s^M;N) = \frac{V^N V'^{M-N}}{Q(M,V,V',T)\Lambda^{3M} N!(M-N)!} \exp\left(-\beta u(s^N)\right) \quad \textbf{(3.44)}$$

Construction of Markov chain implies that a priori probability to move a particle from V′ to V should be equal to the a priori probability to move same particle from V to V′. So considering equation 3.44 probability of acceptance of a trial move of any particle in or out of volume V can be defined as follow:

$$\alpha(N \to N+1) = \frac{V(M-N)}{V'(N+1)} \exp\left(-\beta\left(u(s^{N+1}) - u(S^N)\right)\right) \quad \textbf{(3.45)}$$

$$\alpha(N+1 \to N) = \frac{V(N+1)}{V'(M-N)} \exp\left(-\beta\left(u(s^N) - u(S^{N+1})\right)\right) \quad \textbf{(3.46)}$$

By considering the ideal gas, system is much larger than the interaction system (M→∞, V′→∞(M/V′)→ρ) and also considering the following relation:

$$\mu = k_B T \ln \Lambda^3 \rho \quad \textbf{(3.47)}$$

So in condition of (M/N)→∞, the equation of partition function will be modified as:

$$Q(\mu, V, T) = \sum_{N=0}^{\infty} \frac{\exp(\beta\mu N) V^N}{\Lambda^{3N} N!} \int ds^N \exp(-\beta u(s^N)) \quad \textbf{(3.48)}$$

And the reciprocal equation for probability density will be like:

$$\mathrm{N}_{\mu VT}(s^N; N) \propto \frac{\exp(\beta\mu N) V^N}{\Lambda^{3N} N!} \int ds^N \exp\left(-\beta u(s^N)\right) \quad \textbf{(3.49)}$$

Last two equations (3.48 and 3.49) are known as the final equations of the GCMC simulation method.

There are different distribution samples for MC simulation method for different situations (ensembles) such as Translation, Rotation, Volume changes, Flip Moves, Reptation, Pivot, Displacement, and Insertion and Removal of particles. In grand-canonical simulation, adequate trial moves are:

1- Displacement of the particles. Simulator chooses a random particle and assigns it a displacement then checks the acceptance of this change with probability below:

$$acc(s \to s') = \min(1, \exp(-\beta(u(S'^N) - u(s^N)))) \quad \textbf{(3.50)}$$

2- Insertion and removal of particles. A particle is added to or removed from a randomly selected location. There are two different probability equations for it, one for particle accepting and the other for particle removing in order as following:

$$acc(N \to N+1) = \min\left(1, \frac{V}{\Lambda^3(N+1)} exp\left(\beta\left(\mu - u(N+1) + u(N)\right)\right)\right) \quad \textbf{(3.51)}$$

$$acc(N \to N-1) = \min(1, \frac{\Lambda^3 N}{V} \exp(-\beta(\mu + u(N-1) - u(N)))) \quad \textbf{(3.52)}$$

It was all basic information about the molecular simulation especially for adsorption simulation.

4. SIMULATION METHOD

Molecular simulation methods are playing an important role in the study and application of metal organic framework in different areas. Nowadays widespread use of simulation studies before applying any lab-scale or pilot-scale is very common and very efficient for investment reduction in MOF applying systems. Adsorption experiments are very useful in getting more detailed information about the macroscopic properties of the desired process but such a molecular simulation techniques like MC will help to realize details about microscopic behaviors that are missing parts of the system.

There are different methods of molecular simulation applications. In this study, Accelrys Materials Studio 6 is used for simulating the adsorption applications of sulfur compound containing LPG in different MOFs. Accelrys materials studio 6 provides basis of sampling and molecular simulation for studying chemicals and material including crystalline materials, polymerization and polymer properties, and structure activity relations.

In addition, there are various force-field types as the database of Acclerys Materials Studio, in this study in order to get more accurate results special force-field document is prepared for all materials included in the study.

4.1 Potential Energy and Structural Methods

LJ 12-6 model was used to represent the inter-molecular dispersion-repulsion interactions between atom couples in the structures, using combining rules of Lorentz-Berthelot. In addition to the Lennard-Jones potential Coulombic interactions were added to the inter-molecular potential too. The intra-molecular interactions were contributed to the calculations by adding bond stretch, angle bend, and torsion parameters related to each of the structures. The distant neighbor energies were

supposed to be calculated by the LJ intermolecular interactions. Charges were taken from papers and are placed for each atom separately in all structures.

In All Atoms (AA) modeling, L-J parameters are described for every single atom of the structure including hydrogen atoms bur this method is an expensive method from the aspect of time. Consequently, United Atom (UA) models in which carbon atoms perform most of the simulations and the hydrogen atoms that are connected to them are supposed as united particles. An alternative for this method is the application of Anisotropic United Atom (AUA) method. In AUA force center of the united atoms are supposed to be in pseudo position located somewhere between the hydrogen and carbon atom. This method yields good results for several hydrocarbons with large range of carbon numbers in different temperatures.

For the adsorbate materials, UA system is applied and over-all charges and L-J parameters for the structures were taken from The Transferable Potentials for Phase Equilibria (TraPPE) system as the united structure system of the carbon and hydrogen containing sites. The Transferable Potentials for Phase Equilibria family of force fields is a collection of functional forms and interaction parameters useful for modeling complex chemical systems with molecular mechanics simulation techniques. TraPPE maintains a high degree of accuracy in the prediction of thermophysical properties when applied to a range of different compounds, different state points, different compositions, and different properties. This makes TraPPE one of the few force fields generally suitable for materials and industrial applications. The standard TraPPE nonbonded potential is calculated for all intermolecular interactions and those intramolecular interactions involving (pseudo)atoms separated by four or more bonds and intramolecular Lennard-Jones and Coulomb interactions are excluded.

In the MC simulations for adsorption studies, μVT ensemble or in the other words Grand canonical Monte Carlo (GCMC) ensemble was taken because of the constant temperature, constant volume, and constant chemical potential of the system. In the equilibrium conditions of the simulated system chemical potential energy of the internal adsorbate material is equal to the chemical potential energy of the external one (Haile 1992, Frenkel and Smit 2001, Sadus 2002, Ungerer, Tavitian et al. 2005).

4.2 Adsorbate Structures and Modeling Parameters

LPG is supposed to be including Propane, n-Butane, and i-Butane as the main components by changing in the percentage of each of these material according to extraction well and refining techniques. For this reason in this study single and competitive adsorption simulations were performed for these materials separately and also for Thiophene as the sulfur compound in which is going to be removed from the material mixture. Thiophene is a pollutant available inside the PLG mixture in the scale of ppms then in the binary sorption calculations while fugacity factor for the hydrocarbons are kept constant its amount is supposed to be changing from 10e-4 to 0.01 kPa. Lennard Jones parameters are taken from TraPPE as below:

4.2.1 Propane

Propane is a three carbon alkane with the molecular formula C3H8, normally a gas, but compressible to a transportable liquid. There is no torsion variety for this component so only L-J parameters, bond stretch parameters, and angle-bend parameters are needed.

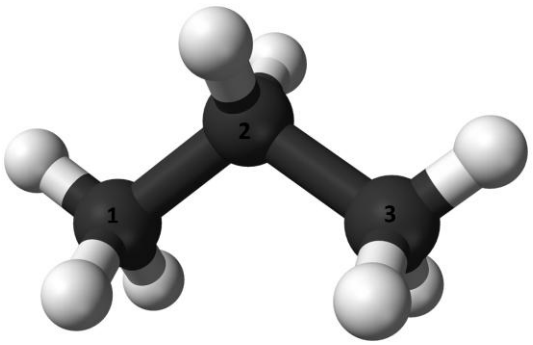

Figure 4.1: Propane structure

Table 4.1: Non-bonded interaction parameters for Propane

Atom (pseudo)	Type	Ɛ/kB [K]	σ [Å]	q[e]
CH3	[CH3]-CHx	98.0	3.750	0
CH2	CHx-[CH2]-CHx	46.0	3.950	0
CH3	[CH3]-CHx	98.0	3.750	0

Bonded interaction parameters for Propane:

Table 4.2: bond length

Stretch	Type	Length [Å]
1-2	CHx-CHy	1.540
2-3	CHx-CHy	1.540

Table 4.3: Angle-bend parameters

Bend	Type	Θ[°]	kΘ/kB [K/rad2]
1-2-3	CHx-(CH2)-CHy	114.0	62500

4.2.2 i-Butane

Isobutane (i-butane), also known as Methylpropane, is a chemical compound with molecular formula C_4H_{10} and is an isomer of butane. It is the simplest alkane with a tertiary carbon. There is no torsion variety for this component so only L-J parameters, bond stretch parameters, and angle-bend parameters are needed.

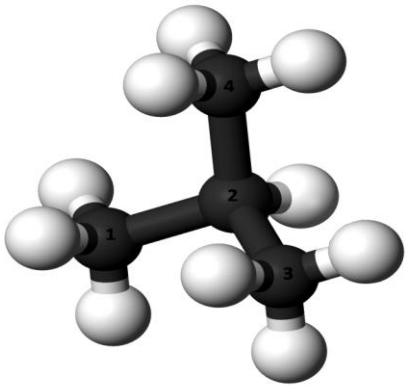

Figure 4.2: i-Butane structure

Table 4.4: Non-bond interaction parameters for i-Butane

Atom(pseudo)	Type	Ɛ/kB [K]	σ [Å]	q[e]
CH3	[CH3]-CHx	98.0	3.750	0
CH	(CHx)2-[CH]-CHx	10.0	4.680	0
CH3	[CH3]-CHx	98.0	3.750	0
CH3	[CH3]-CHx	98.0	3.750	0

Bonded interaction parameters for i-Butane:

Table 4.5: Bond length parameters

Stretch	Type	Length [Å]
1-2	CHx-CHy	1.540
2-3	CHx-CHy	1.540
2-4	CHx-CHy	1.540

Table 4.6: Angle bend parameters

Bend	Type	Θ[°]	kΘ/kB [K/rad2]
1-2-3	CHx-(CH)-CHy	112.0	62500
1-2-4	CHx-(CH)-CHy	112.0	62500
3-2-4	CHx-(CH)-CHy	112.0	62500

4.2.3 n-Butane

Butane is an organic compound with the formula C_4H_{10} that is an alkane with four carbon atoms. Butane is a gas at room temperature and atmospheric pressure. In this material besides L-J, bond length, and angle-bend parameters, torsion parameters should be included in the simulations.

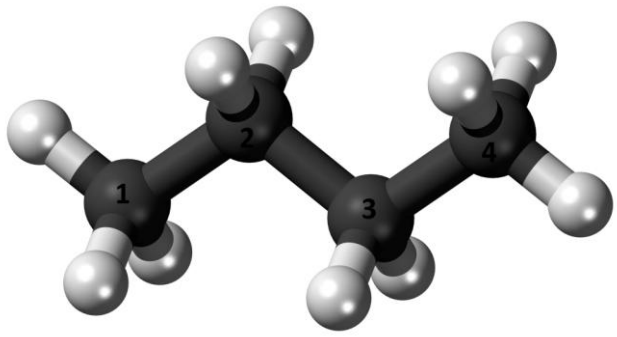

Figure 4.3: n-Butane structure

Table 4.7: Non-bonded interaction parameters for n-Butane

Atom(pseudo)	Type	Ɛ/kB [K]	σ [Å]	q[e]
CH3	[CH3]-CHx	98.0	3.750	0
CH2	CHx-[CH2]-CHx	46.0	3.950	0
CH2	CHx-[CH2]-CHx	46.0	3.950	0
CH3	[CH3]-CHx	98.0	3.750	0

Bonded interaction parameters for n-Butane:

Table 4.8: Bond length parameters

Stretch	Type	Length [Å]
1-2	CHx-CHy	1.540
2-3	CHx-CHy	1.540
3-4	CHx-CHy	1.540

Table 4.9: Angle-bend parameters

Bend	Type	Θ[°]	kΘ/kB [K/rad2]
1-2-3	CHx-(CH2)-CHy	114.0	62500
2-3-4	CHx-(CH2)-CHy	114.0	62500

Table 4.10: Torsion parameters

Torsion	Type	C0/kB [K]	C1/kB [K]	C2/kB [K]	C3/kB [K]
1-2-3-4	CHx-(CH2)-(CH2)-CHy	0.00	355.03	-68.19	791.32

4.2.4 Thiophene

Thiophene, also commonly called thiofuran, is a heterocyclic compound with the formula C4H4S. Consisting of a flat five-membered ring, it is aromatic as indicated by its extensive substitution reactions. It is accepted that this aromatic ring has no torsion variety the only L-J, bond length and angle-bend parameters are enough for simulating it.

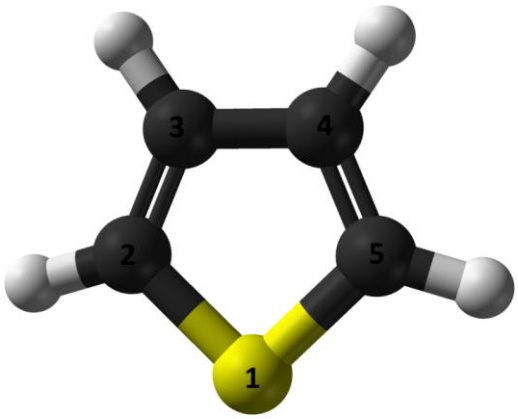

Figure 4.4: Thiophene structure

Table 4.11: Non-bond interaction parameters for Thiophene

Atom(pseudo)	Type	Ɛ/kB [K]	σ [Å]	q[e]
S	CH+[S]+CH	180.0	3.600	0
CH	CH+[CH]+S	50.0	3.695	0
CH	CH+[CH]+CH	50.0	3.695	0
CH	CH+[CH]+CH	50.0	3.695	0
CH	CH+[CH]+S	50.0	3.695	0

Bonded interaction parameters for Thiophene

Table 4.12: Bond length parameters

Stretch	Type	Length [Å]
1-2	CH+S	1.710
2-3	CHx+CHy	1.400
3-4	CHx+CHy	1.400
4-5	CHx+CHy	1.400
5-1	CH+S	1.710

Table 4.13: Angle-bend parameters

Bend	Type	Θ[°]	kΘ/kB [K/rad2]
1-2-3	CH+(CH)+S	11.1.5	rigid
2-3-4	CH+(CH)+CH[+S]	112.4	rigid
3-4-5	CH+(CH)+CH[+S]	112.4	rigid
4-5-1	CH+(CH)+S	111.5	rigid
5-1-2	CH+(S)+CH	92.2	rigid

Before applying these molecules to the simulation process, geometry optimization for all the adsorbate atoms were performed and all the results were compared with the paper articles.

4.3 Adsorbent (MOF) Structures and Modeling Parameters

MOFs are known as cage like structures mainly made from two different parts. One is the metal nod and the other one is the organic part. As there is wide variety of each of these parts, it is possible to build uncountable different MOFs using different metal nods and different organic parts or even using a mixture of each of them in a

single MOF. Different MOFs provides different selectivity and also different permeability demeanor for different materials. Then choosing a proper MOF for a considered system is very critical and demands deep pre-study before any action. In this study, five different MOFs are chosen to be studied to see the performance of each in sulfur removal from LPG. In the incoming parts, simulation parameters and some extra information about each of them are provided. All atomic structures are taken from experimental crystallographic data.

4.3.1 Basosiv M050

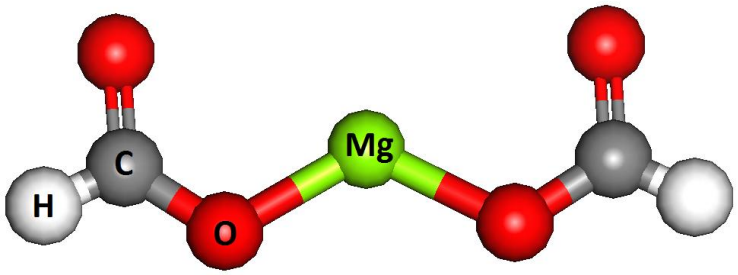

Figure 4.5: Basosiv M050 structure

Table 4.14: Vander Waals parameters for Basosiv M050 (Fischer, Hoffmann et al. 2012)

Atom type	σ [Å]	Ɛ [kcal/mol]	q [e]
H	2.5710	0.044	0.043
C	3.1437	0.1050	0.671
O	3.1180	0.0599	-0.766
Mg	2.6913	0.1110	1.636

Basosiv M050 has a structure of 34.07 Å×29.65 Å× 29.16 Å dimension lengths.

4.3.2 C300

C300 or $wCu_3(BTC)_2$ or copper(II)-benzene-1,3,5-tricarboxylate is a highly porous metal organic framework with copper(II) metal nodes and trimesate ions. Has a light

blue color while containing solvent inside but upon activation becomes darker. Generally, it is believed that this material has 1.5-2 times higher pore volume compared to conventional zeolites.

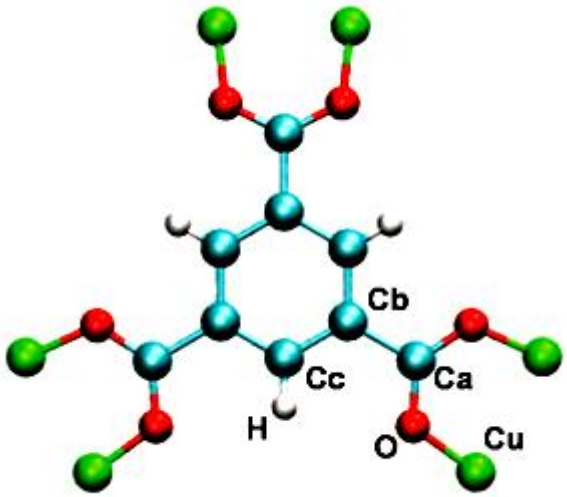

Figure 4.6: C300 structure

Table 4.15: Van der Waals parameters for C300 (Mayo, Olafson et al. 1990)

Atom type	σ [Å]	Ɛ [kcal/mol]	q [e]
H	2.85	7.65	0.15
Ca	3.47	47.86	0.7
Cb	3.47	47.86	0.0
Cc	3.47	47.86	-0.15
O	3.03	48.19	-0.6
Cu	3.114	2.518	1.0

C300 has a cubic structure of 26.29 Å in each dimension.

4.3.3 A100

A100 is used for the name of a large family of MOFs in which the metal node differs from a member to another. They are known as metal-benzenedicarboxylate M (OH)(O2C-C6H4-CO2) in which M stands for the metal like Al, Sc, Cr, Fe, and some other metals. In this study MIL-53,(Al) or A100 is chosen as a member of this

family to be studied. In further studies, other members are considered to be studied and compared with each other and other MOFs.

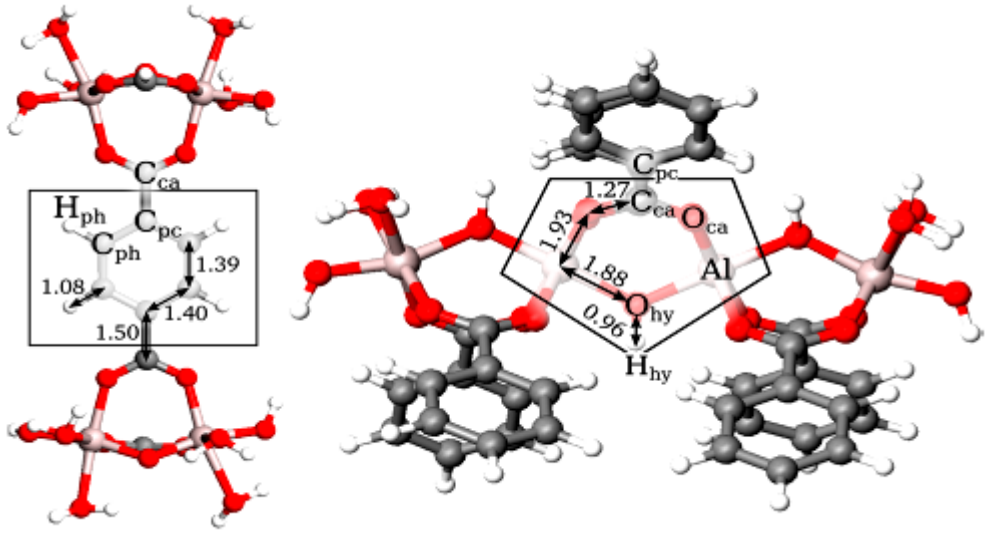

Figure 4.7: A100 structure

Table 4.16: Vand der Waals parameters for A100 (Vanduyfhuys, Verstraelen et al. 2012)

Atom type	σ [Å]	Ɛ [kcal/mol]	q [e]
Al	2.36	0.116	2.078
Cca	1.94	0.056	0.0885
Cpc	1.94	0.056	-0.111
Cph	1.94	0.056	-0.091
Hhy	1.6	0.016	0.515
Hph	1.62	0.020	0.127
Oca	1.82	0.059	-0.74
Ohy	1.82	0.059	-1.322

39.01 Å×30.40 Å× 26.28 Å is the size of the A100 cell in the simulation system.

4.3.4 MOF5

MOF5 is related to a group of metal organic frameworks called IRMOF that contains Zn metal nodes. It is formed from Zn_4O nodes with 1,4- benzodicarboxylic acid among as the linker. As a famous member of this family, this MOF is selected to

be examined in this study. In further studied, other members will be examined and compared to each other and also other MOFs.

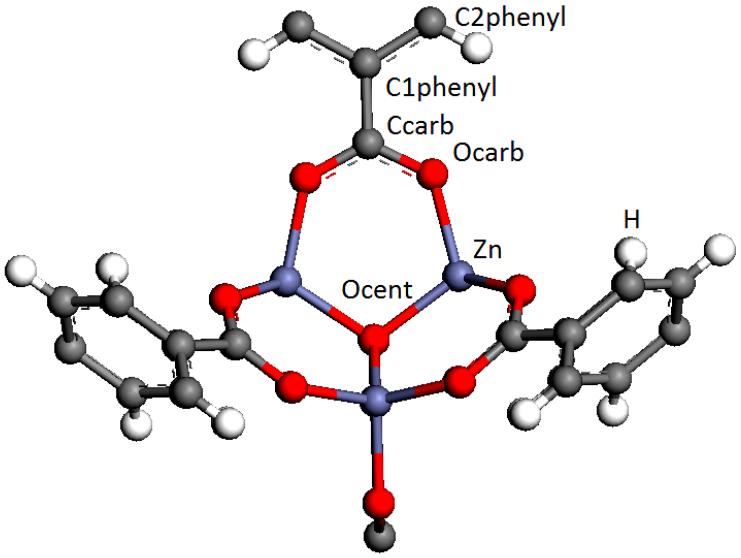

Figure 4.8: MOF5 structure

Table 4.17: Van der Waals parameters for MOF5 (Greathouse and Allendorf 2008)

Atom type	σ [Å]	Ɛ [kcal/mol]	q [e]
Zn	2.311	0.0014	1.2
O_cent	3.088	0.8479	-1.2
O_carb	2.986	0.8479	-0.6
C_carb	3.617	0.1479	0.6
C1_phenyl	3.617	0.1479	-0.1
C2_phenyl	3.617	0.1479	0
H	2.45	0.0380	0.1

MOF5 has a cubic structure and 25.67 Å is the length of cube in each dimension.

4.3.5 Z1200

Zeolitic Imidazolate Frameworks (ZIFs) are ranged in a special class of MOFs are isomorphic with the zeolites from the topological aspects. There are different kinds of ZIFs according to their metal nod (e.g. Fe, Co, Cu, and Zn) which are connected to each other by the imidazole linkers as the organic parts. In this study, Z1200 is taken

to be investigated because studies show that it has high thermal stability and remarkable chemical resistance for different chemicals.

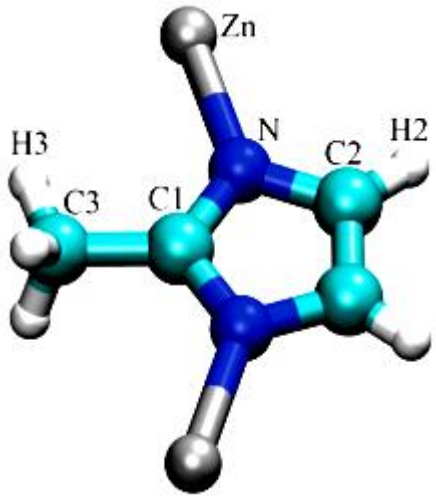

Figure 4.9: Z1200 structure

Table 4.18: Van der Waals parameters for ZIF-8 (Zheng, Sant et al. 2012)

Atom type	σ [Å]	Ɛ [kcal/mol]	q [e]
Zn	2.2	0.0125	0.7362
N	3.648	0.1700	-0.3008
C1	3.8164	0.0860	0.4339
C2	3.8164	0.0860	-0.1924
C3	3.8164	0.1094	-0.6024
H2	2.8185	0.0150	0.1585
H3	2.9745	0.0157	0.1572

Z1200 has the cell dimensions of 16.9901 Å×16.9901 Å× 16.9901 Å as the original size taken from crystallographic databases. In order to be able to choose appropriate cut-off distance as an important item of the simulations enlarging of the MOF structure becomes necessary. Then dimensions changed to 33.9801 Å×33.9801 Å× 33.9801 Å. This process was repeated for all the other MOFs except Cu-BTC because of the large enough dimensions of its cell.

Some simulations were performed in order to find the optimum step for equilibration and production steps for all the MOFs. For all the MOFs except A100, 10^6 for equilibration steps and 10^7 for production steps were seemed to be acceptable but for A100 it was 1.5×10^6 for equilibration steps and 1.5×10^7 for production. United atom techniques were taken for simulations for the adsorbate material and Ewald

summation technique was selected for the electrostatic calculations. Cut-off distance for Van der Waals calculations were in the range or 12Å to 15Å according to the lattice parameters of the MOFs. All simulations were performed in 273K, 283K, 293K, and 303K for all MOFs and every adsorbate inside the LPG separately and also for binary system of thiophene and each of the hydrocarbons in a competitive adsorption conditions.

4.4 Force Field Verification

In order to be sure about the selected force field parameters, some articles in which the same MOFs were experimentally tested for the material similar to adsorbates aimed in this project were selected. Preliminary simulations were done in the same situations as reported in the mentioned articles. Simulation results were compared with those reported in the articles as below.

In figure 4.10 Methane adsorption was tested on C300 at 300 K. The data presented by black triangles are resulted by experimental analysis and the red points are the results of simulations done in this work by using the selected force field parameters (the red line is drawn to guide eyes).

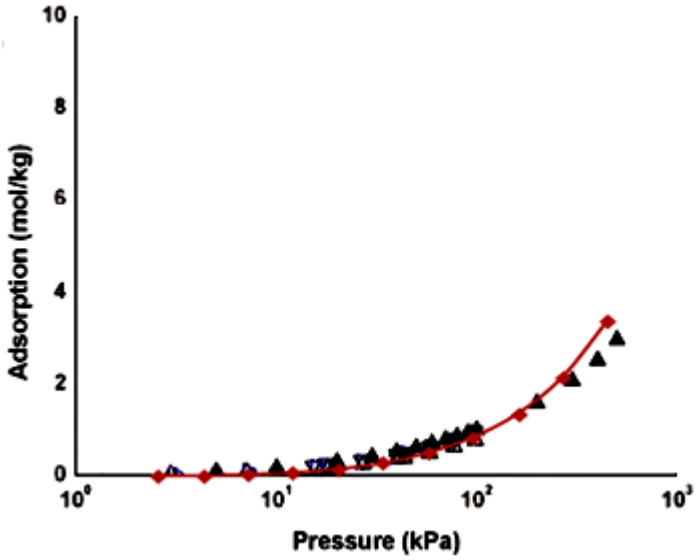

Figure 4.10: C300 & Methane adsorption comparsion in 300K

The comparison in the previous figure shows that force field parameters selected for even C300 or hydrocarbons (Methane in here and Propane and Butane) are suitable to be used in the rest of the simulations. So in the next step by the fixed force field parameters for the hydrocarbon another simulation was tested for MOF5 to fix force field parameters for this MOF.

In the figure 4.11 red points show the experimental Methane adsorption on the MOF5 at 298 K. Blue points are representing the simulation results and a very nice matching is in the result.

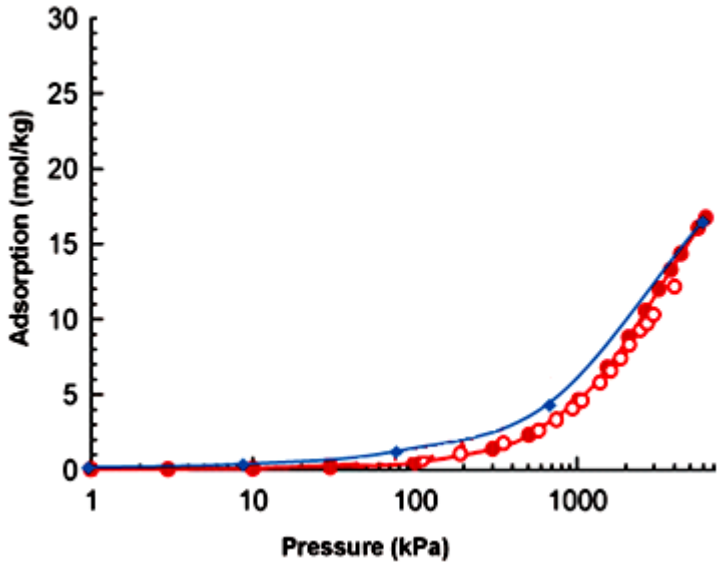

Figure 4.11: MOF5 & Methane adsorption comparsion at 298 K

Until now force field parameters for MOF5 and C300 and also for hydrocarbons are fixed. Now it is time to verify the parameters selected for the Thiophene. In the figure below different adsorption results are seen for Thiophene and MOF5, and the orange data set shows the adsorption results for these materials at 300 K by the selected force field parameters.

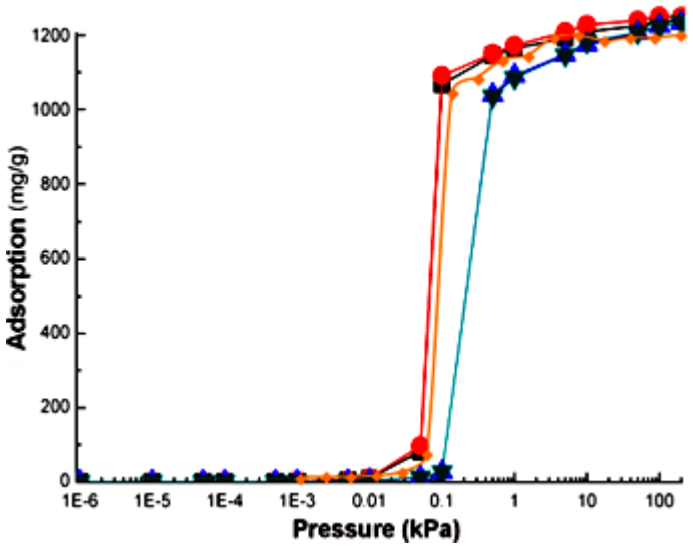

Figure 4.12: MOF5 & Thiophene adsorption comparsion at 300 K

Therefore, adsorption results show that it would be logical to use the force field parameters selected for Thiophene for rest of the simulations.

Testing selected force field parameters for Propane as one of the hydrocarbons by using the force field parameters taken from Methane tests would be logical here. Figure below shows this comparison with an experimental test at 300 K.

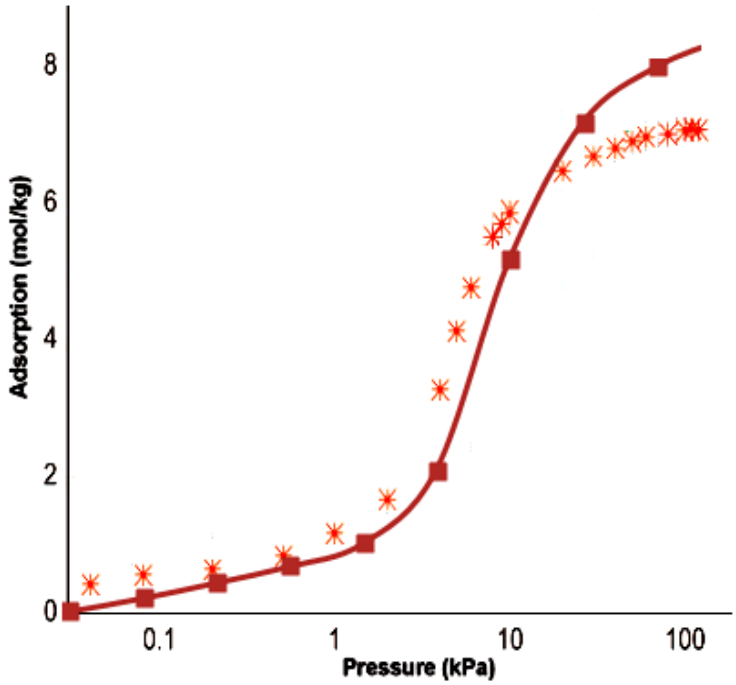

Figure 4.13: C300 & Propane adsorption comparsion at 300 K

Star-like points show the experimental results and the square data set shows the simulation results. Acceptable match of the results shows that fixing parameters for the all materials is going well upto here.

The next step is related to the force field parameter fixing for Z1200.

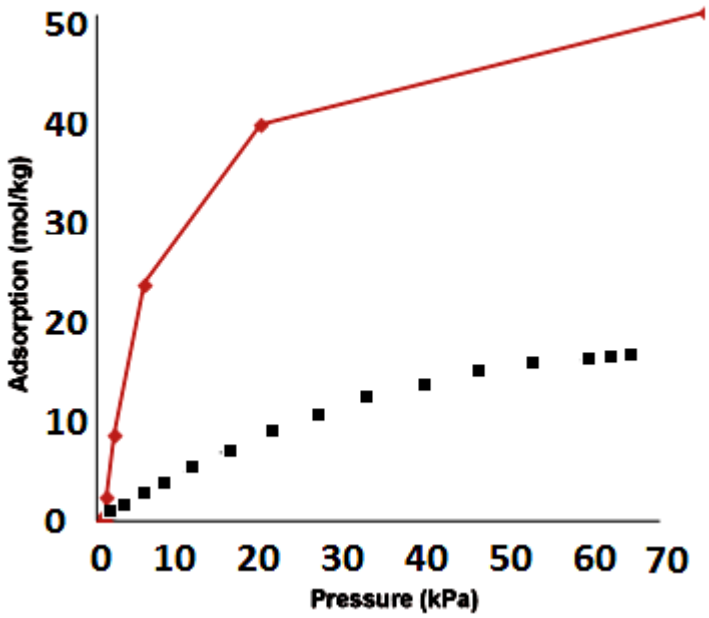

Figure4.14: Z1200 & Methane adsorption comparsion at 300 K

As it can be realized from the figures 4.14, the simulation results for Z1200 and Methane are not matching at 300 K. The best solution for this problem is to use Force Field Refitting method to find the suitable parameters for Z1200. In the next section, we will see how this procedure can be done.

For the other two MOFs, A100 and M050, no suitable experimental tests have been done till now. So by using the experiences gained from other materials, suitable force field parameters are predicted for these MOFs.

4.4.1 Z1200 force field refitting

Force field refitting can be done by changing σ and ε little by little in a logical order. In this work, σ is changing by a 0.02 ratio reduction and ε by 0.1. It is almost a try and error task and all refitted force field parameters are available in appendix A. Some steps of this action is as below:

Table 4.19 – 4.26: Some of the force field parameters applied for Z1200

Type	R0 (σ)	D0 (Ɛ)	e
Zn51	2,2	0,01125	0,7326
N51	3,648	0,153	-0,3008
C151	3,8164	0,0774	0,4339
C251	3,8164	0,0774	-0,1924
C351	3,8164	0,09846	-0,6024
H251	2,8185	0,0135	0,1585
H351	2,9745	0,01413	0,1572

Type	R0 (σ)	D0 (Ɛ)	e
Zn52	2,156	0,01125	0,7326
N52	3,57504	0,153	-0,3008
C152	3,740072	0,0774	0,4339
C252	3,740072	0,0774	-0,1924
C352	3,740072	0,09846	-0,6024
H252	2,76213	0,0135	0,1585
H352	2,91501	0,01413	0,1572

Type	R0 (σ)	D0 (Ɛ)	e
Zn61	2,2	0,01	0,7326
N61	3,648	0,136	-0,3008
C161	3,8164	0,0688	0,4339
C261	3,8164	0,0688	-0,1924
C361	3,8164	0,08752	-0,6024
H261	2,8185	0,012	0,1585
H361	2,9745	0,01256	0,1572

Type	R0 (σ)	D0 (Ɛ)	e
Zn62	2,156	0,01	0,7326
N62	3,57504	0,136	-0,3008
C162	3,740072	0,0688	0,4339
C262	3,740072	0,0688	-0,1924
C362	3,740072	0,08752	-0,6024
H262	2,76213	0,012	0,1585
H362	2,91501	0,01256	0,1572

Type	R0 (σ)	D0 (Ɛ)	e
Zn71	2,2	0,00875	0,7326
N71	3,648	0,119	-0,3008
C171	3,8164	0,0602	0,4339
C271	3,8164	0,0602	-0,1924
C371	3,8164	0,07658	-0,6024
H271	2,8185	0,0105	0,1585
H371	2,9745	0,01099	0,1572

Type	R0 (σ)	D0 (Ɛ)	e
Zn72	2,156	0,00875	0,7326
N72	3,57504	0,119	-0,3008
C172	3,740072	0,0602	0,4339
C272	3,740072	0,0602	-0,1924
C372	3,740072	0,07658	-0,6024
H272	2,76213	0,0105	0,1585
H372	2,91501	0,01099	0,1572

Type	R0 (σ)	D0 (Ɛ)	e
Zn81	2,2	0,0075	0,7326
N81	3,648	0,102	-0,3008
C181	3,8164	0,0516	0,4339
C281	3,8164	0,0516	-0,1924
C381	3,8164	0,06564	-0,6024
H281	2,8185	0,009	0,1585
H381	2,9745	0,00942	0,1572

Type	R0 (σ)	D0 (Ɛ)	e
Zn82	2,156	0,0075	0,7326
N82	3,57504	0,102	-0,3008
C182	3,740072	0,0516	0,4339
C282	3,740072	0,0516	-0,1924
C382	3,740072	0,06564	-0,6024
H282	2,76213	0,009	0,1585
H382	2,91501	0,00942	0,1572

Each of the parameter sets below were applied as the force field parameters for the Z1200 and adsorption simulation was performed for Methane and Z1200 at 300K in

results were compared with the experimental data to see how the changes effect the results and also to see if the results are matching or not.

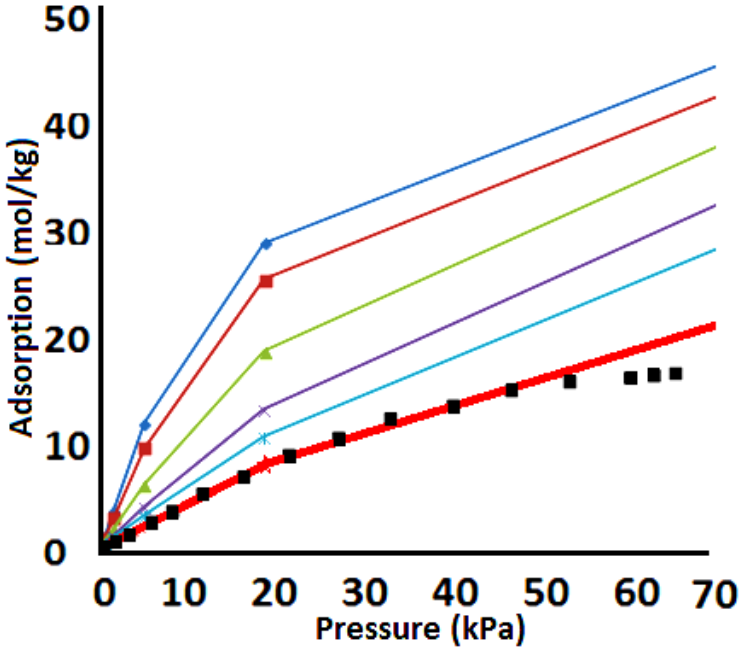

Figure 4.15: Some of the force field refitting results for Z1200

In the figure above there are different simulation results done with different force field parameters produced by mentioned force field refitting method. Data set in bold red color shows acceptable performance when comparing with the experimental data (black points show the experimental results). Figure including all results is available in appendix B.

5. RESULTS AND DISCUSSIONS

First step of simulations are based on the calculation of the adsorption of the components inside the LPG (Propane, i-Butane, n-Butane, and Thiophene). These calculations are done in reder to see if each of the MOFs adsorb these componenets and if yes, how much of these componenets are adsorbed ın any pressure step.

5.1 Adsorption Isotherms

Figure 5.1 shows the the adsorption of LPG components to C300. As it can be easily realized, amount of the Thiophen atoms adsorbed is much more than the other three components and it is a good sign. It shows that C300 has the potential of separating thiophene from LPG. By the temporature increase a reduction in the adsorbed amount of any of the componenets is detected.

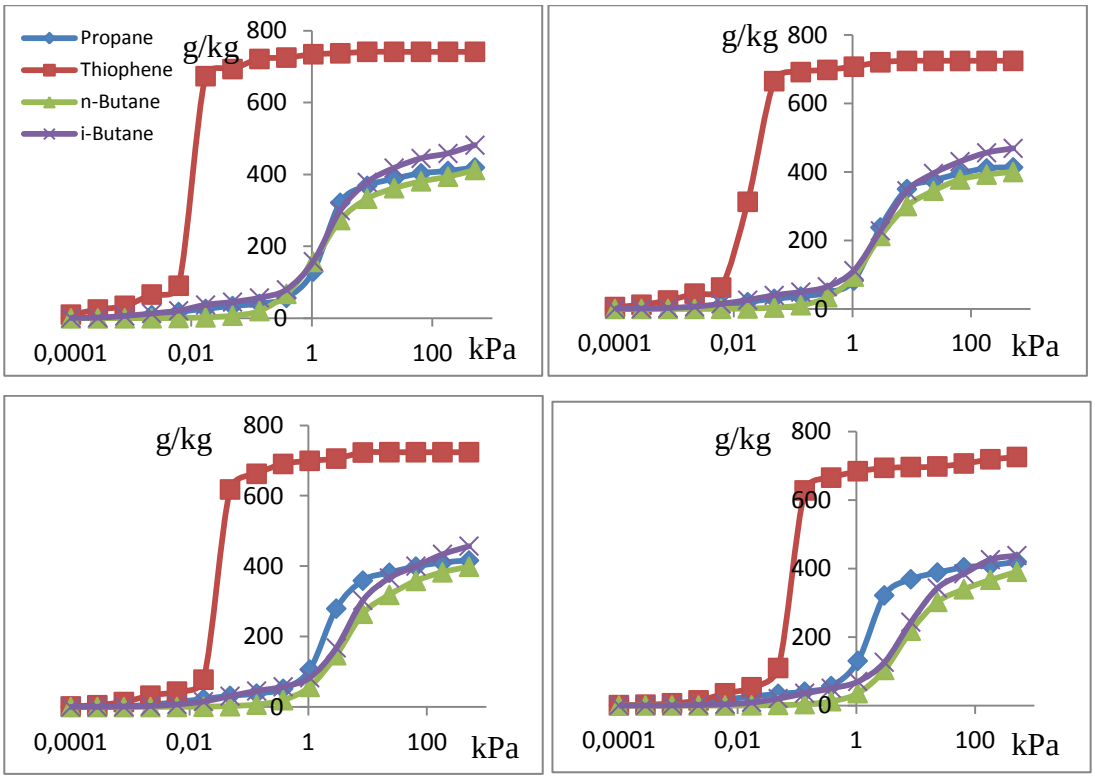

Figure 5.1: Adsorption isotherms of C300. Top left: 273 K ,Top right: 283 K, Bottom left: 293 K, Bottom right: 303 K

Figure below shows the adsorption results for A100 in four differnet temperatures. As the results show this MOF cannot adsorb any of the cvomponenets in low pressures and the first signs of adsorbtion can be realized in around 90 kPa for Thiophene. In one hand seem that this MOF can adsorb thiophene much more than other three components in 506 kPa (LPG pressure in idusterial pipe-lines) but on the other hand it never gets saturated in such amounts of pressure.

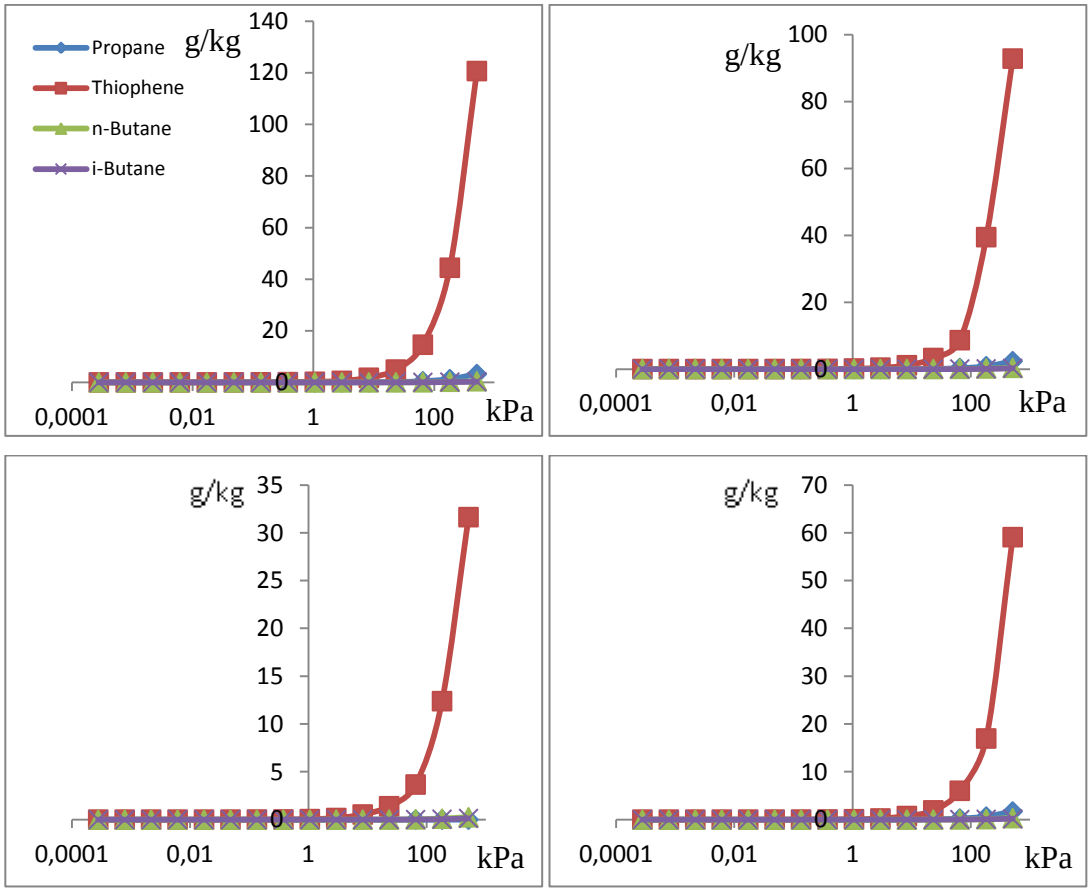

Figure 5.2: Adsorption isotherms of A100. Top left: 273 K ,Top right: 283 K, Bottom left: 293 K, Bottom right: 303 K

Effect of temporature increase is obvious for this MOF ,too. 30 °C increase in temporature causes almost 90 g/kg reduction in the materail adsorbed and also reduces the ratio of the Thiophene adsorbed to the other componenets.

Figure 5.3 represents the adsorption isotherms for M050. According to the simulations, this MOF gets saturated up 506 kPa and it also shows the potential of adsorbing Thiophene more than other components. This MOF also shows a different adsorption pattern for Propane. Maximum capacity of this MOF for thiophene

adsorption seems to be around 250 g/kg nad it is not effected with temperature increase in large scales.

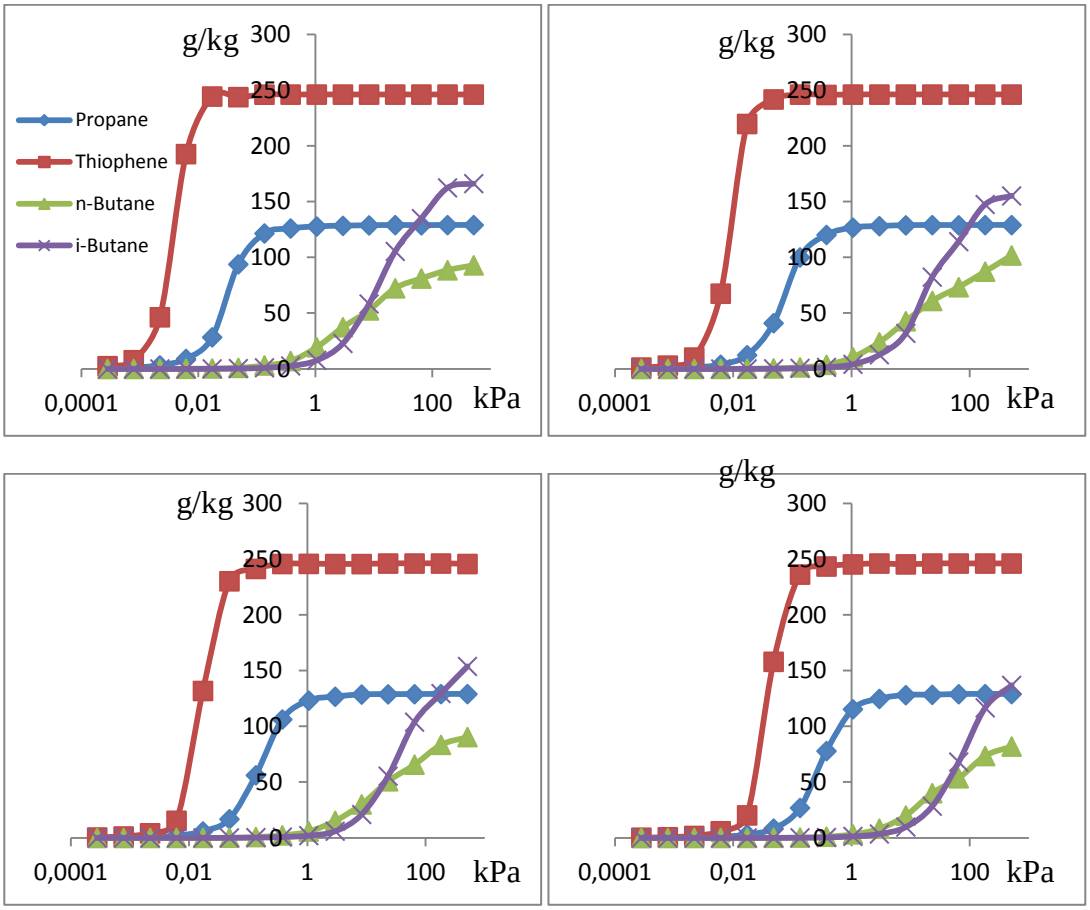

Figure 5.3: Adsorption isotherms of M050. Top left: 273 K ,Top right: 283 K, Bottom left: 293 K, Bottom right: 303 K

The point that takes attention in here is, among the hydrocarbons, Propane get to be adsorbed to the MOF earlier than the other componenets and for some specific aim it also can be useful.

Adsorption isotherms of IRMOF are very similar to those for C300 but the difference is that IRMOF shows more capability in adsorbing materials. Also the adsrbed amount of hydrocarbons is increased in IRMOF (it is about 450 g/kg in average for C300 while it is about 650 for IRMOF) but increase of Thiophene adsorption (it is about 700 g/kg for C300 while it is 1250 g/kg for IRMOF) is more effective.

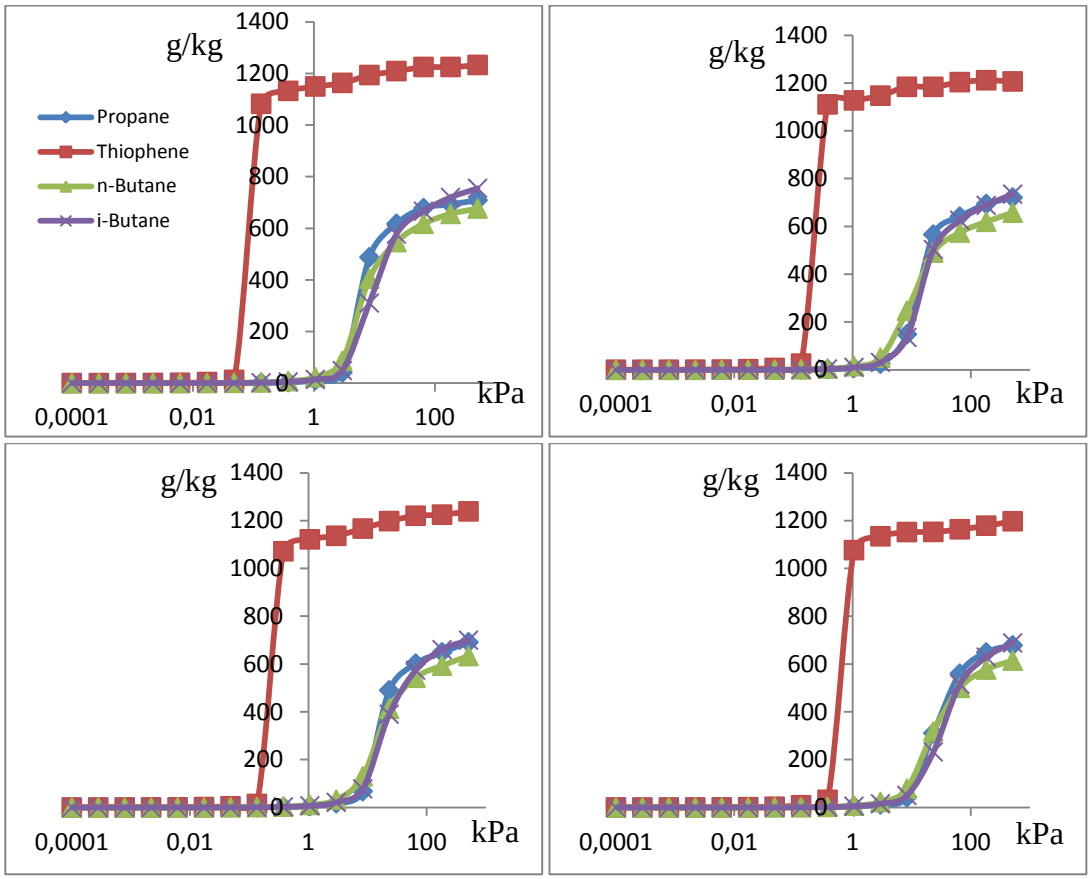

Figure 5.4: Adsorption isotherms of MOF5. Top left: 273 K ,Top right: 283 K, Bottom left: 293 K, Bottom right: 303 K

Results also show that temperature increase cuases more decrease in the amount of material adsorbed for hydrocarbons, so it seems that if the adsorption process be done in the higher temperatures it would be better for Thiıphne separation.

The important point in the isotherms related to ZIF-8 is, in industerial conditions, while it has been saturated by adsorbing maximum amounts of thiophene in its capacity it has not reached to the saturation point for other three components. The negative point for that is the start of adsorption in higher pressures.

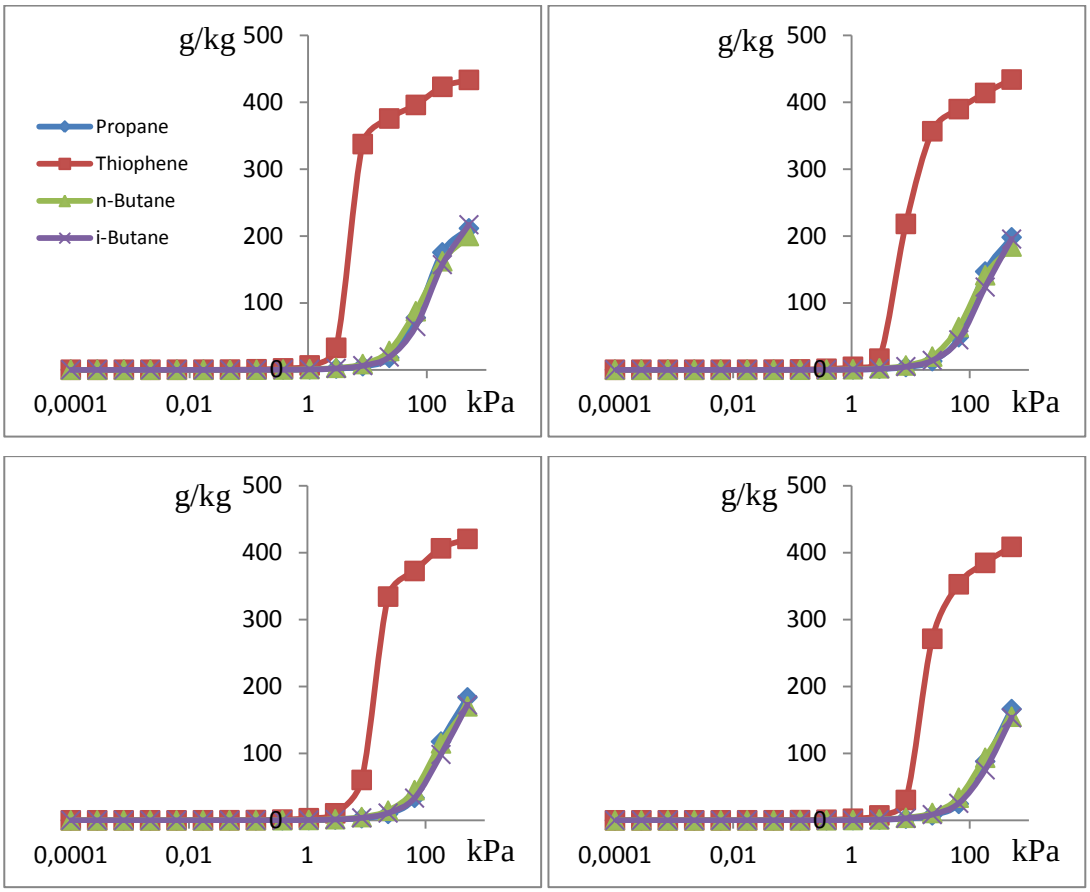

Figure 5.5: Adsorption isotherms of ZIF-8. Top left: 273 K ,Top right: 283 K, Bottom left: 293 K, Bottom right: 303 K

So adsorption isotherms show that all the MOFs show better adsorption performance for the Thiophene comparing with the Propane, i-Butane, and n-Butane. Here ratio of the atoms adsorbed to the MOF structure may be important in order to be able to compare the performance of the MOFs with each other. With increase of pressure in all MOFs for all adsorbates it is obvious that number of the atoms adsorbed by the MOF structure increases but the point here is that Thiophen adsorption increases faster than the other three.

5.2 Efect of Temperature

Temperature is an importat factor in industerial applications. Either increasing or decreasing the temperatur is costy and always people try to make minimum changes in the temperature. So observing the effects of temperature would be very logical in

here. As the adsorption conditions can change by the seasons changing, different possible temperatures were considered to be checked as 273, 283, 293, and 303 K as the possible temperature range accourding to the weathers in the Istanbul. As it incomming diyagrams show that tempearature increase causes a reduction in adsorbed material amount in different pressures before the saturation pressure.

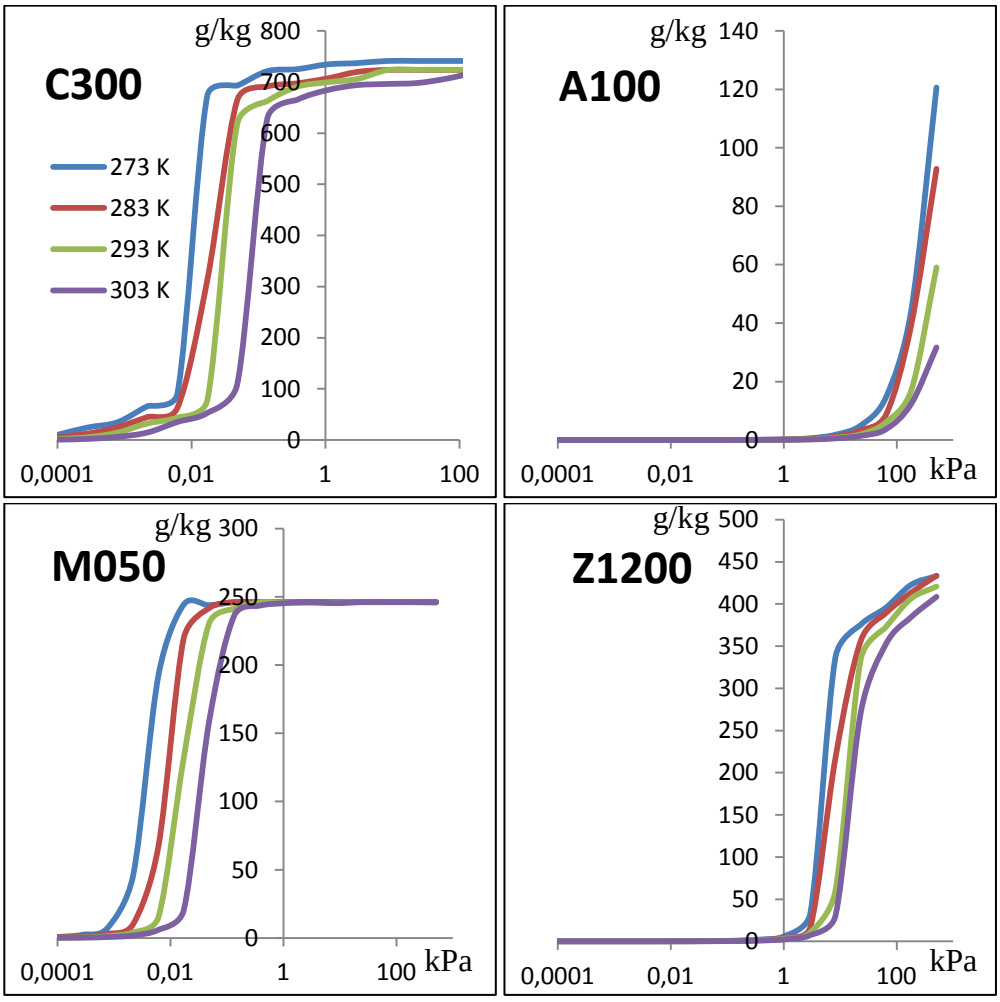

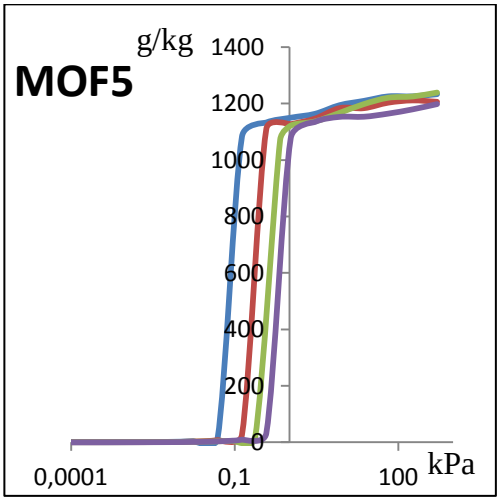

Figure 5.6: Temporature effect on adsorptio

Even after reaching to the saturation pressure some MOFs like C300 show a difference in amount of material adsorbed,too. So theorically working in lower temperatures will seem more logical but we should not forgetr that incresing temperature causes a reduction in adsorption of the hydrocarbons inside the LPG and even some times (such as in ZIF-8) it may end to more reduction in hydrocarbon adsorption than in Thiophene. But generally it is accepted that working in lower temporatures, as much as possible in the industry, is more beneficial.

5.3 Selectivity

The other factor that must be analyzed in the adsorption performance of the MOFs is Selectivity of the MOFs for different adsorbates in the same conditions. Adorption selectivity for Thiophene and each of the hydrocarbons separately is calculated as the ratio between the adsorbed Thiophene and hydrocarbon molecules in each of the MOFs separately divided by the same ratio in the bulk of the gas in contact with the MOF as follow (Demir and Ahunbay 2014):

$$S_{Thiophene/Hydrocarbon} = \frac{x_{Thiophene}/x_{Hydrocarbon}}{y_{Thiophene}/y_{Hydrocarbon}} \qquad \textbf{(5.1)}$$

There are two kinds of selectivity values, one is calcuated by using unary adsorption isotherms which is called ideal adsorption selectivity value and the other one is

calculated by using binary adsorption isotherms and is known as actual adsorption selectivity. As the amount of thiophene is supposed to be less than 1 ppm inside the LPG, the difference between atom numbers of hydrocarbon and thiophene makes actual adsorption results to be untrustable. Then in this part only ideal selectivity are in the point of focus. The ideal selectivity results are as in the below and binary adsoption diyagrams are in appendix C:

MOF	Thiop./Prop.	Thiop./n-But.	Thiop./i-But.
MOF5	50	117	433
A100	64	167	201
M050	820	4452	3692
Z1200	38	11	13
C300	6530	22561	12176

These are dimensionless numbers and only helps us to compare performance of the MOFs with each other. As it can be realized from the numbers above, M050 and C300 have more selectivity ratios for Thiophene with all three hydrocarbones. It means that whenever these MOFs get in contact with Thiophene and LPG hydrocarbons, they will prefer to adsorb Thiphene hundreds of times more than hydrocarbons.So only from the aspect of selectivity, C300 seems to be best material in separating Thiophene from LPG and the second material for this aim is M050.

5.4 Working Capacity

Working Capacity is claculated by subtracting number of adsorbate material atoms remained inside the MOF in the desorption pressure from the number of the atoms adsorbed to the MOF in the adsorption pressure (Demir and Ahunbay 2014):

$$\Delta q = q_{adsorbate\ ,Pads.} - q_{adsorbate,Pdes} \qquad \textbf{(5.2)}$$

In this work we decided the desorption conditions as the ambient conditions in a typical industerial plant in Istanbul, So the by assuming four different temperature paionts (273, 283, 293, and 303 K) and atomospheric pressure with no LPG compounds in the air we did calculations for working capacity.

Table 5.1: Working capacity results for IRMOF

Component	T=273 [k]	T=283[k]	T=293[k]	T=303[k]
Propane	63.28	72.30	67.25	62.28
Thiophene	0.77	1.95	2.81	4.75
n-Butane	42.46	50.65	56.64	58.82
i-Butane	53.74	59.22	62.07	61.01

Table 5.2: Working capacity results for A100

Component	T=273 [k]	T=283[k]	T=293[k]	T=303[k]
Propane	1.94	1.42	1.03	0.98
Thiophene	38.11	29.31	18.67	10.00
n-Butane	0.22	0.17	0.14	0.11
i-Butane	0.06	0.04	0.03	0.02

Table 5.3: Working capacity results for M050

Component	T=273 [k]	T=283[k]	T=293[k]	T=303[k]
Propane	0.69	1.27	3.28	7.61
Thiophene	0.45	0.39	0.33	0.23
n-Butane	31.11	38.64	35.85	33.36
i-Butane	67.65	61.86	54.53	49.23

Table 5.4: Working capacity results for Z1200

Component	T=273 [k]	T=283[k]	T=293[k]	T=303[k]
Propane	103.67	97.14	90.21	81.64
Thiophene	110.02	110.70	107.63	104.77
n-Butane	74.24	68.45	63.36	57.64
i-Butane	58.56	46.08	36.68	28.12

Table 5.5: Working capacity results for MOF5

Component	T=273 [k]	T=283[k]	T=293[k]	T=303[k]
Propane	96.63	98.78	95.03	93.45
Thiophene	6.05	5.77	8.51	8.78
n-Butane	68.75	67.51	65.51	63.83
i-Butane	75.18	72.00	69.21	65.98

According to results, in the temperature range of 273 – 303 K average capacity for C300 is 2.75, for A100 is 24.02, for M050 is 0.35, for MOF5 is 7.28, and for Z1200 it is 108.28. By a galance at the numbers we can realize that Z1200 and A100 are acting better in this area. It seems that C300, M050, and MOF5 which had better performance in previous areas, are not showing preferable performance in working capacity and it mean that in the operation of regenerating MOFs (in order to use them again) it will be a bit hard to remove the adsorped material from MOF structure. For this aim it may be needed to reduce pressure (to do the regeneration in vocuum conditions) or to increase temperature. The point here is that, MOF structure con not tolerate very high temperatures and this issue should be analized separatly to find the optimum regeneration temperature.

5.5 Comparing MOFs with Zeolites

In order to see how the selected MOFs are behaving in comparison to zeolites, three different zeolites are seleceted. These zeolites are MFI, MOR, and all silica zeolite Y. Thiophene adsorption performance of these materials are already been analized in some articles. So in this part simulation results are considered to be copmared with each of the results reported in articles.

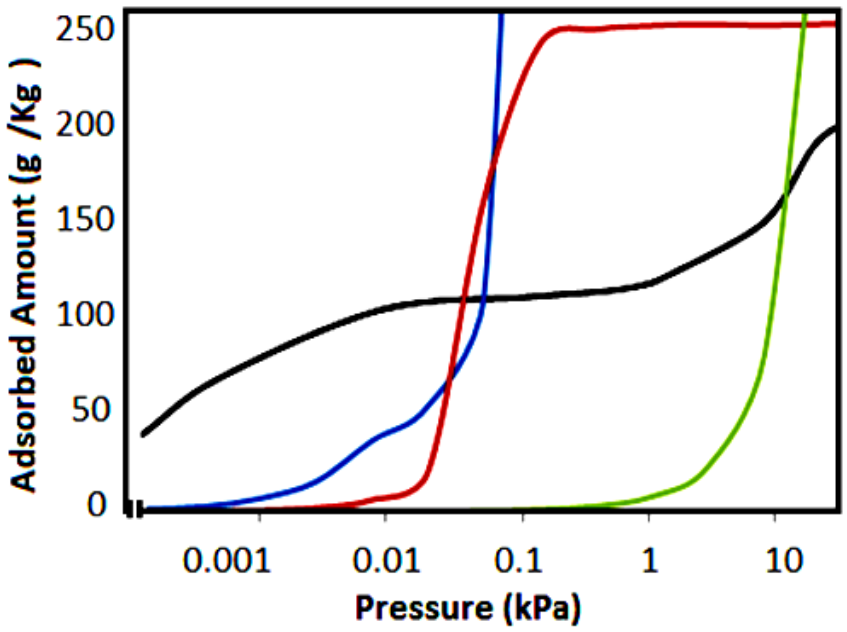

Figure 5.7: Comparing MOFs with MFI zeolite at 298 K. Red line represents M050, green represents MOF5, blue represents C300, and black represents MFI. **(**Yongping Zeng et al, 2012**)**

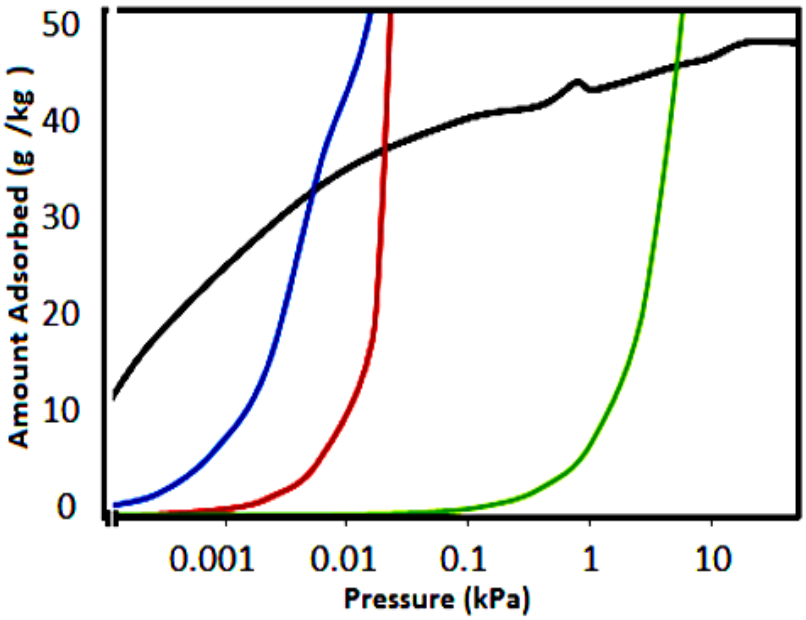

Figure 5.8: Comparing MOFs with MOR zeolite at 298 K. Red line represents M050, green represents MOF5, blue represents C300, and black represents MOR. **(**Yongping Zeng et al, 2012**)**

Thses results show that for both MFI and MOR zeolites adsorbed amout at very low pressures is more then all three best performing MOFs. But in normal pressures and also industerial pressures (4-6 atm) MOFs show better performance. So as industerial

pressure range is important for us, then results show that using MOFs ın such conditions will be more logical.

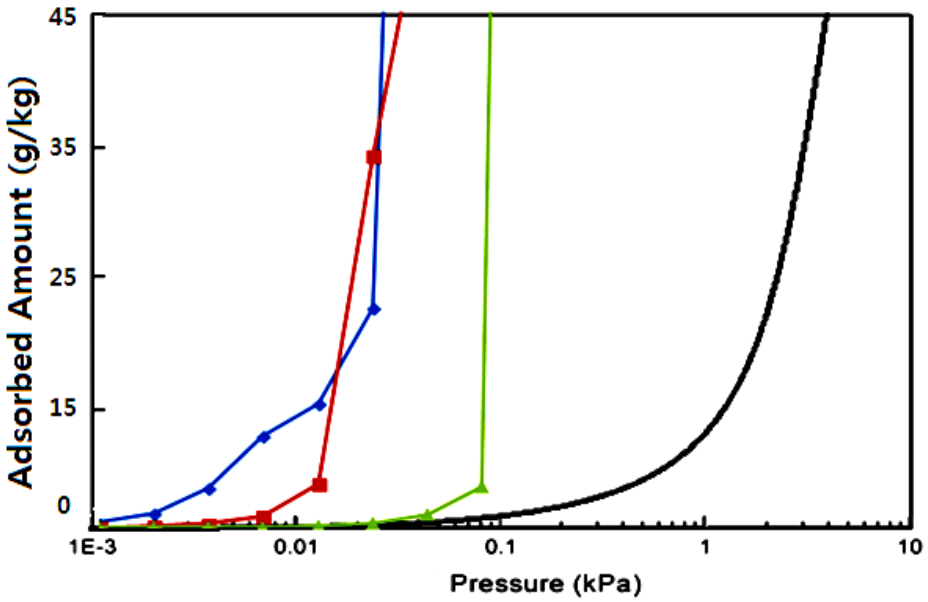

Figure 5.9: Comparing MOFs with all silica zeolite Y zeolite at 363 K. Red line represents M050, green represents MOF5, blue represents C300, and black represents all silica zeolite Y.

In figure 5.9, in which our three best performing MOFs are compared with all silica zeolite Y, results show that even in very low pressures MOFs show better performance in comparing with the mentioned zeolite and it is aother clue saying us using MOFs will be more logical in adsorbing Thiophene from LPG.

CONCLUSIONS

Sulfur removal from LPG is one of the most recent methods for aerosol production besides the other classical LPG usages. In aerosol sector it is also important to produce odorless LPG which is known as ultra clean LPG. There are various methods for sulfur removing from LPG, but most of them are not satisfactory for producing ultra clean LPG for aerosol sector because some of them can not reach to very high levels of purification and some of them are untolerably expensive.

Metal-organic frameworks are one the most recent materials which can be used for this aim with high degrees of confidence. Large variety of these materials is caused by the presence of the countless numbers of organic linkers and metal nodes. By changing metal nodes or organic linkers changes properties of the MOFs and it means that their selectivity and permeabilty can change for different material.

In this study removal of Thiophene from the mixture of i-Butane, n-Butane, and Propane as the main componenets of the LPG gas is aimed. Scince MOFs are some how expensive materials, one of the best ways of examining these materials before any investment is molecular simulation.

By getting advantages of molecular simulation methods it will be possible to produce and examine varieties of different MOFs and consider which one to buy with rational investmant. Molecular simulations can get very close to reality by choosing proper parameters for the systems and material which are used for this aim.

In this study five different MOFs are evaluated by simulation methods. Simulations are realized in four different temperatures starting from 273 K and ending with 303 K. Both sinlge component adsorption and binary adsorptions are simulated and adosrption isotherms, selectivity and working capacity calculation for each of them are performed.

Also all of the MOFs show better adsorption performance for the Thiophene in comparing with other three components, but MOF5 and C300 are showing better performance.

Selectivity analysis shows that also all the selected MOFs are preferring to adsrop Thiophene from the mixture of Propane, i-Butane, n-Butane, and Thiophene, but M050 and C300 are much more selective for this component.

Comparing three of the MOFs which are considered as the best performing ones amoung selected five, results show that using MOFs instead of zeolites will be more logical for separation prosses of Thiophene from LPG by adsorbtion. The only problem in this stage may be the economical aspects and high prices of MOFs.

According to working capacity results, regeneration of C300, MOF5, and M050 will need higher temperatures or lower pressure (than ambient temperature and perssure) or both.

For further studies it is suggested that laboratory scaled experiments and tests be performed for C300, MOF5, and M050 to evaluate simulation results and also to take another step to get to the aim of industerial usage of these materials.

REFERENCES

Achmann, S., G. Hagen, M. Haemmerle, I. Malkowsky, C. Kiener and R. Moos (2010). "Sulfur Removal from Low-Sulfur Gasoline and Diesel Fuel by Metal-Organic Frameworks." Chemical engineering & technology 33(2): 275-280.

Allendorf, M., C. Bauer, R. Bhakta and R. Houk (2009). "Luminescent metal–organic frameworks." Chemical Society Reviews 38(5): 1330-1352.

Anunziata, O. A., G. A. Eimer and L. B. Pierella (1999). "Methane transformation into aromatic hydrocarbons by activation with LPG over Zn-ZSM-11 zeolite." Catalysis letters 58(4): 235-239.

Blanco-Brieva, G., J. M. Campos-Martin, S. Al-Zahrani and J. L. Fierro (2011). "Effectiveness of metal–organic frameworks for removal of refractory organo-sulfur compound present in liquid fuels." Fuel 90(1): 190-197.

Chopard, B. and M. Droz (1998). Cellular automata, Springer.

Collins, D. J. and H.-C. Zhou (2007). "Hydrogen storage in metal–organic frameworks." Journal of materials chemistry 17(30): 3154-3160.

Corma, A., C. Martınez, G. Ketley and G. Blair (2001). "On the mechanism of sulfur removal during catalytic cracking." Applied Catalysis A: General 208(1): 135-152.

De Wild, P., R. Nyqvist, F. De Bruijn and E. Stobbe (2006). "Removal of sulphur-containing odorants from fuel gases for fuel cell-based combined heat and power applications." Journal of power sources 159(2): 995-1004.

Della Rocca, J., D. Liu and W. Lin (2011). "Nanoscale metal–organic frameworks for biomedical imaging and drug delivery." Accounts of chemical research 44(10): 957-968.

Demir, B. and M. G. Ahunbay (2014). "Propane/propylene separation in ion-exchanged zeolite-like metal organic frameworks." Microporous and Mesoporous Materials 198: 185-193.

Farha, O. K., A. Ö. Yazaydın, I. Eryazici, C. D. Malliakas, B. G. Hauser, M. G. Kanatzidis, S. T. Nguyen, R. Q. Snurr and J. T. Hupp (2010). "De

novo synthesis of a metal–organic framework material featuring ultrahigh surface area and gas storage capacities." Nature Chemistry 2(11): 944-948.

Férey, G. (2008). "Hybrid porous solids: past, present, future." Chemical Society Reviews 37(1): 191-214.

Fischer, M., F. Hoffmann and M. Fröba (2012). "Metal–organic frameworks and related materials for hydrogen purification: Interplay of pore size and pore wall polarity." RSC Advances 2(10): 4382-4396.

Frenkel, D. and B. Smit (2001). Understanding molecular simulation: from algorithms to applications, Academic press.

Greathouse, J. A. and M. D. Allendorf (2008). "Force field validation for molecular dynamics simulations of IRMOF-1 and other isoreticular zinc carboxylate coordination polymers." The Journal of Physical Chemistry C 112(15): 5795-5802.

Haile, J. (1992). Molecular dynamics simulation, Wiley, New York.

Herm, Z. R., E. D. Bloch and J. R. Long (2013). "Hydrocarbon separations in metal–organic frameworks." Chemistry of Materials 26(1): 323-338.

Horcajada, P., T. Chalati, C. Serre, B. Gillet, C. Sebrie, T. Baati, J. F. Eubank, D. Heurtaux, P. Clayette and C. Kreuz (2010). "Porous metal-organic-framework nanoscale carriers as a potential platform for drug delivery and imaging." Nature materials 9(2): 172-178.

Horcajada, P., C. Serre, G. Maurin, N. A. Ramsahye, F. Balas, M. Vallet-Regi, M. Sebban, F. Taulelle and G. Férey (2008). "Flexible porous metal-organic frameworks for a controlled drug delivery." Journal of the American Chemical Society 130(21): 6774-6780.

Horcajada, P., C. Serre, M. Vallet-Regí, M. Sebban, F. Taulelle and G. Férey (2006). "Metal–organic frameworks as efficient materials for drug delivery." Angewandte Chemie 118(36): 6120-6124.

Huelsenbeck, J. P. and F. Ronquist (2001). "MRBAYES: Bayesian inference of phylogenetic trees." Bioinformatics 17(8): 754-755.

Khan, N. A. and S. H. Jhung (2013). "Effect of central metal ions of analogous metal-organic frameworks on the adsorptive removal of benzothiophene from a model fuel." Journal of hazardous materials 260: 1050-1056.

Klontzas, E., A. Mavrandonakis, E. Tylianakis and G. E. Froudakis (2008). "Improving hydrogen storage capacity of MOF by functionalization of the organic linker with lithium atoms." Nano letters 8(6): 1572-1576.

Koelman, J. and P. Hoogerbrugge (1993). "Dynamic simulations of hard-sphere suspensions under steady shear." EPL (Europhysics Letters) 21(3): 363.

Kreno, L. E., K. Leong, O. K. Farha, M. Allendorf, R. P. Van Duyne and J. T. Hupp (2011). "Metal–organic framework materials as chemical sensors." Chemical Reviews 112(2): 1105-1125.

Li, J.-R., R. J. Kuppler and H.-C. Zhou (2009). "Selective gas adsorption and separation in metal–organic frameworks." Chemical Society Reviews 38(5): 1477-1504.

Li, J.-R., Y. Ma, M. C. McCarthy, J. Sculley, J. Yu, H.-K. Jeong, P. B. Balbuena and H.-C. Zhou (2011). "Carbon dioxide capture-related gas adsorption and separation in metal-organic frameworks." Coordination Chemistry Reviews 255(15): 1791-1823.

Lin, X., J. Jia, P. Hubberstey, M. Schröder and N. R. Champness (2007). "Hydrogen storage in metal–organic frameworks." CrystEngComm 9(6): 438-448.

Liu, Y., J. F. Eubank, A. J. Cairns, J. Eckert, V. C. Kravtsov, R. Luebke and M. Eddaoudi (2007). "Assembly of Metal–Organic Frameworks (MOFs) Based on Indium-Trimer Building Blocks: A Porous MOF with soc Topology and High Hydrogen Storage." Angewandte Chemie International Edition 46(18): 3278-3283.

Lu, G. and J. T. Hupp (2010). "Metal− organic frameworks as sensors: a ZIF-8 based Fabry− Pérot device as a selective sensor for chemical vapors and gases." Journal of the American Chemical Society 132(23): 7832-7833.

Mason, J. A., M. Veenstra and J. R. Long (2014). "Evaluating metal–organic frameworks for natural gas storage." Chemical Science 5(1): 32-51.

Mayo, S. L., B. D. Olafson and W. A. Goddard (1990). "DREIDING: a generic force field for molecular simulations." Journal of Physical Chemistry 94(26): 8897-8909.

McDonald, I. (1972). "NpT-ensemble Monte Carlo calculations for binary liquid mixtures." Molecular Physics 23(1): 41-58.

Millward, A. R. and O. M. Yaghi (2005). "Metal-organic frameworks with exceptionally high capacity for storage of carbon dioxide at room temperature." Journal of the American Chemical Society 127(51): 17998-17999.

Murray, L. J., M. Dincă and J. R. Long (2009). "Hydrogen storage in metal–organic frameworks." Chemical Society Reviews 38(5): 1294-1314.

Nevers, A. D. (1987). Odor-fading prevention from organosulfur-odorized liquefied petroleum gas, Google Patents.

Pan, L., D. H. Olson, L. R. Ciemnolonski, R. Heddy and J. Li (2006). "Separation of hydrocarbons with a microporous metal–organic framework." Angewandte Chemie 118(4): 632-635.

Ray, J. R. (1991). "Microcanonical ensemble Monte Carlo method." Physical Review A 44(6): 4061.

Sadus, R. J. (2002). Molecular simulation of fluids, Elsevier.

Satoh, A. (2003). Introduction to Molecular-Microsimulation for Colloidal Dispersions, Elsevier.

Stock, N. and S. Biswas (2011). "Synthesis of metal-organic frameworks (MOFs): routes to various MOF topologies, morphologies, and composites." Chemical reviews 112(2): 933-969.

Suh, M. P., H. J. Park, T. K. Prasad and D.-W. Lim (2011). "Hydrogen storage in metal–organic frameworks." Chemical reviews 112(2): 782-835.

Sumida, K., D. L. Rogow, J. A. Mason, T. M. McDonald, E. D. Bloch, Z. R. Herm, T.-H. Bae and J. R. Long (2011). "Carbon dioxide capture in metal–organic frameworks." Chemical reviews 112(2): 724-781.

Sun, D., S. Ma, Y. Ke, D. J. Collins and H.-C. Zhou (2006). "An interweaving MOF with high hydrogen uptake." Journal of the American Chemical Society 128(12): 3896-3897.

Tanabe, K. K. and S. M. Cohen (2011). "Postsynthetic modification of metal–organic frameworks—a progress report." Chemical Society Reviews 40(2): 498-519.

Taylor, K. M., W. J. Rieter and W. Lin (2008). "Manganese-Based Nanoscale Metal− Organic Frameworks for Magnetic Resonance Imaging." Journal of the American Chemical Society 130(44): 14358-14359.

Ting, V. and H. Doan (2014). Use of waste TPA in the synthesis of a metal organic framework (MOF) for use in hydrogen storage. Scientific conference on Oil Refining and Pertrochemical Engineering (ORPE 2014), University of Bath.

Tiwari, M., S. Sahu, R. Bhangare, P. Ajmal and G. Pandit (2013). "Estimation of polycyclic aromatic hydrocarbons associated with size segregated combustion aerosols generated from household fuels." Microchemical Journal 106: 79-86.

Ungerer, P., B. Tavitian and A. Boutin (2005). Applications of molecular simulation in the oil and gas industry: Monte Carlo methods, Editions Technip.

Valleau, J. P. and L. K. Cohen (1980). "Primitive model electrolytes. I. Grand canonical Monte Carlo computations." The Journal of chemical physics 72(11): 5935-5941.

Vanduyfhuys, L., T. Verstraelen, M. Vandichel, M. Waroquier and V. Van Speybroeck (2012). "Ab Initio Parametrized Force Field for the Flexible Metal–Organic Framework MIL-53 (Al)." Journal of Chemical Theory and Computation 8(9): 3217-3231.

Wu, H., W. Zhou and T. Yildirim (2009). "High-capacity methane storage in metal− organic frameworks M2 (dhtp): The important role of open metal sites." Journal of the American Chemical Society 131(13): 4995-5000.

Yazaydın, A. O. z. r., R. Q. Snurr, T.-H. Park, K. Koh, J. Liu, M. D. LeVan, A. I. Benin, P. Jakubczak, M. Lanuza and D. B. Galloway (2009). "Screening of metal− organic frameworks for carbon dioxide capture from flue gas using a combined experimental and modeling approach." Journal of the American Chemical Society 131(51): 18198-18199.

Yoo, Y., Z. Lai and H.-K. Jeong (2009). "Fabrication of MOF-5 membranes using microwave-induced rapid seeding and solvothermal secondary growth." Microporous and Mesoporous Materials 123(1): 100-106.

Zhang, H.-X., H.-L. Huang, C.-X. Li, H. Meng, Y.-Z. Lu, C.-L. Zhong, D.-H. Liu and Q.-Y. Yang (2012). "Adsorption behavior of metal–organic frameworks for thiophenic sulfur from diesel oil." Industrial & Engineering Chemistry Research 51(38): 12449-12455.

Zheng, B., M. Sant, P. Demontis and G. B. Suffritti (2012). "Force field for molecular dynamics computations in flexible ZIF-8 framework." The Journal of Physical Chemistry C 116(1): 933-938.

APPENDICES

APPENDIX A: Z1200 force field refitting tables
APPENDIX B: Z1200 refitted results
APPENDIX C: Binary adsorption diagrams

Appendix A:

Table A.1: First set of force field parameters for Z1200 (σ is constant and ε is changing)

Type	R0 (σ) 1	e	D0 (Ɛ) 1	D0 (Ɛ) 2	D0 (Ɛ) 3	D0 (Ɛ) 4	D0 (Ɛ) 5	D0 (Ɛ) 6	D0 (Ɛ) 7	D0 (Ɛ) 8
Zn	2.2	0.7326	0.01125	0.01	0.00875	0.0075	0.00625	0.005	0.00375	0.0025
N	3.648	-0.3008	0.153	0.136	0.119	0.102	0.085	0.068	0.051	0.034
C1	3.8164	0.4339	0.0774	0.0688	0.0602	0.0516	0.043	0.0344	0.0258	0.0172
C2	3.8164	-0.1924	0.0774	0.0688	0.0602	0.0516	0.043	0.0344	0.0258	0.0172
C3	3.8164	-0.6024	0.09846	0.08752	0.07658	0.06564	0.0547	0.04376	0.03282	0.02188
H2	2.8185	0.1585	0.0135	0.012	0.0105	0.009	0.0075	0.006	0.0045	0.003
H3	2.9745	0.1572	0.01413	0.01256	0.01099	0.00942	0.00785	0.00628	0.00471	0.00314

Table A.2: Second set of force field parameters for Z1200 (σ is constant and ε is changing)

Type	R0 (σ) 2	e	D0 (Ɛ) 1	D0 (Ɛ) 2	D0 (Ɛ) 3	D0 (Ɛ) 4	D0 (Ɛ) 5	D0 (Ɛ) 6	D0 (Ɛ) 7	D0 (Ɛ) 8
Zn	2.156	0.7326	0.01125	0.01	0.00875	0.0075	0.00625	0.005	0.00375	0.0025
N	3.57504	-0.3008	0.153	0.136	0.119	0.102	0.085	0.068	0.051	0.034
C1	3.740072	0.4339	0.0774	0.0688	0.0602	0.0516	0.043	0.0344	0.0258	0.0172
C2	3.740072	-0.1924	0.0774	0.0688	0.0602	0.0516	0.043	0.0344	0.0258	0.0172
C3	3.740072	-0.6024	0.09846	0.08752	0.07658	0.06564	0.0547	0.04376	0.03282	0.02188
H2	2.76213	0.1585	0.0135	0.012	0.0105	0.009	0.0075	0.006	0.0045	0.003
H3	2.91501	0.1572	0.01413	0.01256	0.01099	0.00942	0.00785	0.00628	0.00471	0.00314

Table A.3: Third set of force field parameters for Z1200 (σ is constant and ε is changing)

Type	R0 (σ) 3	e	D0 (Ɛ) 1	D0 (Ɛ) 2	D0 (Ɛ) 3	D0 (Ɛ) 4	D0 (Ɛ) 5	D0 (Ɛ) 6	D0 (Ɛ) 7	D0 (Ɛ) 8
Zn	2.112	0.7326	0.01125	0.01	0.00875	0.0075	0.00625	0.005	0.00375	0.0025
N	3.50208	-0.3008	0.153	0.136	0.119	0.102	0.085	0.068	0.051	0.034
C1	3.663744	0.4339	0.0774	0.0688	0.0602	0.0516	0.043	0.0344	0.0258	0.0172
C2	3.663744	-0.1924	0.0774	0.0688	0.0602	0.0516	0.043	0.0344	0.0258	0.0172
C3	3.663744	-0.6024	0.09846	0.08752	0.07658	0.06564	0.0547	0.04376	0.03282	0.02188
H2	2.70576	0.1585	0.0135	0.012	0.0105	0.009	0.0075	0.006	0.0045	0.003
H3	2.85552	0.1572	0.01413	0.01256	0.01099	0.00942	0.00785	0.00628	0.00471	0.00314

Table A.4: Forth set of force field parameters for Z1200 (σ is constant and ε is changing)

Type	R0 (σ) 4	e	D0 (Ɛ) 1	D0 (Ɛ) 2	D0 (Ɛ) 3	D0 (Ɛ) 4	D0 (Ɛ) 5	D0 (Ɛ) 6	D0 (Ɛ) 7	D0 (Ɛ) 8
Zn	2.068	0.7326	0.01125	0.01	0.00875	0.0075	0.00625	0.005	0.00375	0.0025
N	3.42912	-0.3008	0.153	0.136	0.119	0.102	0.085	0.068	0.051	0.034
C1	3.587416	0.4339	0.0774	0.0688	0.0602	0.0516	0.043	0.0344	0.0258	0.0172
C2	3.587416	-0.1924	0.0774	0.0688	0.0602	0.0516	0.043	0.0344	0.0258	0.0172
C3	3.587416	-0.6024	0.09846	0.08752	0.07658	0.06564	0.0547	0.04376	0.03282	0.02188
H2	2.64939	0.1585	0.0135	0.012	0.0105	0.009	0.0075	0.006	0.0045	0.003
H3	2.79603	0.1572	0.01413	0.01256	0.01099	0.00942	0.00785	0.00628	0.00471	0.00314

Table A.5: Fifth set of force field parameters for Z1200 (σ is constant and ε is changing)

Type	R0 (σ) 5	e	D0 (Ɛ) 1	D0 (Ɛ) 2	D0 (Ɛ) 3	D0 (Ɛ) 4	D0 (Ɛ) 5	D0 (Ɛ) 6	D0 (Ɛ) 7	D0 (Ɛ) 8
Zn	2.024	0.7326	0.01125	0.01	0.00875	0.0075	0.00625	0.005	0.00375	0.0025
N	3.35616	-0.3008	0.153	0.136	0.119	0.102	0.085	0.068	0.051	0.034
C1	3.511088	0.4339	0.0774	0.0688	0.0602	0.0516	0.043	0.0344	0.0258	0.0172
C2	3.511088	-0.1924	0.0774	0.0688	0.0602	0.0516	0.043	0.0344	0.0258	0.0172
C3	3.511088	-0.6024	0.09846	0.08752	0.07658	0.06564	0.0547	0.04376	0.03282	0.02188
H2	2.59302	0.1585	0.0135	0.012	0.0105	0.009	0.0075	0.006	0.0045	0.003
H3	2.73654	0.1572	0.01413	0.01256	0.01099	0.00942	0.00785	0.00628	0.00471	0.00314

Table A.6: Sixth set of force field parameters for Z1200 (σ is constant and ε is changing)

Type	R0 (σ) 6	e	D0 (Ɛ) 1	D0 (Ɛ) 2	D0 (Ɛ) 3	D0 (Ɛ) 4	D0 (Ɛ) 5	D0 (Ɛ) 6	D0 (Ɛ) 7	D0 (Ɛ) 8
Zn	1.98	0.7326	0.01125	0.01	0.00875	0.0075	0.00625	0.005	0.00375	0.0025
N	3.2832	-0.3008	0.153	0.136	0.119	0.102	0.085	0.068	0.051	0.034
C1	3.43476	0.4339	0.0774	0.0688	0.0602	0.0516	0.043	0.0344	0.0258	0.0172
C2	3.43476	-0.1924	0.0774	0.0688	0.0602	0.0516	0.043	0.0344	0.0258	0.0172
C3	3.43476	-0.6024	0.09846	0.08752	0.07658	0.06564	0.0547	0.04376	0.03282	0.02188
H2	2.53665	0.1585	0.0135	0.012	0.0105	0.009	0.0075	0.006	0.0045	0.003
H3	2.67705	0.1572	0.01413	0.01256	0.01099	0.00942	0.00785	0.00628	0.00471	0.00314

Table A.7: Seventh set of force field parameters for Z1200 (σ is constant and ε is changing)

Type	R0 (σ) 7	e	D0 (Ɛ) 1	D0 (Ɛ) 2	D0 (Ɛ) 3	D0 (Ɛ) 4	D0 (Ɛ) 5	D0 (Ɛ) 6	D0 (Ɛ) 7	D0 (Ɛ) 8
Zn	1.936	0.7326	0.01125	0.01	0.00875	0.0075	0.00625	0.005	0.00375	0.0025
N	3.21024	-0.3008	0.153	0.136	0.119	0.102	0.085	0.068	0.051	0.034
C1	3.358432	0.4339	0.0774	0.0688	0.0602	0.0516	0.043	0.0344	0.0258	0.0172
C2	3.358432	-0.1924	0.0774	0.0688	0.0602	0.0516	0.043	0.0344	0.0258	0.0172
C3	3.358432	-0.6024	0.09846	0.08752	0.07658	0.06564	0.0547	0.04376	0.03282	0.02188
H2	2.48028	0.1585	0.0135	0.012	0.0105	0.009	0.0075	0.006	0.0045	0.003
H3	2.61756	0.1572	0.01413	0.01256	0.01099	0.00942	0.00785	0.00628	0.00471	0.00314

Table A.8: Eighth set of force field parameters for Z1200 (σ is constant and ε is changing)

Type	R0 (σ) 8	e	D0 (Ɛ) 1	D0 (Ɛ) 2	D0 (Ɛ) 3	D0 (Ɛ) 4	D0 (Ɛ) 5	D0 (Ɛ) 6	D0 (Ɛ) 7	D0 (Ɛ) 8
Zn	1.892	0.7326	0.01125	0.01	0.00875	0.0075	0.00625	0.005	0.00375	0.0025
N	3.13728	-0.3008	0.153	0.136	0.119	0.102	0.085	0.068	0.051	0.034
C1	3.282104	0.4339	0.0774	0.0688	0.0602	0.0516	0.043	0.0344	0.0258	0.0172
C2	3.282104	-0.1924	0.0774	0.0688	0.0602	0.0516	0.043	0.0344	0.0258	0.0172
C3	3.282104	-0.6024	0.09846	0.08752	0.07658	0.06564	0.0547	0.04376	0.03282	0.02188
H2	2.42391	0.1585	0.0135	0.012	0.0105	0.009	0.0075	0.006	0.0045	0.003
H3	2.55807	0.1572	0.01413	0.01256	0.01099	0.00942	0.00785	0.00628	0.00471	0.00314

Table A.9: Ninth set of force field parameters for Z1200 (σ is constant and ε is changing)

Type	R0 (σ) 9	e	D0 (Ɛ) 1	D0 (Ɛ) 2	D0 (Ɛ) 3	D0 (Ɛ) 4	D0 (Ɛ) 5	D0 (Ɛ) 6	D0 (Ɛ) 7	D0 (Ɛ) 8
Zn	1.848	0.7326	0.01125	0.01	0.00875	0.0075	0.00625	0.005	0.00375	0.0025
N	3.06432	-0.3008	0.153	0.136	0.119	0.102	0.085	0.068	0.051	0.034
C1	3.205776	0.4339	0.0774	0.0688	0.0602	0.0516	0.043	0.0344	0.0258	0.0172
C2	3.205776	-0.1924	0.0774	0.0688	0.0602	0.0516	0.043	0.0344	0.0258	0.0172
C3	3.205776	-0.6024	0.09846	0.08752	0.07658	0.06564	0.0547	0.04376	0.03282	0.02188
H2	2.36754	0.1585	0.0135	0.012	0.0105	0.009	0.0075	0.006	0.0045	0.003
H3	2.49858	0.1572	0.01413	0.01256	0.01099	0.00942	0.00785	0.00628	0.00471	0,00314

Appendix B:

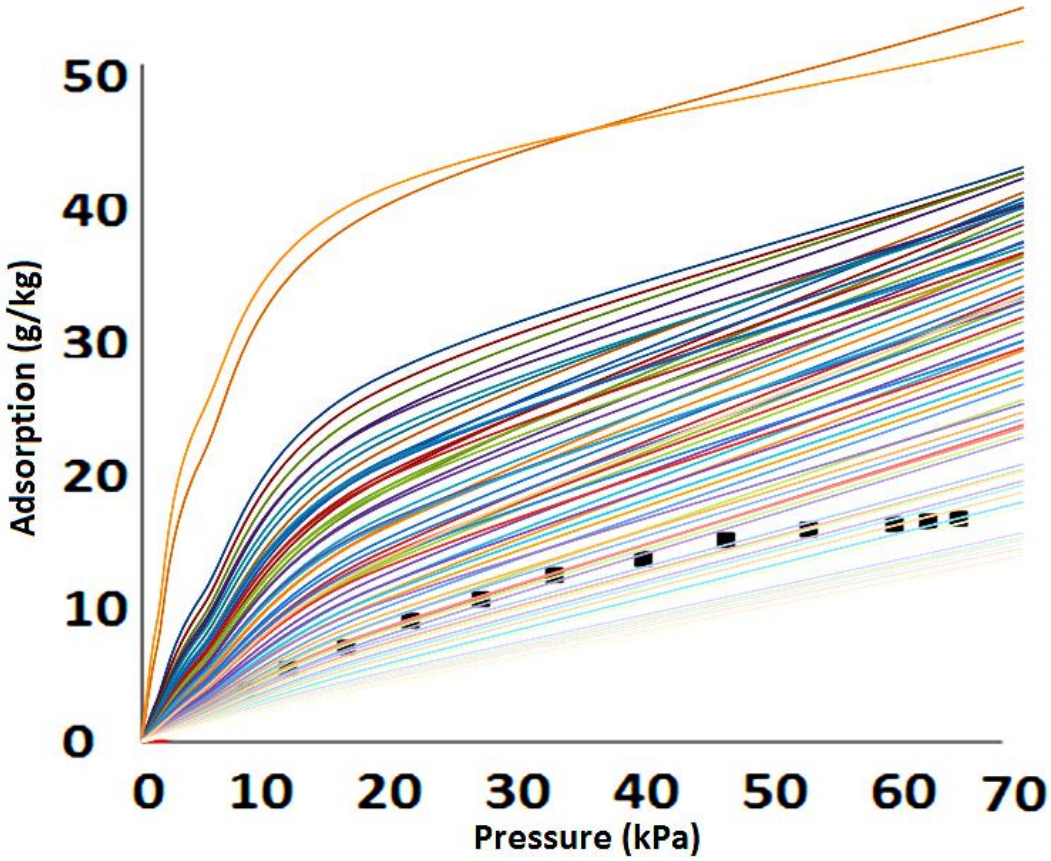

Figure B.1: All the simulation results by different force fields for Z1200

Appendix C:

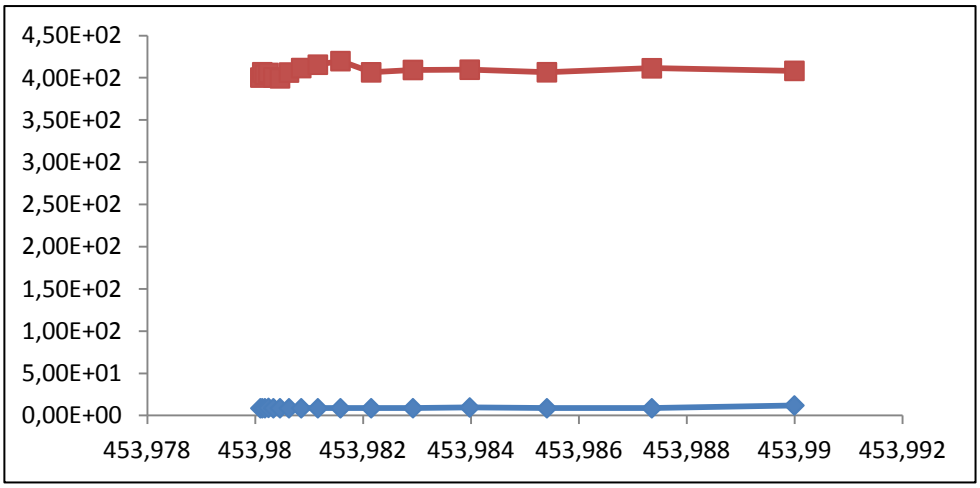

Figure C. 1: Thiophene and Propane binary adsorption diagram at 273K for C300. Red represents Propane amount and blue represents Thiophene amount

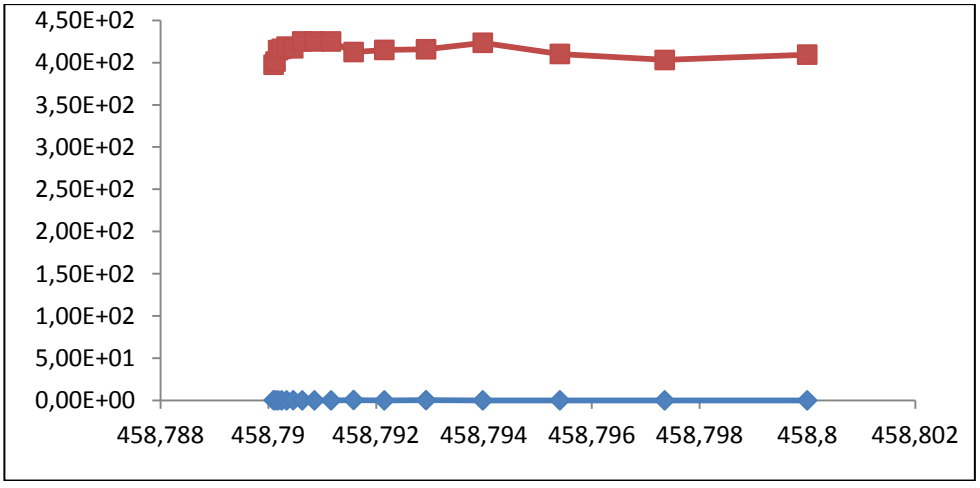

Figure C. 2: Thiophene and Propane binary adsorption diagram at 283K for C300. Red represents Propane amount and blue represents Thiophene amount.

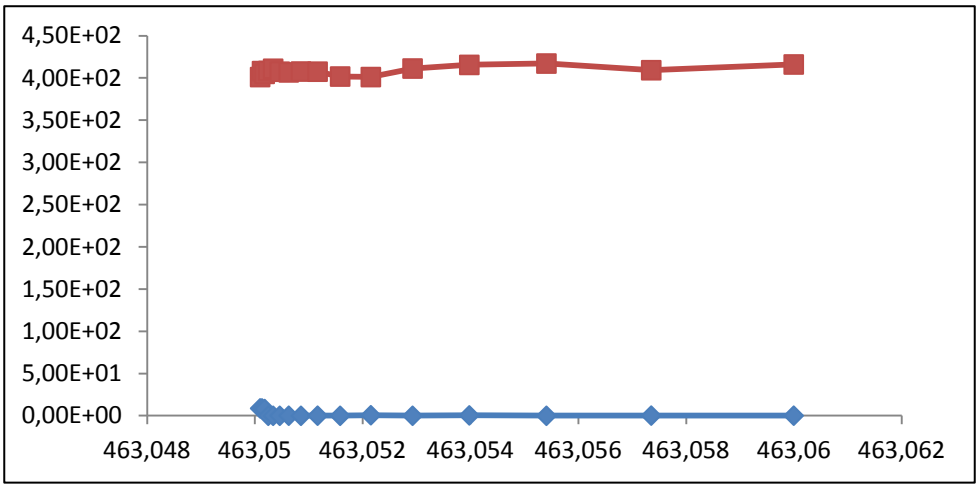

Figure C. 3: Thiophene and Propane binary adsorption diagram at 293K for C300. Red represents Propane amount and blue represents Thiophene amount.

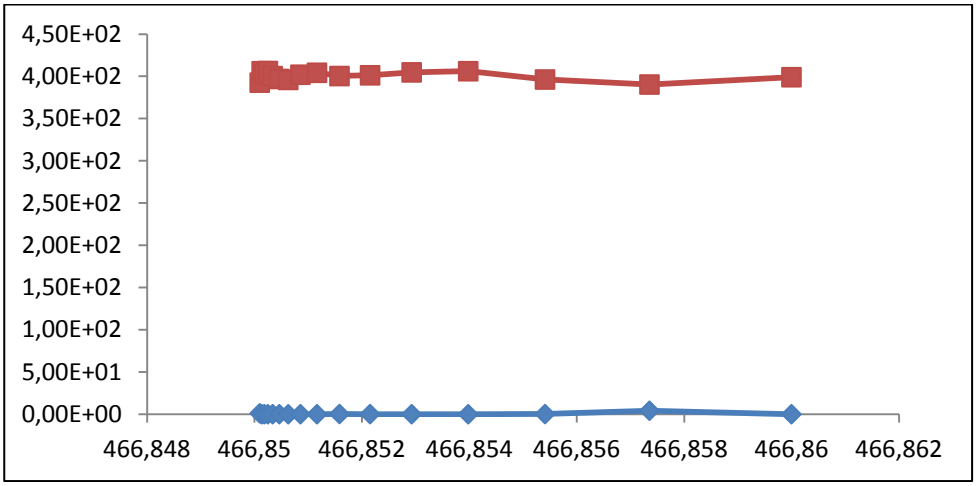

Figure C. 4: Thiophene and Propane binary adsorption diagram at 303K for C300. Red represents Propane amount and blue represents Thiophene amount.

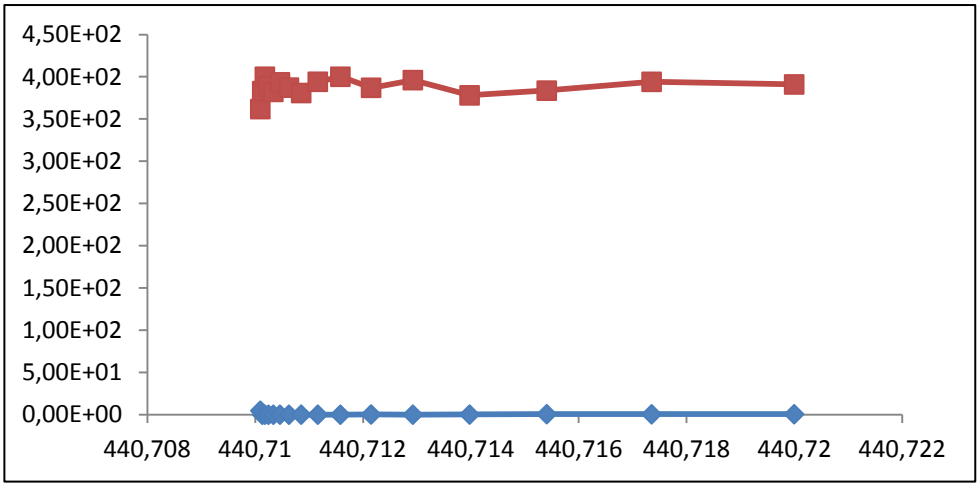

Figure C. 5: Thiophene and Propane binary adsorption diagram at 303K for C300. Red represents n-Butane amount and blue represents Thiophene amount.

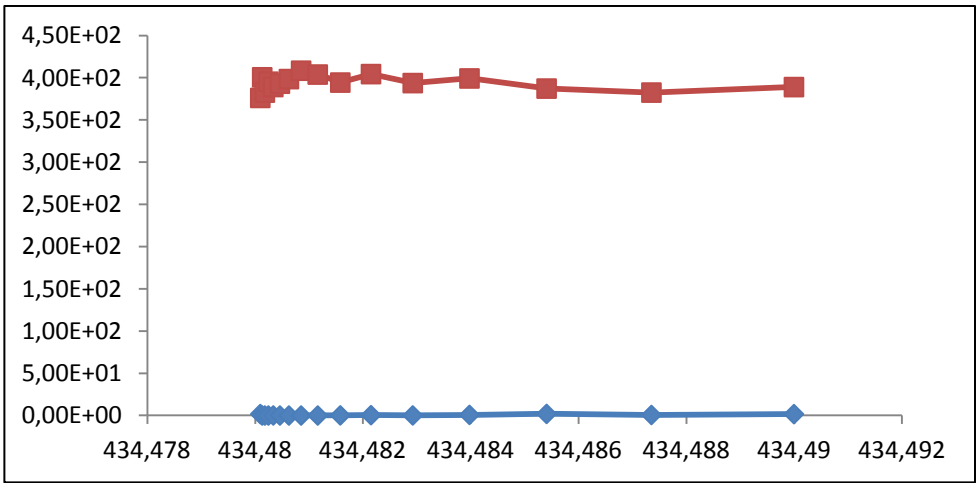

Figure C. 6: Thiophene and Propane binary adsorption diagram at 293K for C300. Red represents n-Butane amount and blue represents Thiophene amount.

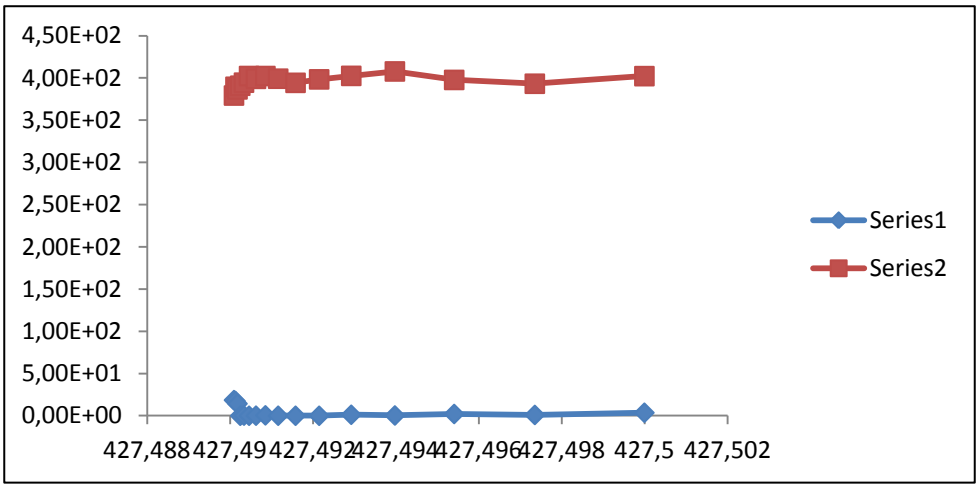

Figure C. 7: Thiophene and Propane binary adsorption diagram at 283K for C300. Red represents n-Butane amount and blue represents Thiophene amount.

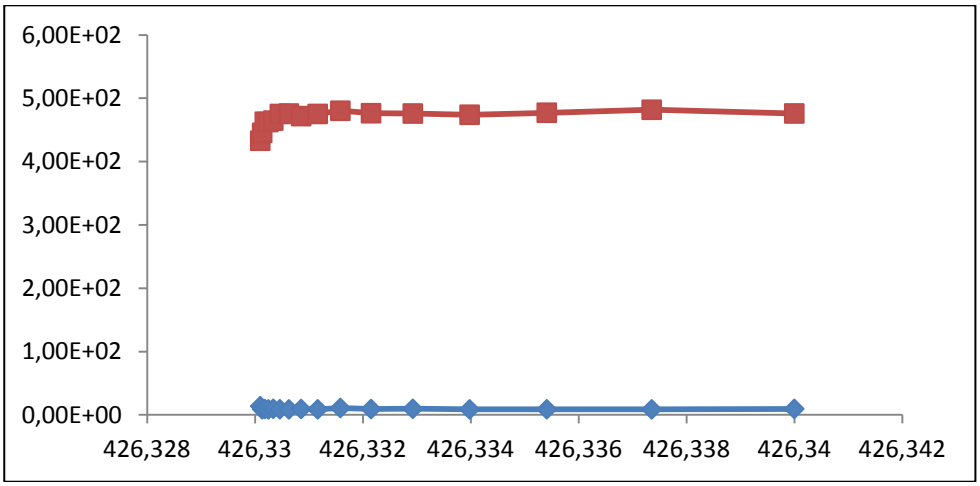

Figure C. 8: Thiophene and Propane binary adsorption diagram at 273K for C300. Red represents i-Butane amount and blue represents Thiophene amount.

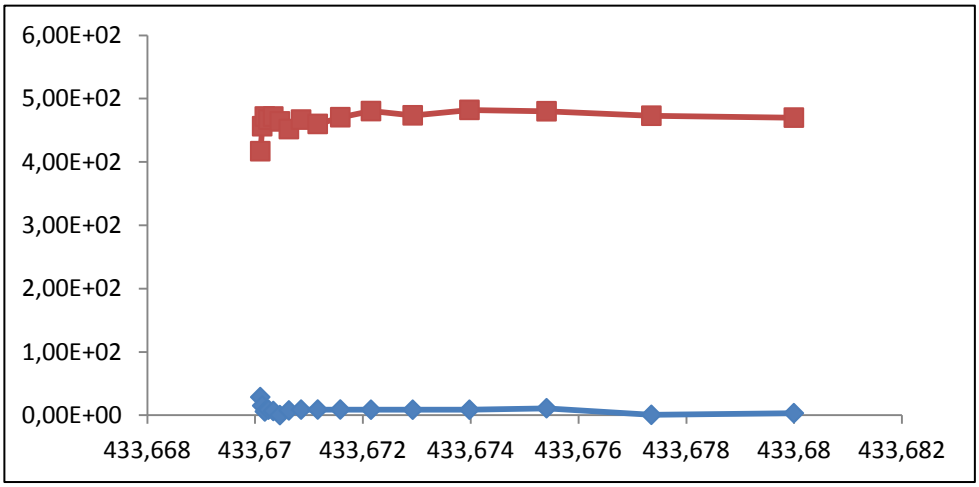

Figure C. 9: Thiophene and Propane binary adsorption diagram at 283K for C300. Red represents i-Butane amount and blue represents Thiophene amount.

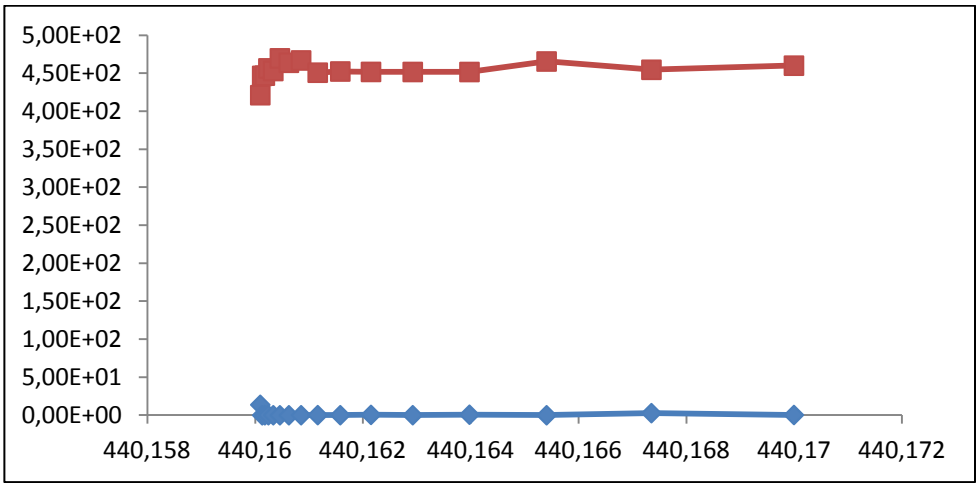

Figure C. 10: Thiophene and Propane binary adsorption diagram at 293K for C300. Red represents i-Butane amount and blue represents Thiophene amount.

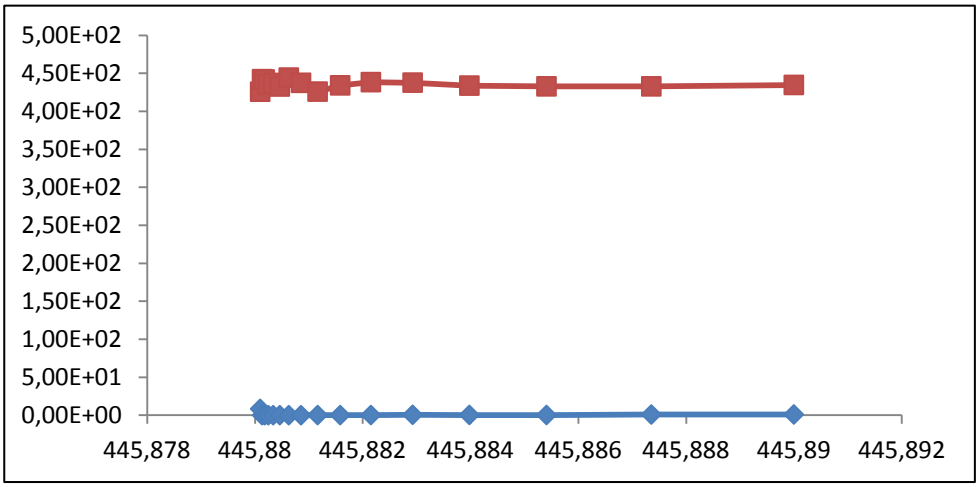

Figure C. 11: Thiophene and Propane binary adsorption diagram at 303K for C300. Red represents i-Butane amount and blue represents Thiophene amount.

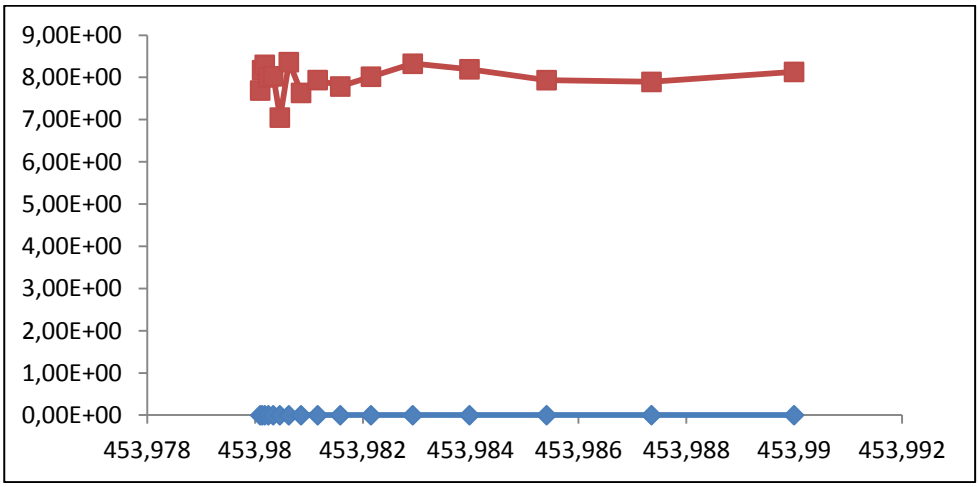

Figure C. 12: Thiophene and Propane binary adsorption diagram at 273K for A100. Red represents Propane amount and blue represents Thiophene amount.

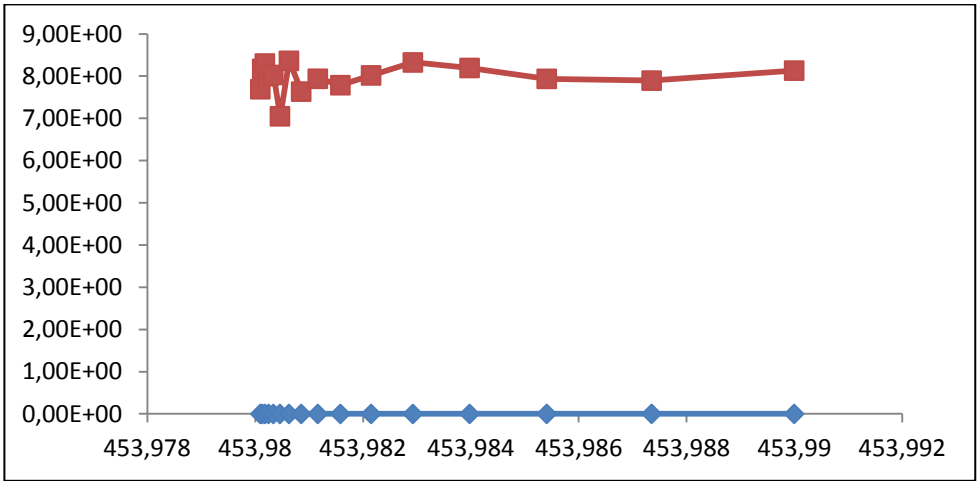

Figure C. 13: Thiophene and Propane binary adsorption diagram at 283K for A100. Red represents Propane amount and blue represents Thiophene amount.

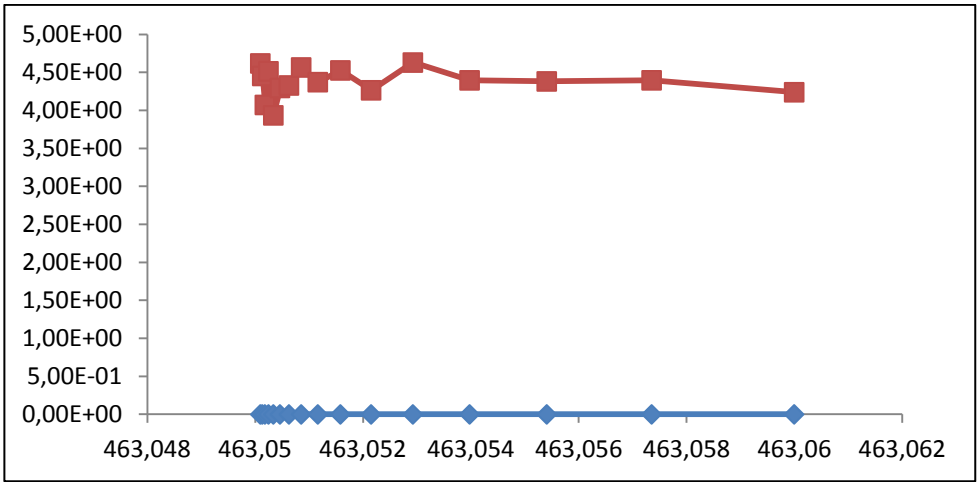

Figure C. 14: Thiophene and Propane binary adsorption diagram at 293K for A100. Red represents Propane amount and blue represents Thiophene amount.

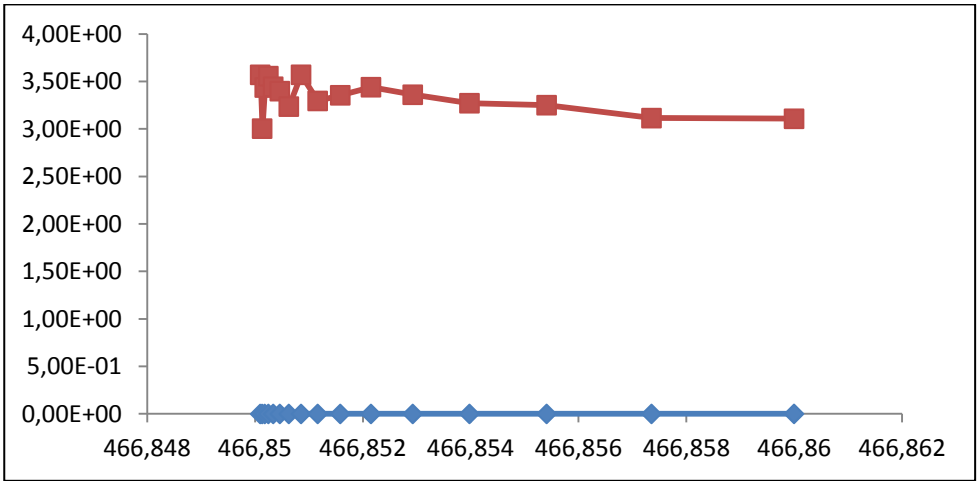

Figure C. 15: Thiophene and Propane binary adsorption diagram at 303K for A100. Red represents Propane amount and blue represents Thiophene amount.

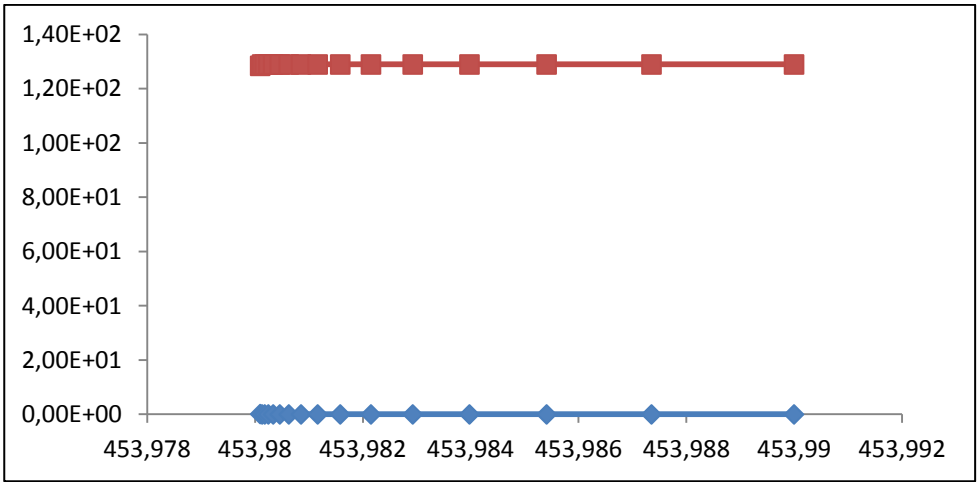

Figure C. 16: Thiophene and Propane binary adsorption diagram at 273K for M050. Red represents Propane amount and blue represents Thiophene amount.

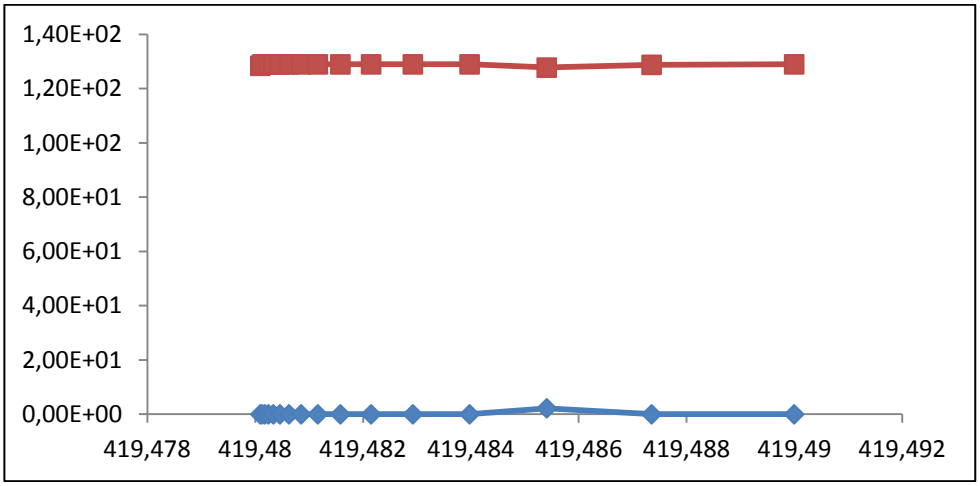

Figure C. 17: Thiophene and Propane binary adsorption diagram at 283K for M050. Red represents Propane amount and blue represents Thiophene amount.

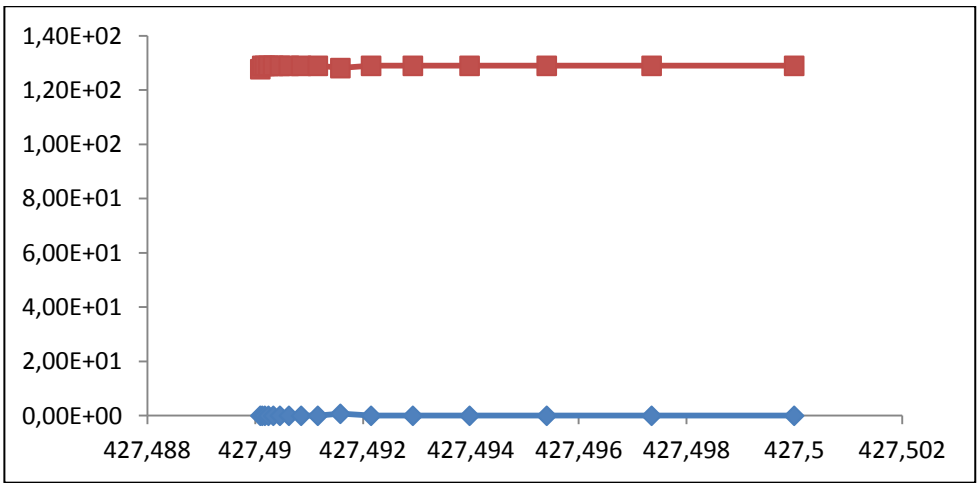

Figure C. 18: Thiophene and Propane binary adsorption diagram at 293K for M050. Red represents Propane amount and blue represents Thiophene amount.

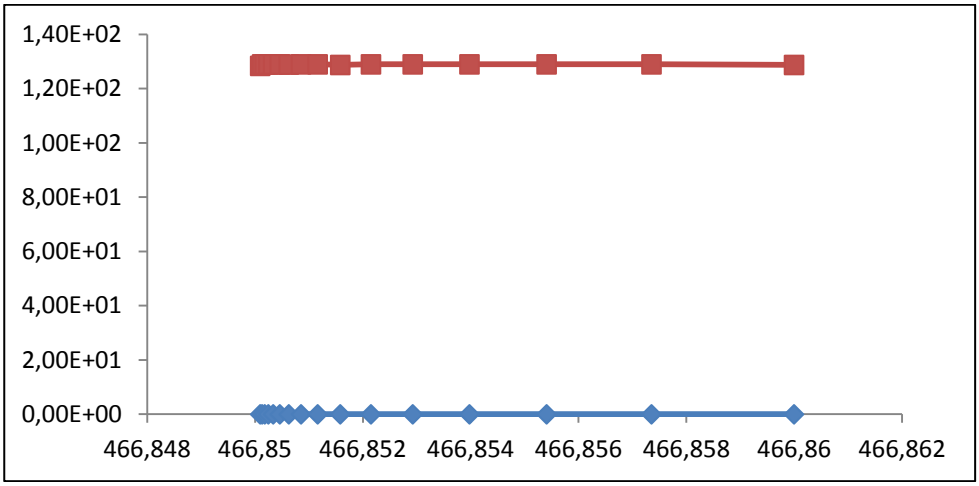

Figure C. 19: Thiophene and Propane binary adsorption diagram at 303K for M050. Red represents Propane amount and blue represents Thiophene amount.

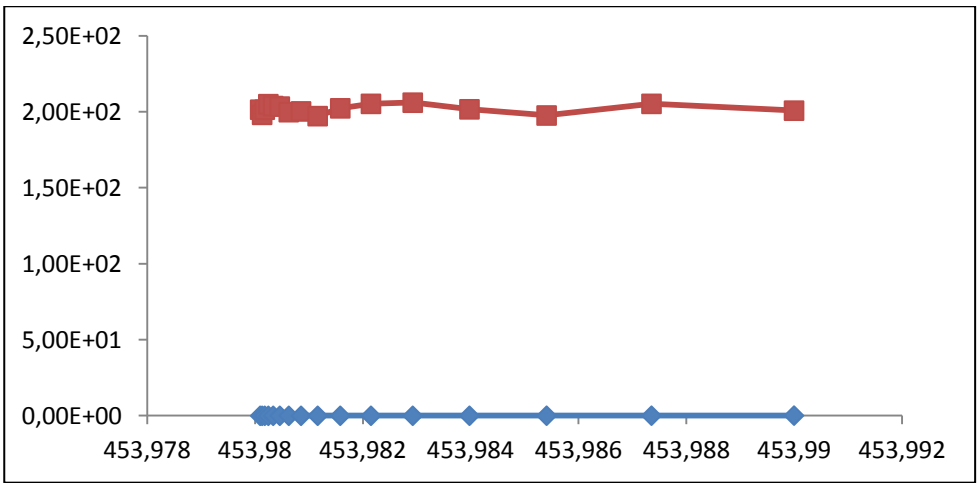

Figure C. 20: Thiophene and Propane binary adsorption diagram at 273K for ZIF8. Red represents Propane amount and blue represents Thiophene amount.

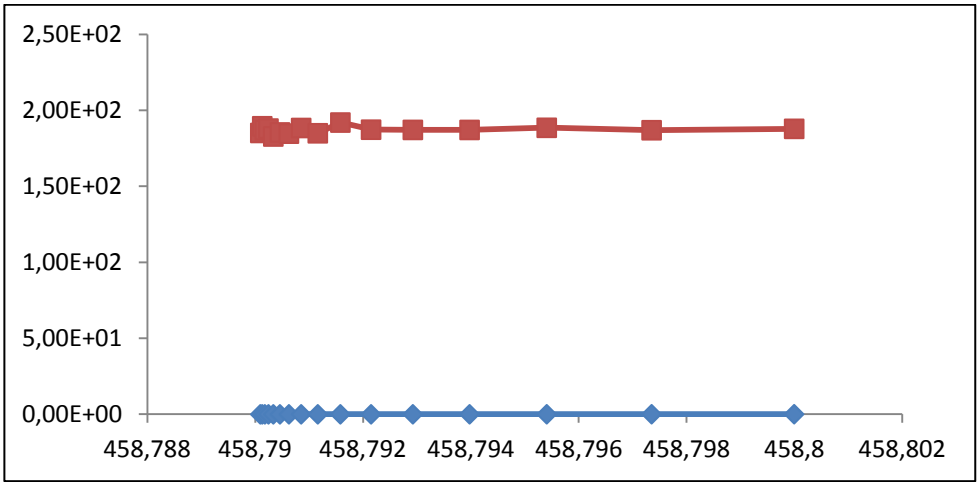

Figure C. 21: Thiophene and Propane binary adsorption diagram at 283K for ZIF8. Red represents Propane amount and blue represents Thiophene amount

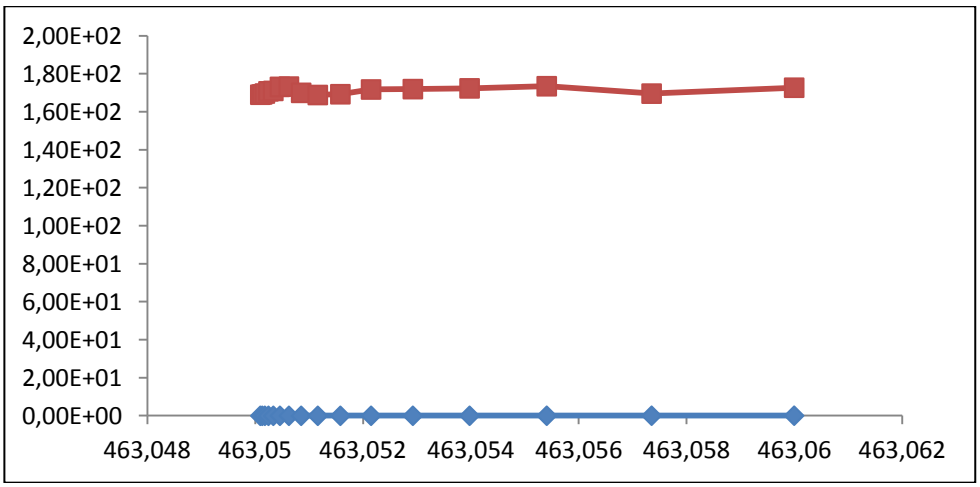

Figure C. 22: Thiophene and Propane binary adsorption diagram at 293K for ZIF8. Red represents Propane amount and blue represents Thiophene amount.

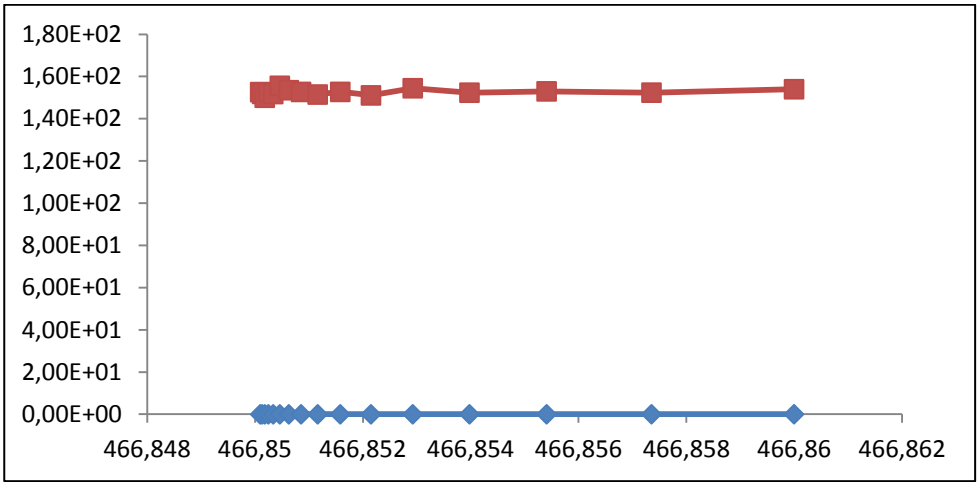

Figure C. 23: Thiophene and Propane binary adsorption diagram at 303K for ZIF8. Red represents Propane amount and blue represents Thiophene amount.

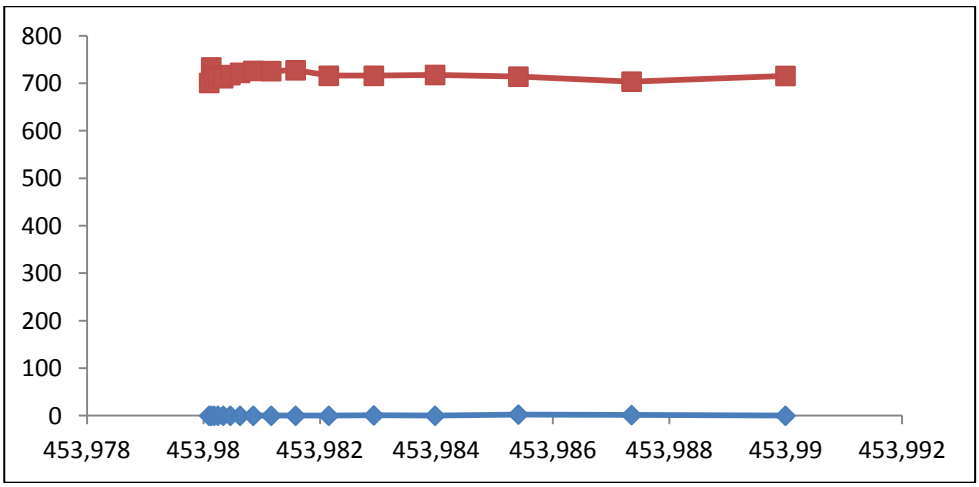

Figure C. 24: Thiophene and Propane binary adsorption diagram at 273K for M050. Red represents Propane amount and blue represents Thiophene amount.

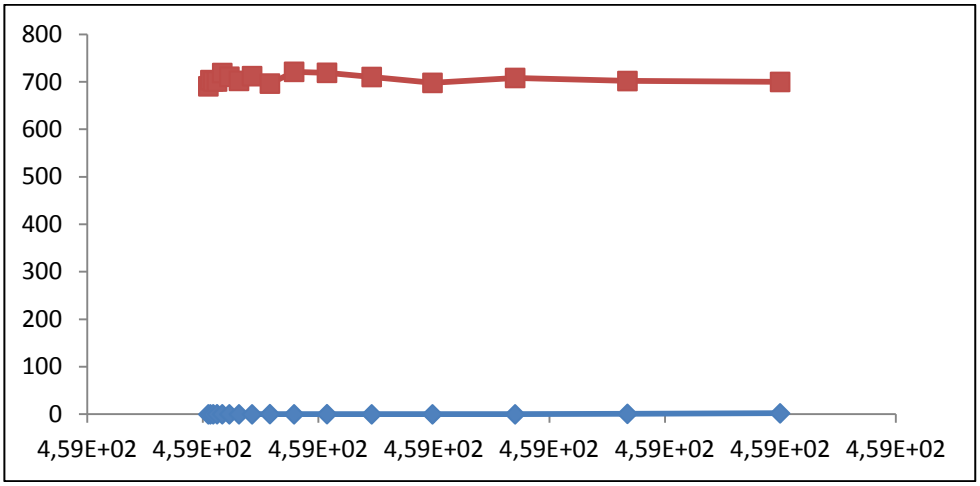

Figure C. 25: Thiophene and Propane binary adsorption diagram at 283K for M050. Red represents Propane amount and blue represents Thiophene amount.

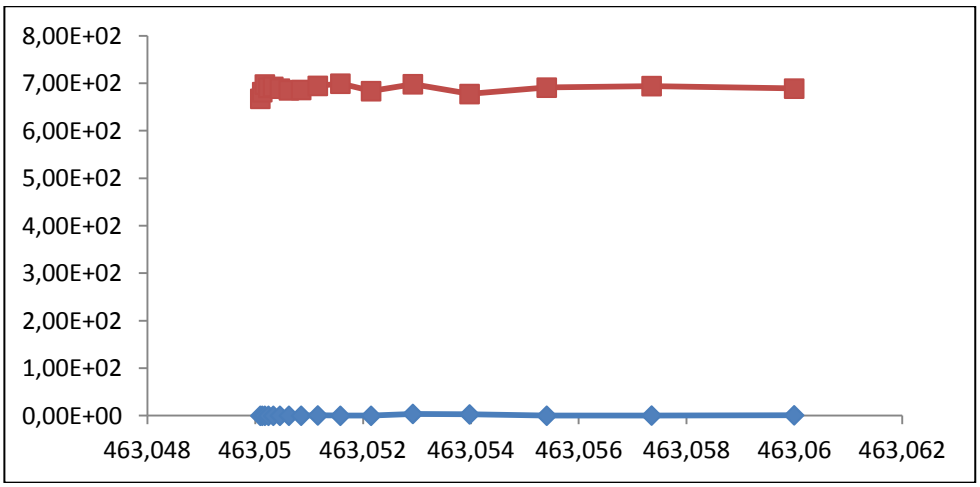

Figure C. 26: Thiophene and Propane binary adsorption diagram at 293K for M050. Red represents Propane amount and blue represents Thiophene amount.

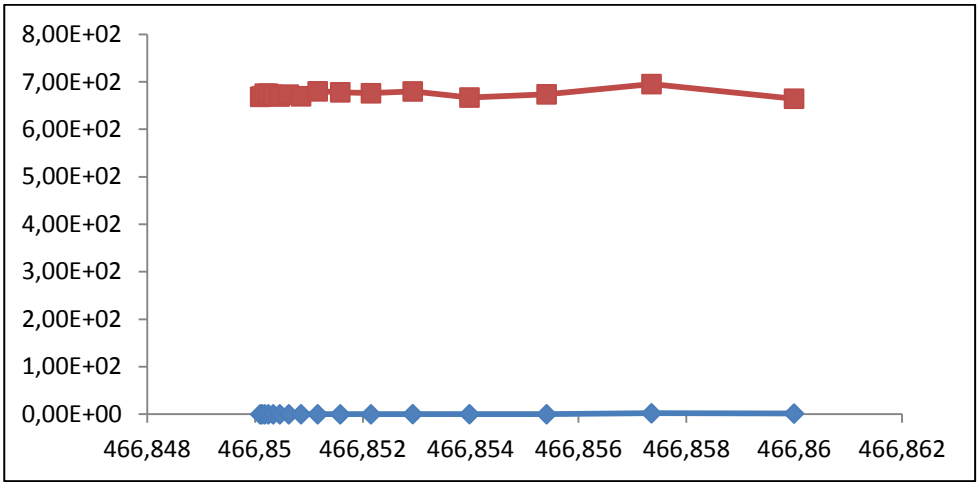

Figure C. 27: Thiophene and Propane binary adsorption diagram at 303K for M050. Red represents Propane amount and blue represents Thiophene amount.

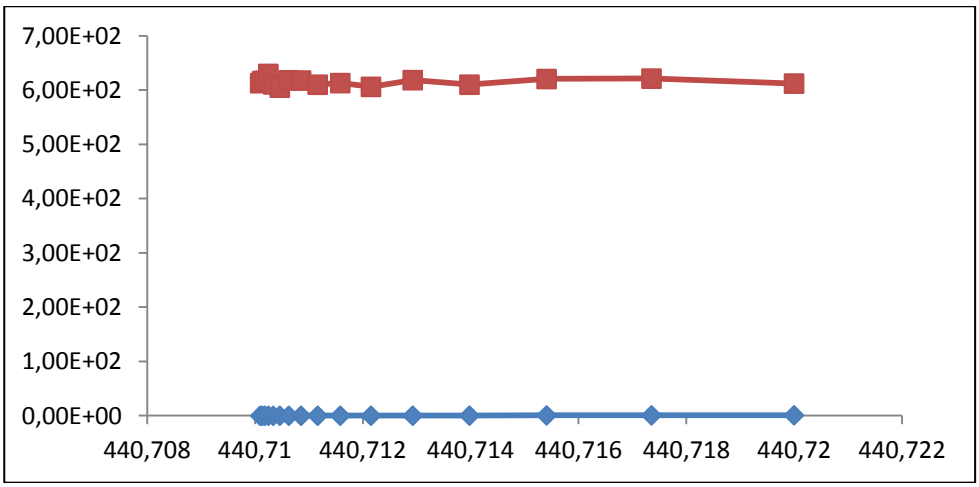

Figure C. 28: Thiophene and n-Butane binary adsorption diagram at 303K for IRMOF. Red represents n-Butane amount and blue represents Thiophene amount.

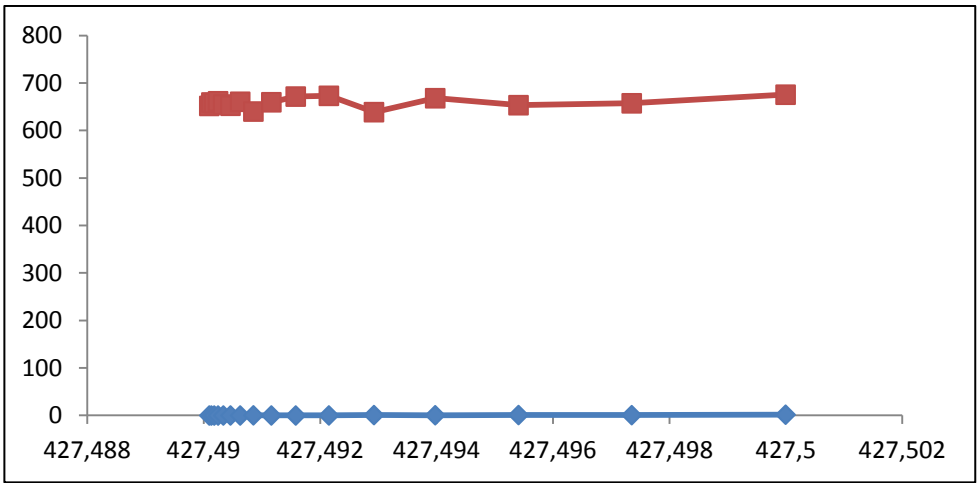

Figure C. 29: Thiophene and n-Butane binary adsorption diagram at 283K for IRMOF. Red represents n-Butane amount and blue represents Thiophene amount.

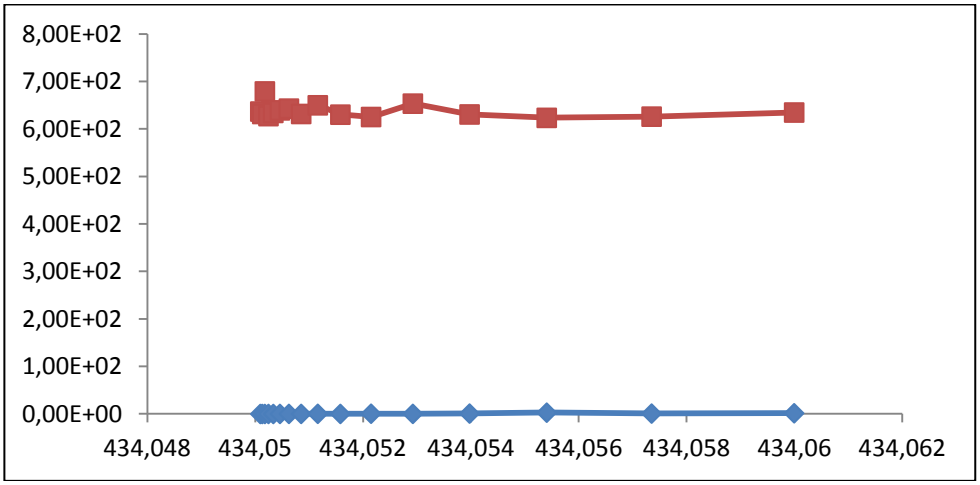

Figure C. 30: Thiophene and n-Butane binary adsorption diagram at 293K for IRMOF. Red represents n-Butane amount and blue represents Thiophene amount

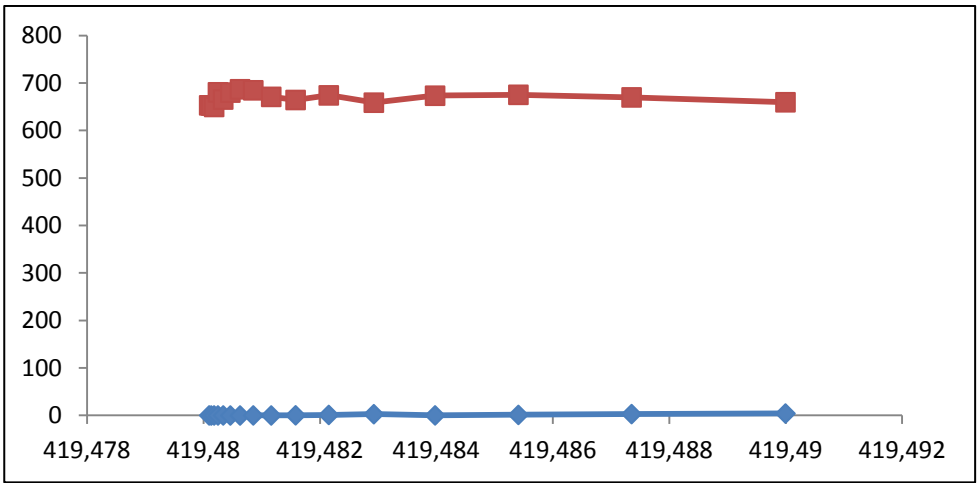

Figure C. 31: Thiophene and n-Butane binary adsorption diagram at 273K for IRMOF. Red represents n-Butane amount and blue represents Thiophene amount.

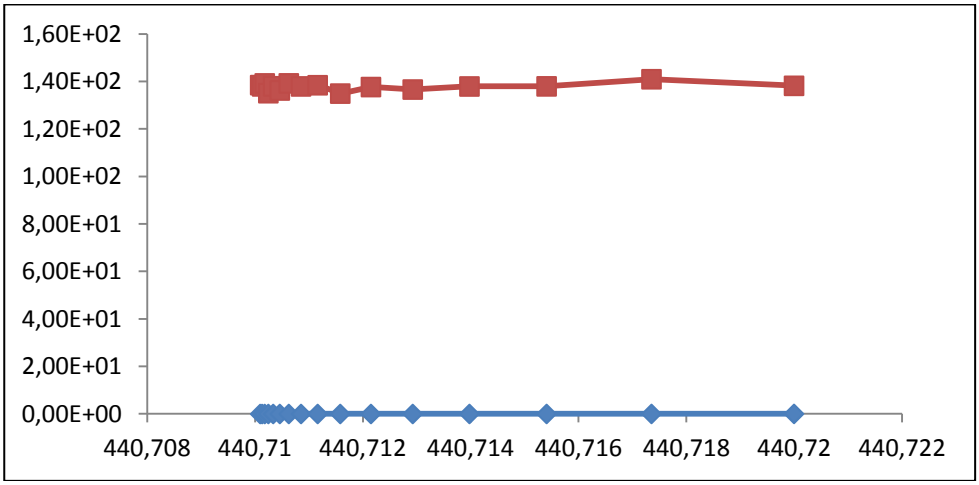

Figure C. 32: Thiophene and n-Butane binary adsorption diagram at 303K for ZIF8. Red represents n-Butane amount and blue represents Thiophene amount.

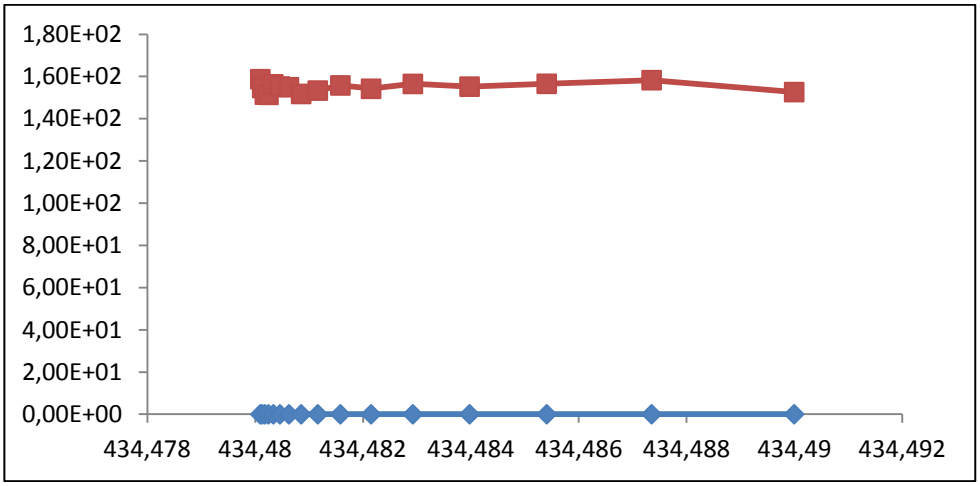

Figure C. 33: Thiophene and n-Butane binary adsorption diagram at 293K for ZIF8. Red represents n-Butane amount and blue represents Thiophene amount.

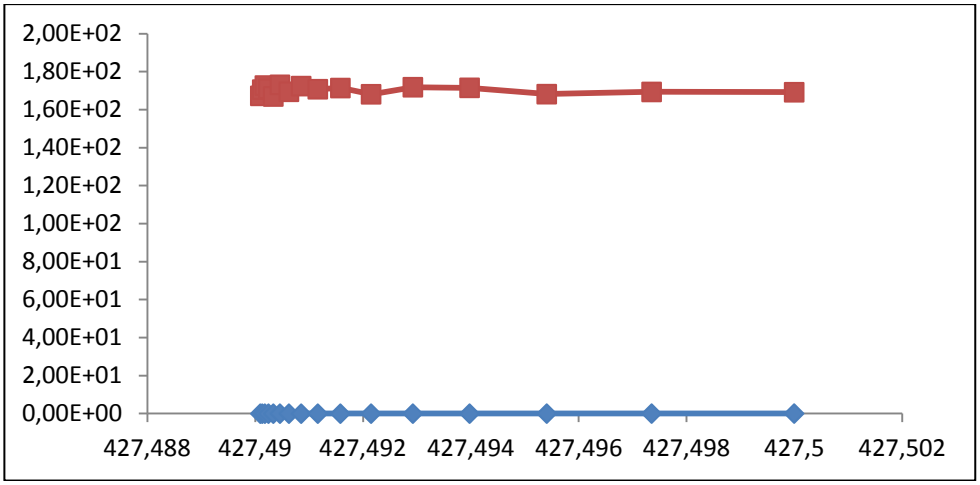

Figure C. 34: Thiophene and n-Butane binary adsorption diagram at 283K for ZIF8. Red represents n-Butane amount and blue represents Thiophene amount.

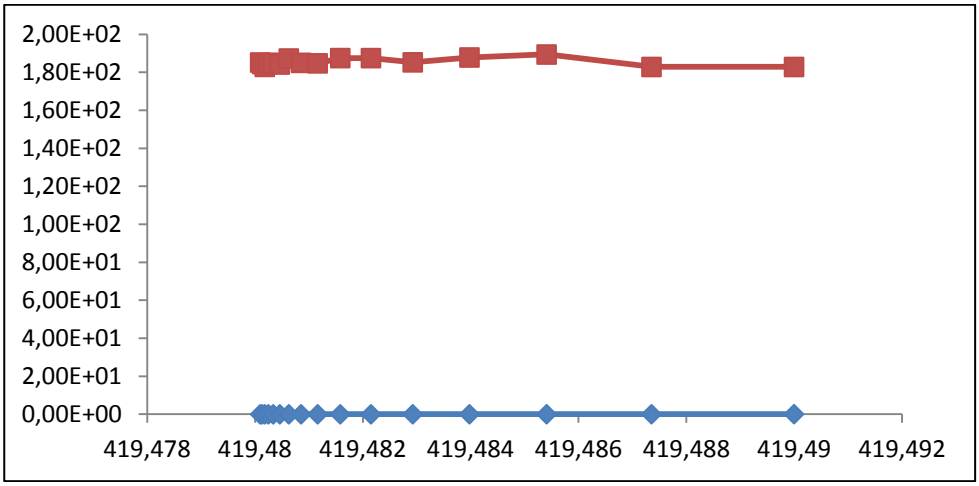

Figure C. 35: Thiophene and n-Butane binary adsorption diagram at 273K for ZIF8. Red represents n-Butane amount and blue represents Thiophene amount.

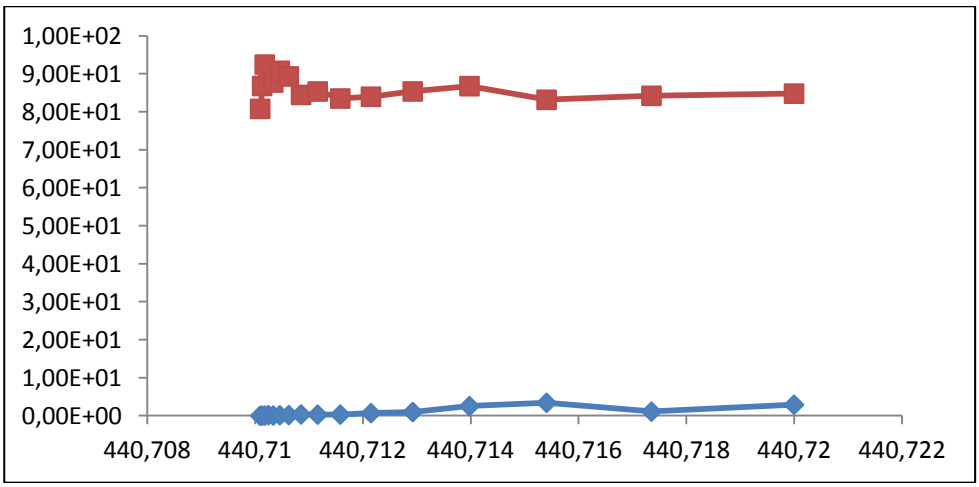

Figure C. 36: Thiophene and n-Butane binary adsorption diagram at 303K for M050. Red represents n-Butane amount and blue represents Thiophene amount.

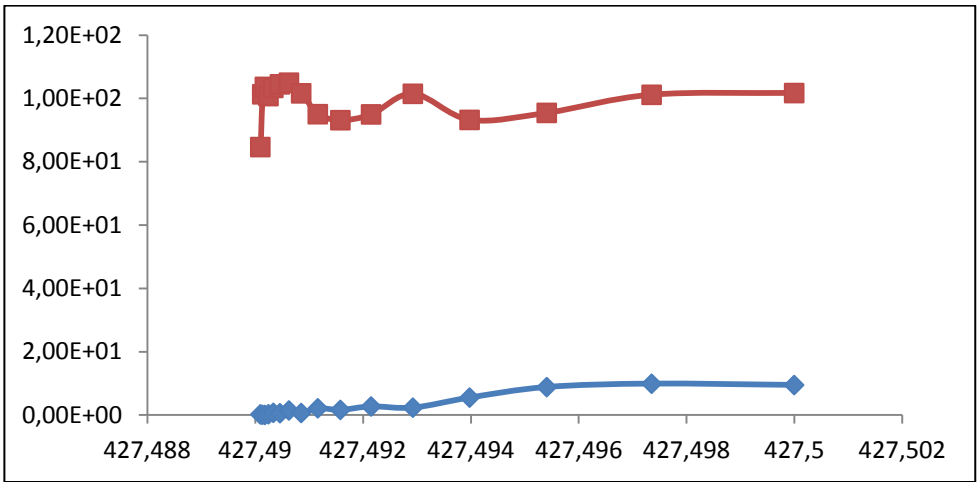

Figure C. 37: Thiophene and n-Butane binary adsorption diagram at 283K for M050. Red represents n-Butane amount and blue represents Thiophene amount.

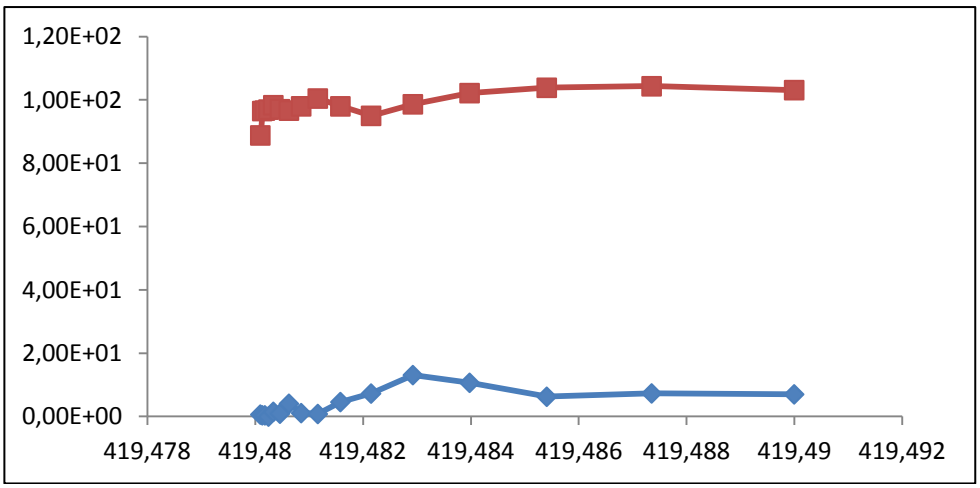

Figure C. 38: Thiophene and n-Butane binary adsorption diagram at 273K for M050. Red represents n-Butane amount and blue represents Thiophene amount.

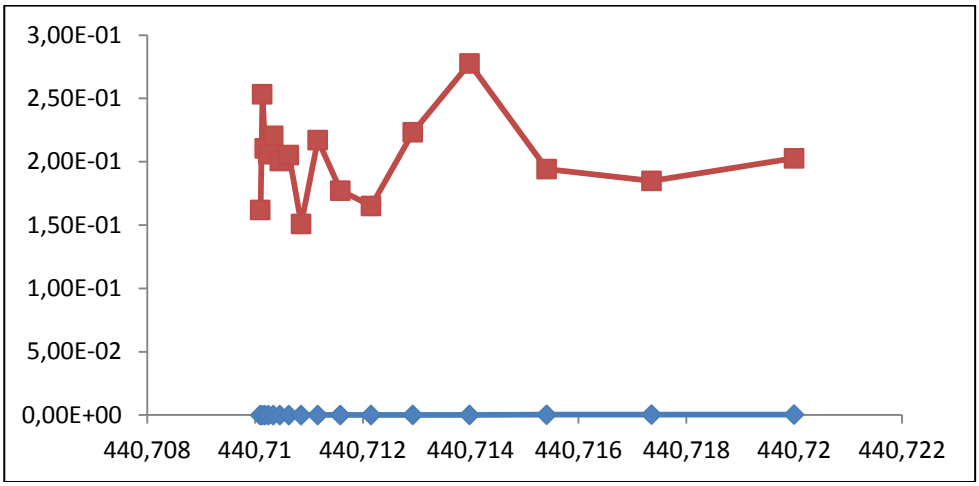

Figure C. 39: Thiophene and n-Butane binary adsorption diagram at 303K for A100. Red represents n-Butane amount and blue represents Thiophene amount.

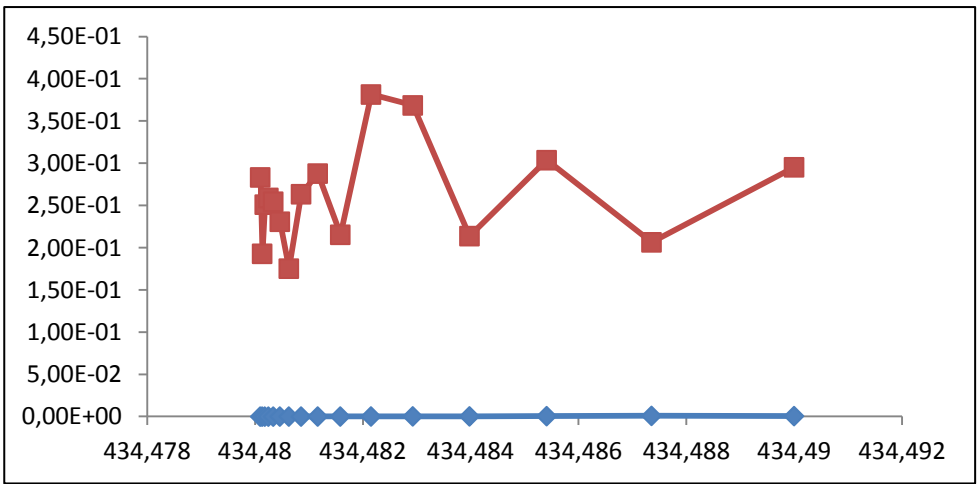

Figure C. 40: Thiophene and n-Butane binary adsorption diagram at 293K for A100. Red represents n-Butane amount and blue represents Thiophene amount.

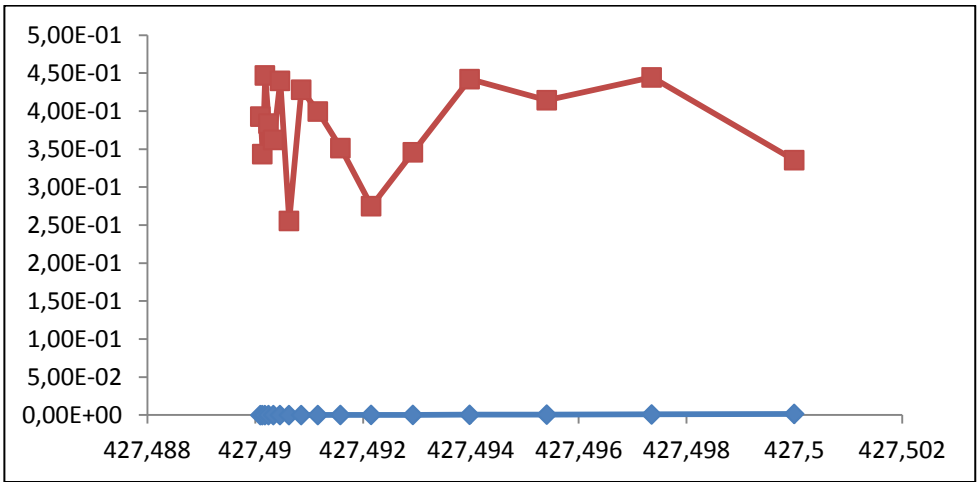

Figure C. 41: Thiophene and n-Butane binary adsorption diagram at 283K for A100. Red represents n-Butane amount and blue represents Thiophene amount.

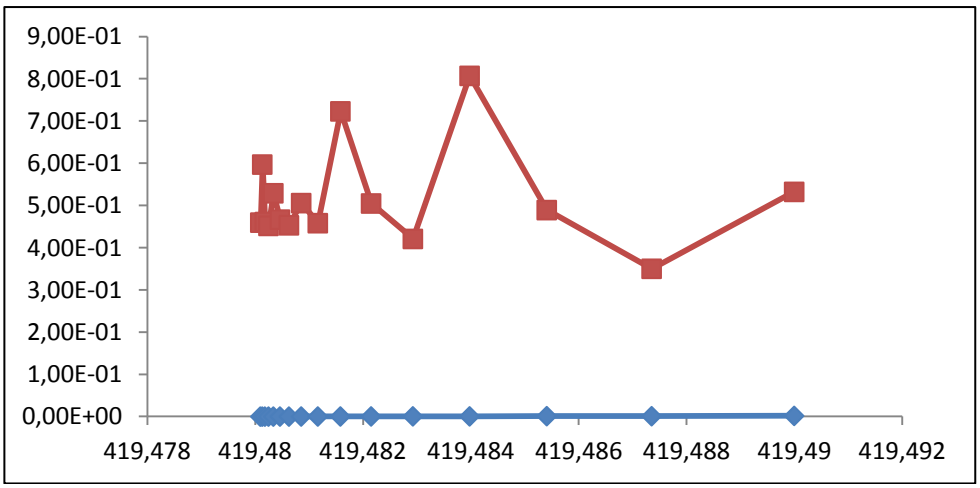

Figure C. 42: Thiophene and n-Butane binary adsorption diagram at 273K for A100. Red represents n-Butane amount and blue represents Thiophene amount.

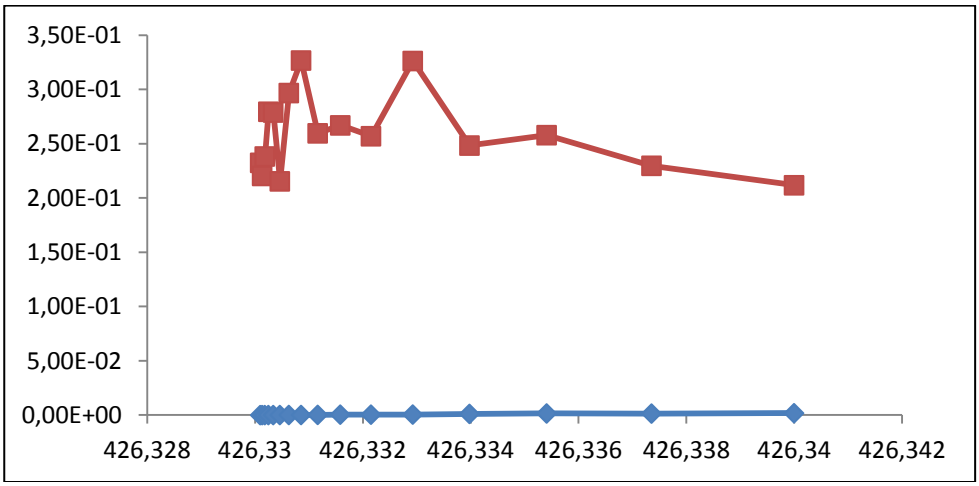

Figure C. 43: Thiophene and i-Butane binary adsorption diagram at 273K for A100. Red represents i-Butane amount and blue represents Thiophene amount.

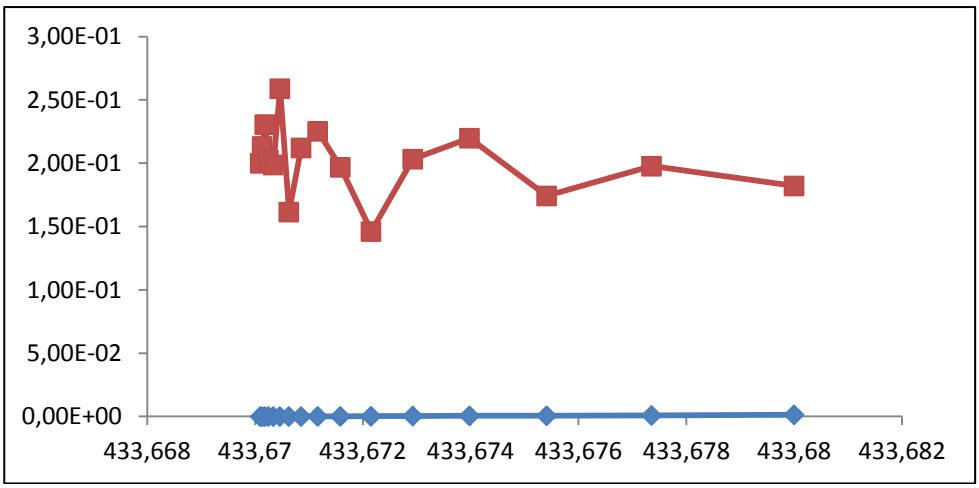

Figure C. 44: Thiophene and i-Butane binary adsorption diagram at 283K for A100. Red represents i-Butane amount and blue represents Thiophene amount.

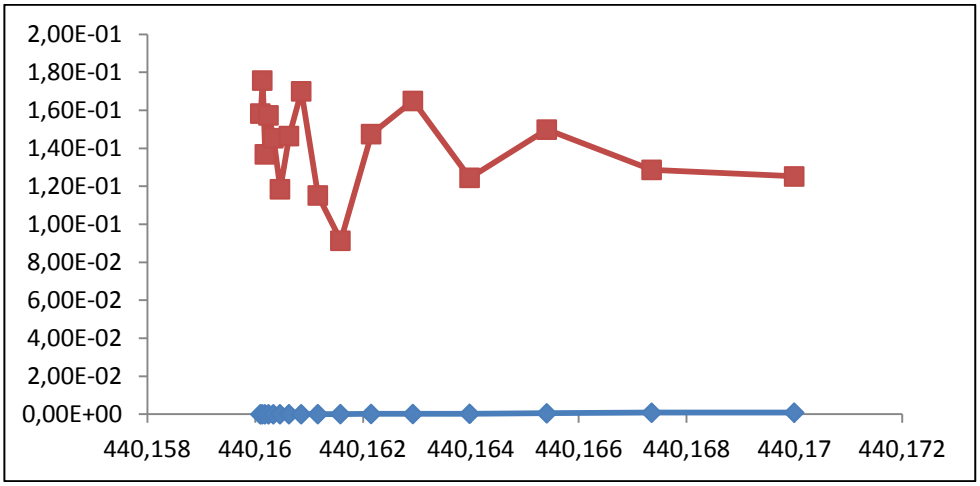

Figure C. 45: Thiophene and i-Butane binary adsorption diagram at 293K for A100. Red represents i-Butane amount and blue represents Thiophene amount.

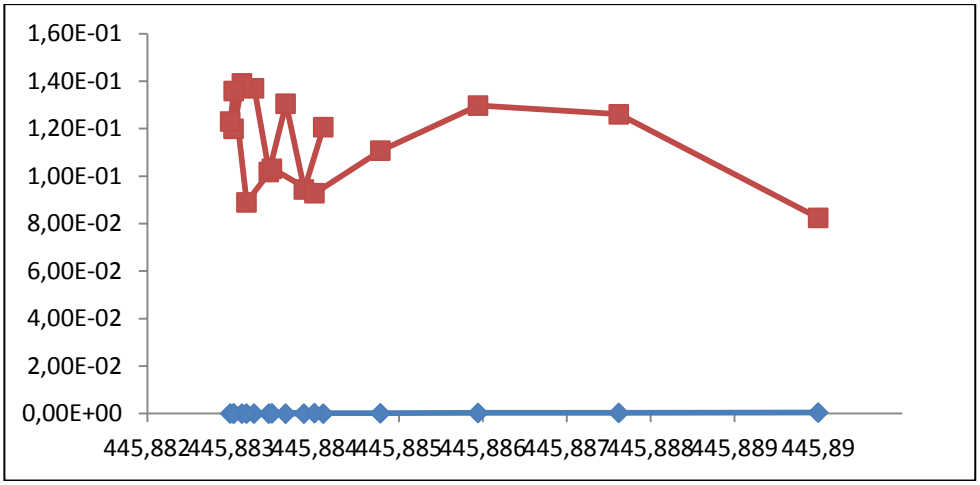

Figure C. 46: Thiophene and i-Butane binary adsorption diagram at 303K for A100. Red represents i-Butane amount and blue represents Thiophene amount.

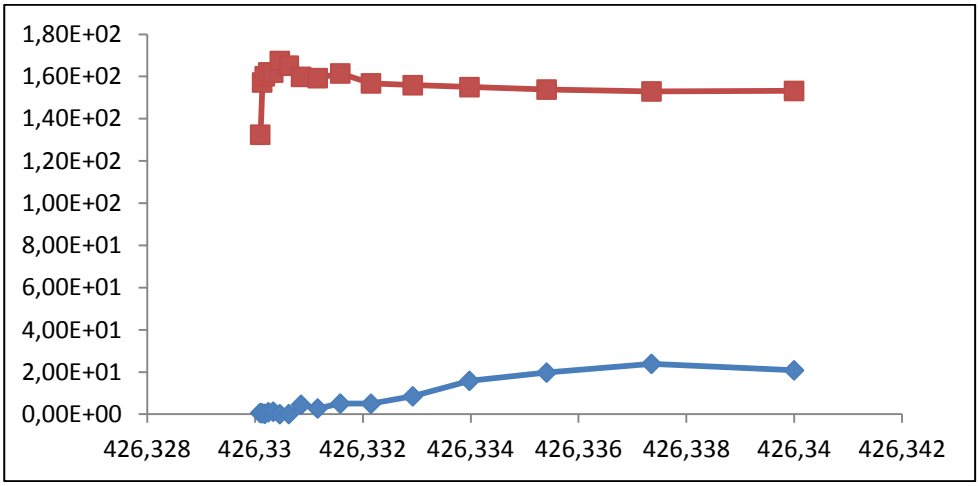

Figure C. 47: Thiophene and i-Butane binary adsorption diagram at 273K for M050. Red represents i-Butane amount and blue represents Thiophene amount.

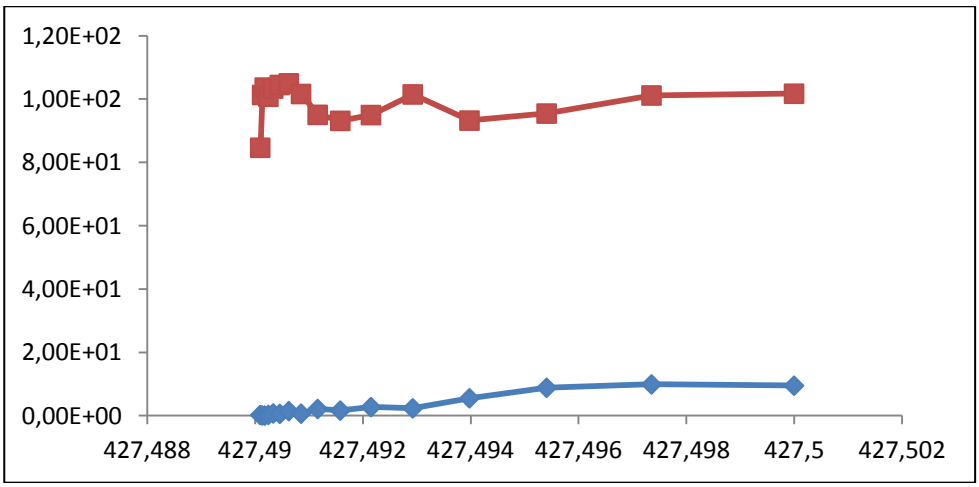

Figure C. 48: Thiophene and i-Butane binary adsorption diagram at 283K for M050. Red represents i-Butane amount and blue represents Thiophene amount.

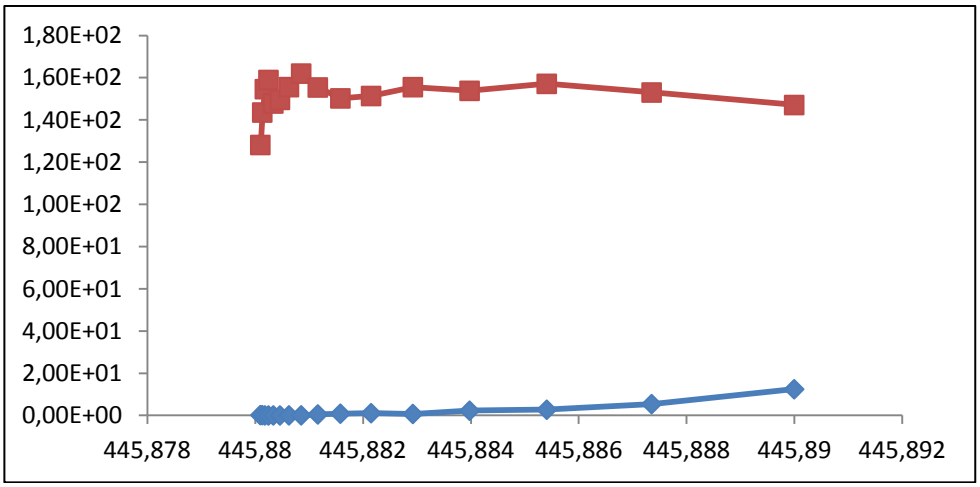

Figure C. 49: Thiophene and i-Butane binary adsorption diagram at 303K for M050. Red represents i-Butane amount and blue represents Thiophene amount.

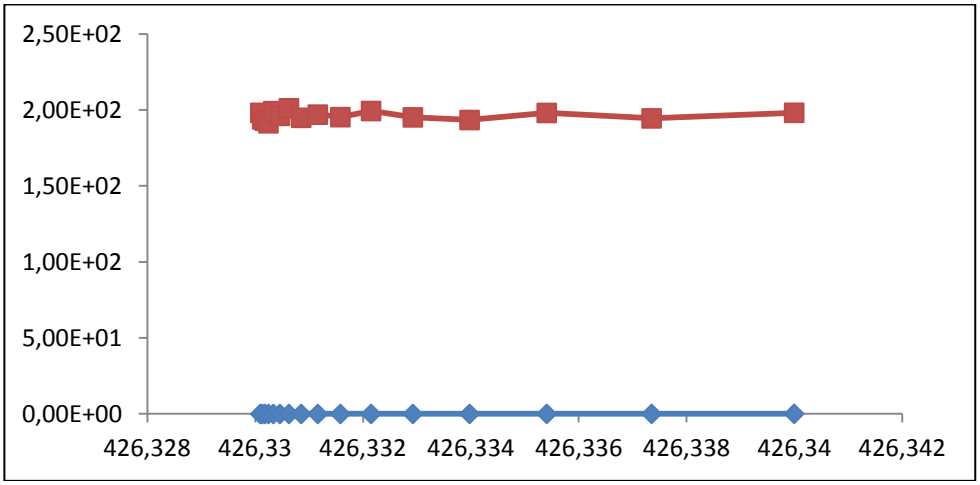

Figure C. 50: Thiophene and i-Butane binary adsorption diagram at 273K for ZIF8. Red represents i-Butane amount and blue represents Thiophene amount.

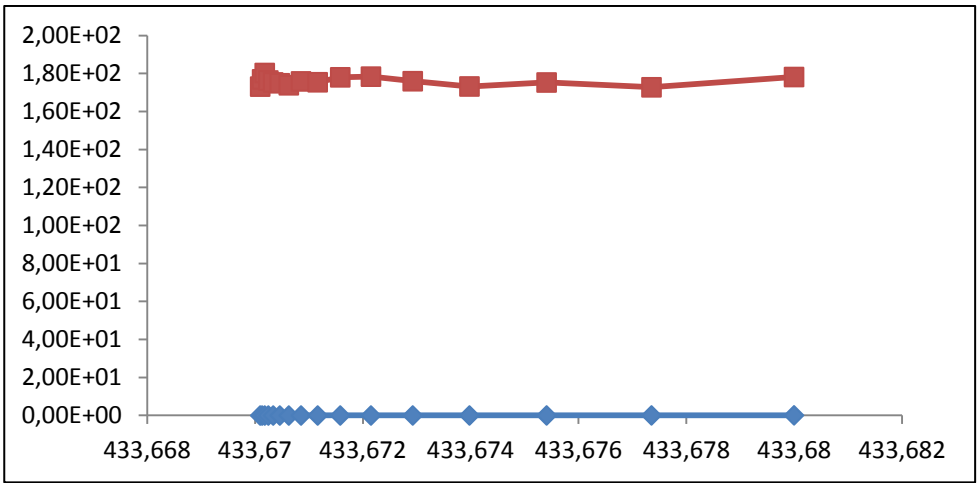

Figure C. 51: Thiophene and i-Butane binary adsorption diagram at 283K for ZIF8. Red represents i-Butane amount and blue represents Thiophene amount.

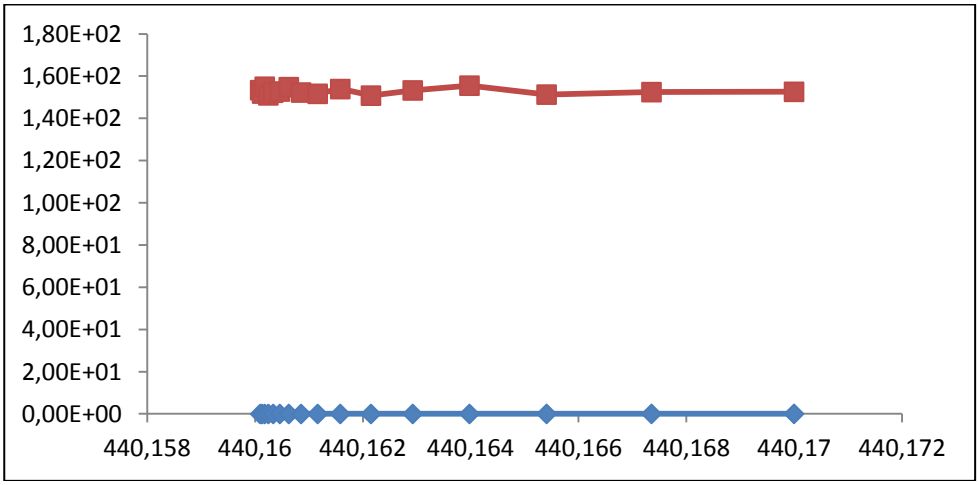

Figure C. 52: Thiophene and i-Butane binary adsorption diagram at 283K for ZIF8. Red represents i-Butane amount and blue represents Thiophene amount.

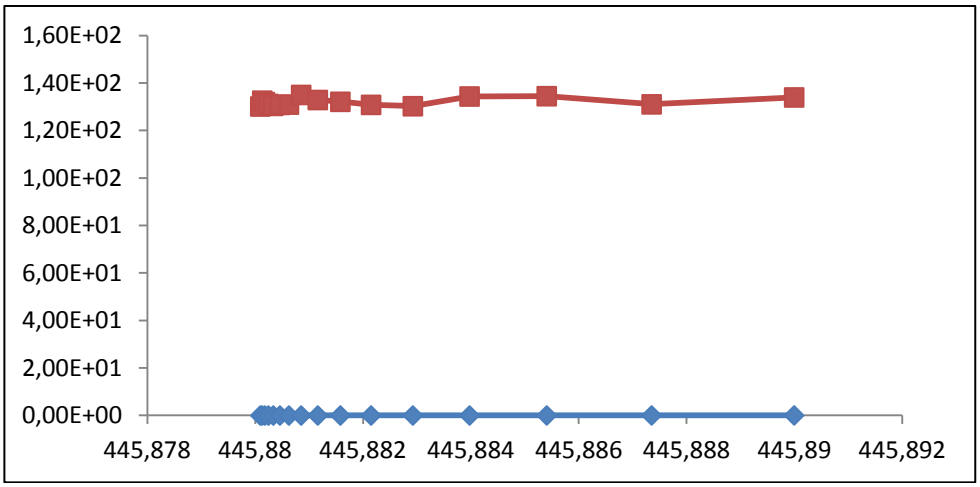

Figure C. 53: Thiophene and i-Butane binary adsorption diagram at 303K for ZIF8. Red represents i-Butane amount and blue represents Thiophene amount.

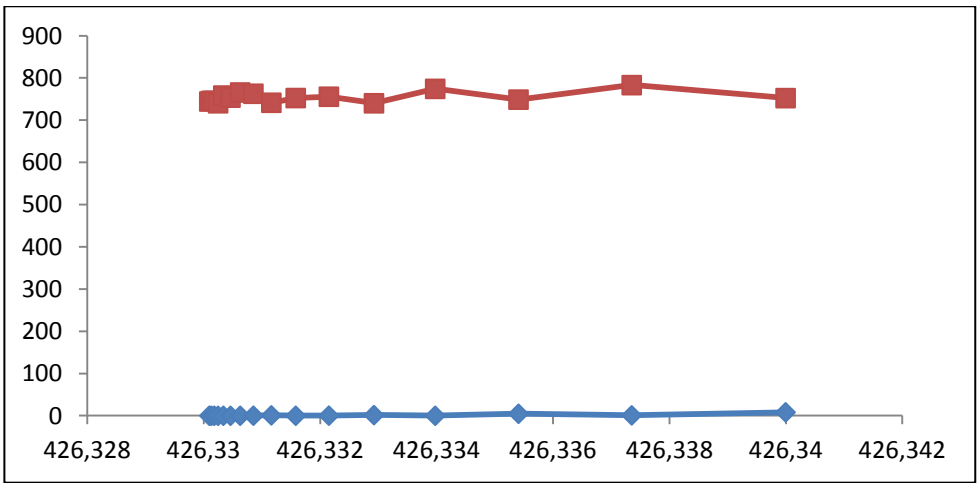

Figure C. 54: Thiophene and i-Butane binary adsorption diagram at 273K for IRMOF. Red represents i-Butane amount and blue represents Thiophene amount.

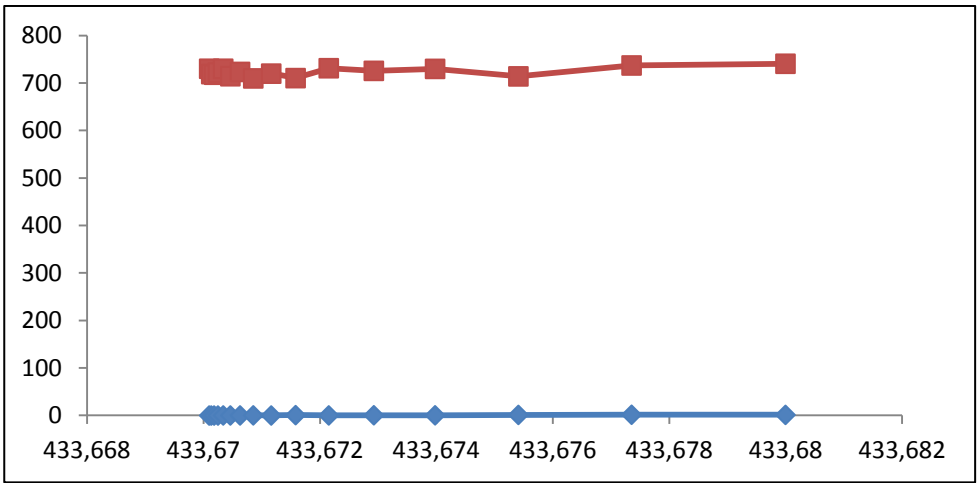

Figure C. 55: Thiophene and i-Butane binary adsorption diagram at 283K for IRMOF. Red represents i-Butane amount and blue represents Thiophene amount

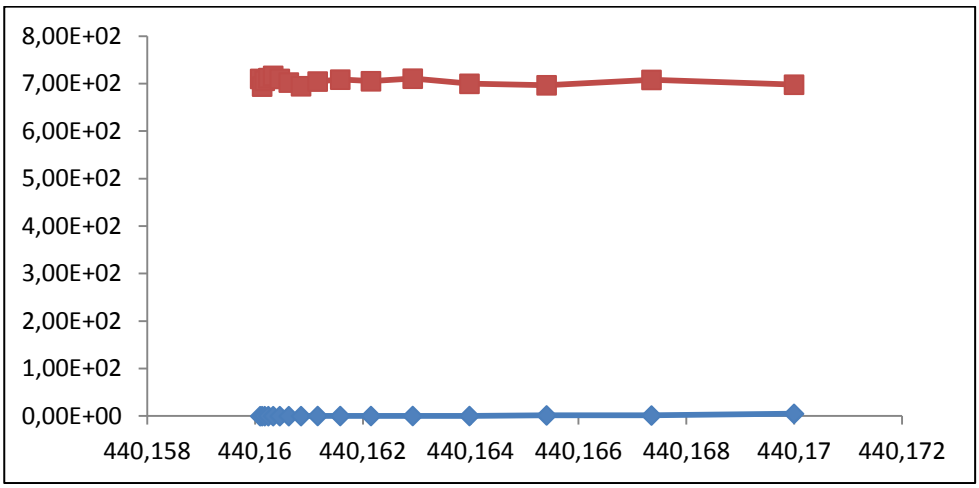

Figure C. 56: Thiophene and i-Butane binary adsorption diagram at 293K for IRMOF. Red represents i-Butane amount and blue represents Thiophene amount.

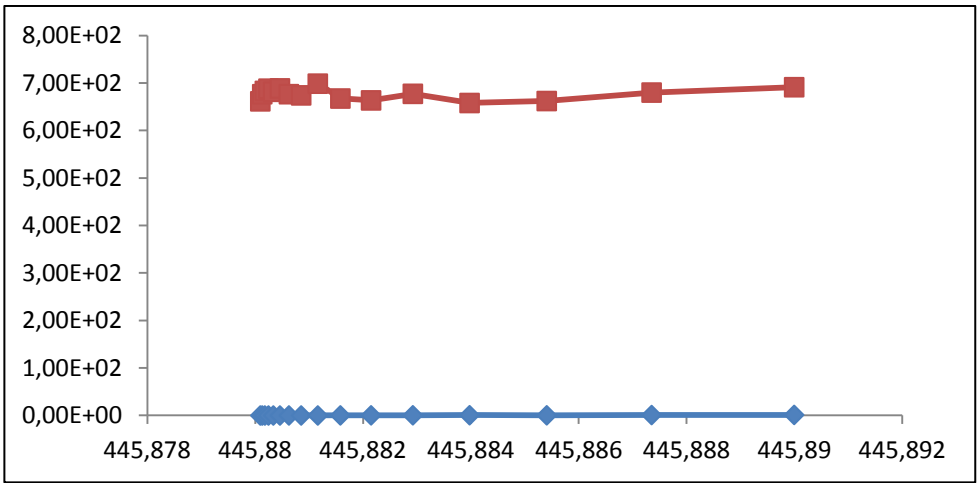

Figure C. 57: Thiophene and i-Butane binary adsorption diagram at 303K for IRMOF. Red represents i-Butane amount and blue represents Thiophene amount.

Appendix C:

Table C.1: Sulfur compounds inside LPG

Sulfur compound	**Molecular weight (kg/kmol)**	**Boiling point (˚C)**	**Density (kg/m^3)**	**Average amount inside LPG (ppm)**
H_2S	34,08	-60,3	1539	476
COS	60,075	-50	2510	1.3
C_2H_6S	62,14	35	845,3	13.04
CH_4S	48,11	6	1999	1
C_2H_6S	62,14	37	846	4.3
C_4H_8S	88,17	119	998,7	1.14
$C_{14}H_{12}S$	212,31	365	1182	<1
$C_2H_6S_2$	94,20	110	1060	<1
C_8H_6S	134,20	221	1150	<1
$C_{12}H_8S$	184,26	332	1252	<1

CURRICULUM VITAE

Name Surname: Masoud TEYMOURFAMIANASL

Place and Date of Birth: Miyandoab/ Iran – 04.04.1989

Address: Istanbul Technical University, Faculty of Chemical Engineering, 34469 Maslak, Istanbul, Turkey

e-mail: m_famian@yahoo.com

B.Sc.: Urmiya University of Technology, Department of Chemical Engineering- Petro-Chemical Engineering